

**Geophysical characterization of the lithology  
and structure of the Olobanita Well Field,  
Lower Lake Baringo Basin, Kenya Rift:  
Implication on Groundwater occurrence**

By

**Mogaka Daniel Nyaberi**

**Reg. No. I56/71802/2008**

Dissertation submitted to the University of Nairobi in  
partial fulfilment of the requirements for the degree of  
Master of Science in Geology (Applied Geophysics)

**UNIVERSITY OF NAIROBI**

**August 2010**

University of NAIROBI Library



0478751 1

## Disclaimer

This document describes work undertaken as part of a programme of study at the University of Nairobi. All views and opinions expressed therein remain the sole responsibility of the author, and do not necessarily represent those of the University.

## Declaration

This is my original work and has not been submitted for a degree in any other University.

Signed..........Date.....6/9/2010.....

**Mogaka Daniel Nyaberi**

The dissertation has been submitted for examination with my knowledge as University supervisor

Signed..........Date.....6/9/2010.....

**Professor Justus Obiko Barongo**

## Abstract

The task of the research project is the use of geophysical technologies for the characterization of the lithology and structure beneath the Olobanita well field, and determine their implications on the groundwater drilling operations in the basin. Development of the aquifer since the 2000's to date by the government agencies and its development partners through drilling, has resulted in generation over time of data and information on its water resources. Consequently, borehole collapse problems have been reported that have resulted from the drilling activities. This has been used by my research as a guide to the study of the subsurface of the well field. Geophysical techniques employed includes electrical resistivity (vertical electrical sounding (VES) and electrical resistivity tomography (ERT)), magnetics and geospatial techniques like geographical information systems (GIS) and global positioning system (GPS) for development of maps.

The Olobanita Basin with an area of 625km<sup>2</sup>, a volcano-sedimentary basin is located in the Central Kenya Rift, Nakuru district of Rift Valley Province. It is located between latitudes 0°00'N and 0°15' S and longitudes 36°00' and 36°15' E. For the study, establishments on the subsurface geology of the wellfield were made from; borehole geologic logs, vertical electrical sounding interpreted data, electrical resistivity tomographic interpreted data and magnetic data analysis results and reports by other researchers.

The vertical electrical sounding and the 2-Dimension (2D) Resistivity imaging allowed a distinction to be made between very high resistive volcanic sands, the moderately high resistivity freshwater saturated zone and the very low resistive clays in localised areas. The geological interpretation of the surveys correlated very well with the borehole data. Vertical faults have resulted in minor down-throwing of blocks in areas close to the rift wall on the east and some few metres to the west margins of the VES grid area. It is concluded that the well-field lies in a volcano-sedimentary basin, where the results from the analysis shows that there exists volcanic sand and silt formation to a depth of about 40 metres underlain by volcanic ashes and fragments to a depth of about 80 metres with intercalations of hard rock formations mainly; welded tuffs and trachyte. These loose unconsolidated geologic materials are vulnerable to collapsing by any chance of disturbance. To the depth beyond 80 metres to about 300 metres exists loose sediments with rounded fragments; thus, contributes to the borehole blockage and collapsing challenges.

# Contents

Disclaimer.....	i
Declaration.....	ii
Abstract.....	iii
Contents.....	iv
List of Tables.....	viii
List of Figures.....	ix
Dedication.....	xvi
Acknowledgement.....	xvii
CHAPTER ONE.....	1
1.0 INTRODUCTION.....	1
1.1 Background Information.....	1
1.2. Statement of the research problem.....	3
1.3. Location.....	4
1.4. Physiography.....	6
1.4.1 Topography.....	6
1.4.2 Drainage.....	6
1.5 . Climate.....	6
1.6. Soils and land use.....	7
1.6.1 Soils.....	7
1.6.2 Land use.....	7
1.7. Vegetation.....	8
1.8. Communication.....	8
1.9. Justification and significance.....	8
1.9.1 Justification.....	8

1.9.2 Significance.....	8
1.10. Aim and Objectives.....	9
1.10.1 Aim.....	9
1.10.2 Objectives.....	9
1.11. Previous works.....	9
CHAPTER TWO.....	11
2.0 GEOLOGY AND HYDROGEOLOGY.....	11
2.1. Geology.....	11
2.1.1 Regional geology.....	11
2.1.2 Geology of the study area.....	11
2.2. Hydrogeology.....	16
2.2.1 Regional hydrogeology.....	16
2.2.1.1 Groundwater Conditions of Lower Baringo Basin.....	18
CHAPTER THREE.....	21
3.0 BASIC THEORY.....	21
3.1. Introduction.....	21
3.2 Basic Principles.....	22
3.2.1 Vertical Electrical Sounding.....	22
3.2.2 Electrical resistivity tomography.....	24
3.2.3 Magnetic Method.....	26
CHAPTER FOUR.....	28
4.0 DATA AQUITION.....	28
4.1 Introduction.....	28
4.2 Aquition of Pleriminary Data.....	28
4.2.1 Drilling operations data.....	29
4.2.2 Geologic Logging Data.....	29

4.3 Acquisition of Field Data.....	30
4.3.1 Instrumentation.....	30
4.3.2 Fieldwork.....	35
CHAPTER FIVE.....	40
5.0 DATA PROCESSING AND INTERPRETATION.....	40
5.1 Introduction.....	40
5.2 Vertical Electrical Sounding.....	40
5.2.1 Data Processing.....	40
5.2.2 Interpretation of the data.....	43
5.3 Electrical Resistivity Tomography data.....	46
5.3.1 Processing raw.....	46
5.3.2 Interpretation.....	46
5.4 Magnetic data.....	48
5.4.1 Processing.....	48
5.4.1 Interpretation.....	52
CHAPTER SIX.....	58
6.0 DISCUSSION OF RESULTS.....	58
6.1 Introduction.....	58
6.2 Relationship between borehole lithology/structure and collapsing of boreholes.....	58
6.3 Lithological interpretation of geophysical results.....	59
6.4 Structural interpretation of geophysical data.....	82
6.5 Relationship between borehole lithology/structure and geophysical results and hence collapsing of boreholes.....	88
6.6 Groundwater.....	90
CHAPTER SEVEN.....	91
7.0 CONCLUSION AND RECOMMENDATIONS.....	91

REFERENCES..... 93

APPENDICES.....96

APPENDIX A. Magnetic profiles (1-4) running in the area in the West to East direction  
covering 2500 metres at intervals of 100 metres showing subsurface magnetic  
materials and faultzones.....96

APPENDIX B. Concrete field data on borehole competition report-Olobanita Borehole No. 1  
showing areas affected by collapsing during drilling operations..... 98



# List of Tables

1.1 Safe Yield from Water Resources by Major Drainage Basins in Kenya	
Safe yield in '000 cubic meters per day.....	2
2.1 Stratigraphic Table.....	12
3.1 Geophysical tools and the specific parameters they measure.....	21
6.1 Formation resistivities from interpreted model of station 13.....	61
6.2 General relationship between F and grain-sizes established in NW-Europe.....	61
6.3 Resistivity Ranges for Materials in BH2.....	62
6.4 Formation resistivities from interpreted model of abandoned BHX.....	64
6.5 Resistivity Ranges for geologic materials in BHX.....	64
6.6 Formation resistivities from interpreted model of BH6.....	66
6.7 Shows the interpreted subsurface geology and their resistivities for BH2.....	69
6.8 Shows the interpreted subsurface geology and their resistivities for abandoned BHX.....	70

# List of Figures

- 1.1 The central Kenya Rift with the study area shown in a square.....4
- 1.2 Map showing the Olobanita well field within the Lower Baringo Basin, Central Kenya Rift.....5
- 1.3 Showing the average annual rainfall across Kenya. Source FEWSNET 2009.....7
- 2.1 The geological map of the study area.....16
- 3.1 Showing the current and potential electrode arrangement in the field.....22
- 3.2 Electrical resistivity tomography geophysical section or profile.....25
- 3.3 Magnetic field due to a simple bar magnetic.....26
- 4.1 SYSCAL R2 electrical resistivity equipment which was employed in VES data collection.....31
- 4.2 Field data collection using SYSCAL R1 switch 72 Electrical Resistivity Tomography meter.....32
- 4.3 SINTREX Total Field Proton Precession Magnetometer used in the field.....33
- 4.4 A schematic of the proton precession magnetometer.....34
- 4.5 The grid within the study area where the VES data was collected.....35
- 4.6 The grid within the study area where the magnetic data was collected.....38
- 5.1 Format of inputting raw Ves data to be interpreted by use of the AGI EarthImager 1D inversion and modeling software.....40

5.2 Raw data from the field in an input ASCII.....	41
5.3. Input file in figure 5.2 and output file for processed results entered in the Resist.for.....	41
5.4 Shows next stage of processed Ves data.....	42
5.5 Shows final stage of pprocessed Ves data.....	42
5.6 Measured and modeled data as read by AGI Earthimager 1D software.....	43
5.7 Inverted measured data of station 17.....	44
5.8 An interpreted model showing the subsurface of the station 17 in the study area.....	44
5.9 Interpreted model (station 13 at BH2) showing curve and layered resistivity model.....	45
5.10 Interpreted model (station 16 at BH1) showing curve and layered resistivity model.....	45
5.11 Data in a format as imported from the field machine for interpretation by RES2DINV software.....	46
5.12 Data in format of figure 4.8. read by RES2DINV software.....	47
5.13 Profile 1 showing the vertical slice obtained from borehole 2.....	47
5.14 Profile 1 showing the vertical slice acquired from BH X.....	48
5.15. Format of magnetic field data to be interpolated.....	49
5.16 Reading data using interpol.for program.....	49

5.17	Data resulting from interpolation of magnetic field data.....	50
5.18	Format of interpolated data used in correct.for program.....	50
5.19	Reading data using correct.for program.....	50
5.20	Corrected magnetic data.....	51
5.21	Data reading using euler deconvolution freeware.....	51
5.22	Data entered in surfer for plotting.....	52
5.23	Initial plot of the processed magnetic data in interpretation.....	53
5.24a	Magnetic profile 1 about 100metres to the north of BH2.....	53
5.24b	Shows fault zones in magnetic profile 1 of the study area.....	54
5.25a	Magnetic profile 1 about 10 metres to the north of BH2.....	55
5.25b	Shows fault zones in magnetic profile 1 of the study area.....	55
5.26a	Magnetic profile 4 about 200 metres to the south of BH2.....	56
5.26b	Magnetic profile 4 showing fault zones.....	56
5.27a	Magnetic profile 3 about 200 metres to the south of BH2.....	57
5.27b	Magnetic profile 3 showing fault zones.....	57
6.1	Geologic log of Olobanita Borehole no. 2 .....	60
6.2	Interpreted model at station 13 (at BH2) showing curve and layered resistivity model.....	61
6.3	Geological log of Olobanita abandoned Borehole X.....	63

6.4	Interpreted model at the abandoned BHX showing curve and layered resistivity model.....	64
6.5	Geological log of Olobanita Borehole 6.....	65
6.6	Interpreted model at the abandoned BH6 showing curve and layered resistivity.....	66
6.7a	Vertical electrical sounding interpreted models (profile 1 W-E).....	67
6.7b	Vertical electrical sounding interpreted models (profile 2 W-E).....	67
6.7c	Vertical electrical sounding interpreted models (profile 3 W-E).....	67
6.7d	Vertical electrical sounding interpreted models (profile 4 W-E).....	68
6.8i	Interpreted model at station 1.....	71
6.8ii	Interpreted model at station 2.....	71
6.8iii	Interpreted model at station 3.....	71
6.8iv	Interpreted model at station 4.....	71
6.8v	Interpreted model at station 5.....	72
6.8vi	Interpreted model at station 6.....	72
6.8vii	Interpreted model at station 7.....	72
6.8viii	Interpreted model at station 8.....	72
6.8ix	Interpreted model at station 9.....	72
6.8x	Interpreted model at station 10.....	72
6.8xi	Interpreted model at station 11.....	73

6.8xii	Interpreted model at station 12.....	73
6.8xiii	Interpreted model at station 13.....	73
6.8xiv	Interpreted model at station 14.....	73
6.8xv	Interpreted model at station 15.....	73
6.8xvi	Interpreted model at station 16.....	73
6.8xvii	Interpreted model at station 17.....	74
6.8xviii	Interpreted model at station 18.....	74
6.8xix	Interpreted model at station 19.....	74
6.8xx	Interpreted model at station 20.....	74
6.8xxi	Interpreted model at station 21.....	74
6.8xxii	Interpreted model at station 22.....	74
6.8xxiii	Interpreted model at station 23.....	75
6.8xxiv	Interpreted model at station 24.....	75
6.8xxv.	Interpreted model at station 25.....	75
6.8xxvi	Interpreted model at station 26.....	75
6.8xxvii	Interpreted model at station 27.....	75
6.8xxviii	Interpreted model at station 28.....	75
6.9a	Profile 1 Vertical section of true resistivity in the N-S direction (contours in ohm.m).....	77
6.9b	Profile 2 Vertical section of true resistivity in the N-S direction (contours in ohm.m).....	77

6.9c Profile 3 Vertical section of true resistivity in the N-S direction (contours in ohm.m).....	78
6.9d Profile 4 Vertical section of true resistivity in the N-S direction (contours in ohm.m).....	78
6.9e Profile 5 Vertical section of true resistivity in the N-S direction (contours in ohm.m).....	79
6.9f Profile 6 Vertical section of true resistivity in the N-S direction (contours in ohm.m).....	79
6.9g Profile 7 Vertical section of true resistivity in the N-S direction (contours in ohm.m).....	80
6.10a Profile 1 Vertical section of true resistivity in the W-E direction (contours in ohm.m).....	80
6.10b Profile 2 Vertical section of true resistivity in the W-E direction (contours in ohm.m).....	81
6.10c Profile 3 Vertical section of true resistivity in the W-E direction (contours in ohm.m).....	81
6.11 Profile 4 Vertical section of true resistivity in the W-E direction (contours in ohm.m).....	82
6.12a Horizontal section of true resistivity at 50 m depth (contours in ohm.m).....	83
6.12b Horizontal section of true resistivity at 100 m depth (contours in ohm.m).....	83
6.12c Horizontal section of true resistivity at 150 m depth (contours in ohm.m).....	84
6.12d Horizontal section of true resistivity at 200 m depth (contours in ohm.m).....	84
6.12e Horizontal section of true resistivity at 250 m depth (contours in ohm.m).....	85
6.12f Horizontal section of true resistivity at 300 m depth (contours in ohm.m).....	85
6.12g Horizontal section of true resistivity at 350 m depth (contours in ohm.m).....	86
6.13 Magnetic profile processed to a depth of 1000m.....	86
6.14 Profile 1 showing the vertical slice acquired from abandoned BHX.....	87
6.15 Magnetic profile through the abandoned BHX.....	87

6.16. Shows correlation of ERT profile, geologic log and VES model and the specific areas where collapsing occurred during drilling of BH2.....88

6.17. Shows correlation of ERT profile, geologic log and VES model and the specific areas where collapsing occurred during drilling of BHX.....89



## Dedication

This Dissertation has been dedicated to my daughter, Amygrace Kerubo whose love for her future propelled my hard work.

## Acknowledgements

“Having come this far, means I have been carried on the shoulders of some giants” [Shakespeare]. To these, I am greatly indebted.

Firstly, my appreciation to the Government of France whose sponsorship through CIFEG made this study a success. My gratitude also for the permission granted to pursue the degree by the Kenya Government through my employer; the Ministry of Water and Irrigation.

Secondly, I wish to express my profound gratitude to my supervisor – Prof. Justus Obiko Barongo for his important guidance and helpful comments from the beginning of the project, fieldwork supervision till this finalized report. Every time’s discussion with him made my dissertation improve and I really learnt and improved a lot from him. Furthermore, I am thankful to the Olobanita local people for their immense support and willingness to co-operate during the fieldwork. My heartfelt thanks go to my colleagues in the Geophysics course and colleagues from Ministry of Water and Irrigation, Data Base Division for all the support received.

Consequently, I am grateful to the Rift Valley Water Services Board, for they willingly offered information on boreholes and some consultancy reports. I wish to also acknowledge the kind co-operation of the Department of Mines and Geology, Kenya, who made available their Proton processing magnetometer instrument for this study.

I am highly indebted also to my spouse, Lydia and our daughter Amygrace and my mother who stood by me during the course of the study and whose encouragement, moral and prayer support kept me going. To God be all the Glory.

# CHAPTER ONE

## 1.0 INTRODUCTION

### 1.1 Background Information

Fresh water is a finite and vulnerable resource, essential to sustain life, development and the environment. The world's freshwater resources are under increasing pressure; so, many still lack access to adequate water supply for basic needs. Growth in population, increased economic activity and improved standards of living lead to increased competition for, and conflicts over the limited freshwater resource.

Current estimates indicate that the total volume of water on earth is about  $1.4 \times 10^9 \text{ km}^3$  of which about 97% is in the seas or oceans and therefore saline, 77% of freshwater is locked up in icecaps and glaciers, leaving negligible percentage in easily accessible sources like lakes and rivers. Kenya is classified as a chronically water-scarce country. The country's natural endowment of freshwater is limited by an annual renewable freshwater supply of only 647 cubic meters per capita. Globally, a country is categorized as "water-stressed" if its annual renewable freshwater supplies are between 1,000 and 1,700 cubic meters per capita and "water-scarce" if its renewable freshwater supplies are less than 1,000 cubic meters per capita (World Bank, 2000). Kenya uses both surface and groundwater resources to meet the current demand. The magnitudes of annual renewable water from surface and groundwater resources differ. The volume of annual renewable surface water is on the order of 19.7 billion cubic meters per year ( $\text{m}^3/\text{yr}$ ) while the volume of renewable groundwater is on the order of 2.1 billion  $\text{m}^3/\text{yr}$  (Tuinhof, 2001). Renewable groundwater is therefore approximately one-tenth as large as renewable surface water.

Only a certain proportion of renewable water can be used (known as the safe yield), while the remainder is either technically inaccessible or required to safeguard environmental and ecological processes. Even though all water up to the safe yield can be tapped, it can only be accessed at a steeply increasing cost. The safe yield for surface water is estimated to be on the order of 7.4 billion  $\text{m}^3/\text{yr}$ , while the estimated safe yield from groundwater is on the order of 1.0 billion  $\text{m}^3/\text{yr}$  (refer to Table 1.1.).

Table 1.1: Safe Yield from Water Resources by Major Drainage Basins in Kenya Safe yield in '000 cubic meters per day

Basin	Surface Water	%	Groundwater	%	Total	%
Lake Basin	11,993	59.2	539	18.7	12,532	54.2
Rift Valley	211	1.0	586	20.3	797	3.4
Athi River	582	2.9	405	14.0	987	4.2
Tana River	6,789	33.5	685	23.8	7,474	32.3
Ewaso Ng'iro	674	3.3	663	23.0	1,337	5.8
<b>Totals</b>	<b>20,249</b>	<b>100</b>	<b>2,878</b>	<b>100</b>	<b>23,127</b>	<b>100</b>

Source: Surface water data from Republic of Kenya 1992; Groundwater data from Tuinhof 2001.

Groundwater has considerable potential for boosting water supplies. Kenya's geology and hydrogeology favor economic exploitation of groundwater resources, with an estimated annual safe yield of 1.0 billion m<sup>3</sup> per year. These resources are spread over five hydrological areas: (1) the volcanic rocks area in the Rift Valley; (2) the volcanic rocks area outside of the Rift Valley; (3) the metamorphic basement rocks' area; (4) the eastern Quaternary sedimentary rocks' area; and (5) the western Quaternary sedimentary rocks' area.

It is estimated that less than 10% of Kenya's available groundwater resource is currently used (MoWI, 2006). The advent of technology has made the quest for water for all purpose in life to drift from ordinary search for water to prospecting for steady and reliable subsurface or groundwater. While available groundwater resources must be used for economic growth, at the same time it is important to avoid creating undesirable impacts on groundwater leading to a decline in the value of the resource. This calls for proper management, both to ensure resource sustainability and to maintain quality.

Groundwater is one of the major sources of fresh water for supply to Nakuru town and its peri-urban residents. Besides Kabatini and Baharini well fields, Olobanita well field contributes immensely towards the grid supply of water to the town. Nakuru is one of the towns in Kenya encompassed with the increasing growth in population and the subsequent socio-economic pursuits (including urbanization, industrial production, tourism and agricultural activities) and the demand for water is increasing rapidly (GOK, 1999), thus the need to develop groundwater resources to its full potential. Despite the great contribution of Olobanita well field as a water

source to Nakuru town, the development of groundwater supply has largely been affected by the collapsing of boreholes during the drilling operations. There is also increasing dependence on groundwater in this area with little appraisal on the sustainability of this resource steer clear of the appropriateness to environment, though a reliable source of fresh water.

## 1.2. Statement of the research problem

The potential volume of the surface water resources is highly declining leading to increase in the dependence to a high proportion on groundwater resources. Deforestation, land fragmentation, cultivation of wetlands and rapid increase in human settlements have had negative impacts on water resources resulting in reduced stream flows and ground water. Groundwater is one of the major pre-requisites for a decent life and indeed any form of life. Nakuru town, being the fourth largest town in Kenya, relies heavily on groundwater explored from its hinterland in order to meet the water requirements for her fast growing population and its peri-urban areas. There is increased abstraction of groundwater in the main well-fields which include Olobanita, Baharini and Kabatini in Nakuru without proper knowledge of the aquifer structure and lithology. The appropriate utilization of groundwater has not been possible and the water scarcity has still remained an issue of great concern. This fact is attributable to various groundwater exploration and extraction problems. The collapsing of freshly drilled boreholes, the poor siting of boreholes that result in low uneconomical well-yields and drying up of shallow boreholes are some of the key concerns affecting the Olobanita well-field, one of the key fields designed for groundwater supply to Nakuru town.

The geophysical studies have come up with incontrovertible results pertaining to the physical characteristics of the subsurface and their comparison to Stratigraphic correlation monitored from the geologic logs which are practically excellent. This study endeavored to establish the geology, hydrogeology and geological structures of Olobanita well-field which will form a basis into the future understanding of the groundwater regime of the area in its various aspects like recharge, discharge, pollution and effectiveness in groundwater development in the well-field. Consequently, the difficulty posed by the lithology and geological and tectonic structures to groundwater drilling operations were investigated. Thus the application of these methods revealed the type of lithology and structure that lead to the collapsing of freshly drilled boreholes in the well-field.

### 1.3. Location

Olobanita well-field, herein referred as the study area, occurs within the Lower Baringo Basin, Central Kenya Rift (see Figure 1.1). The well field is a volcano-sedimentary sub-basin with an area of 625km<sup>2</sup>. It is located between latitudes 0°00'N and 0°15' S and longitudes 36°00' and 36°15' E (see Figure 1.2).

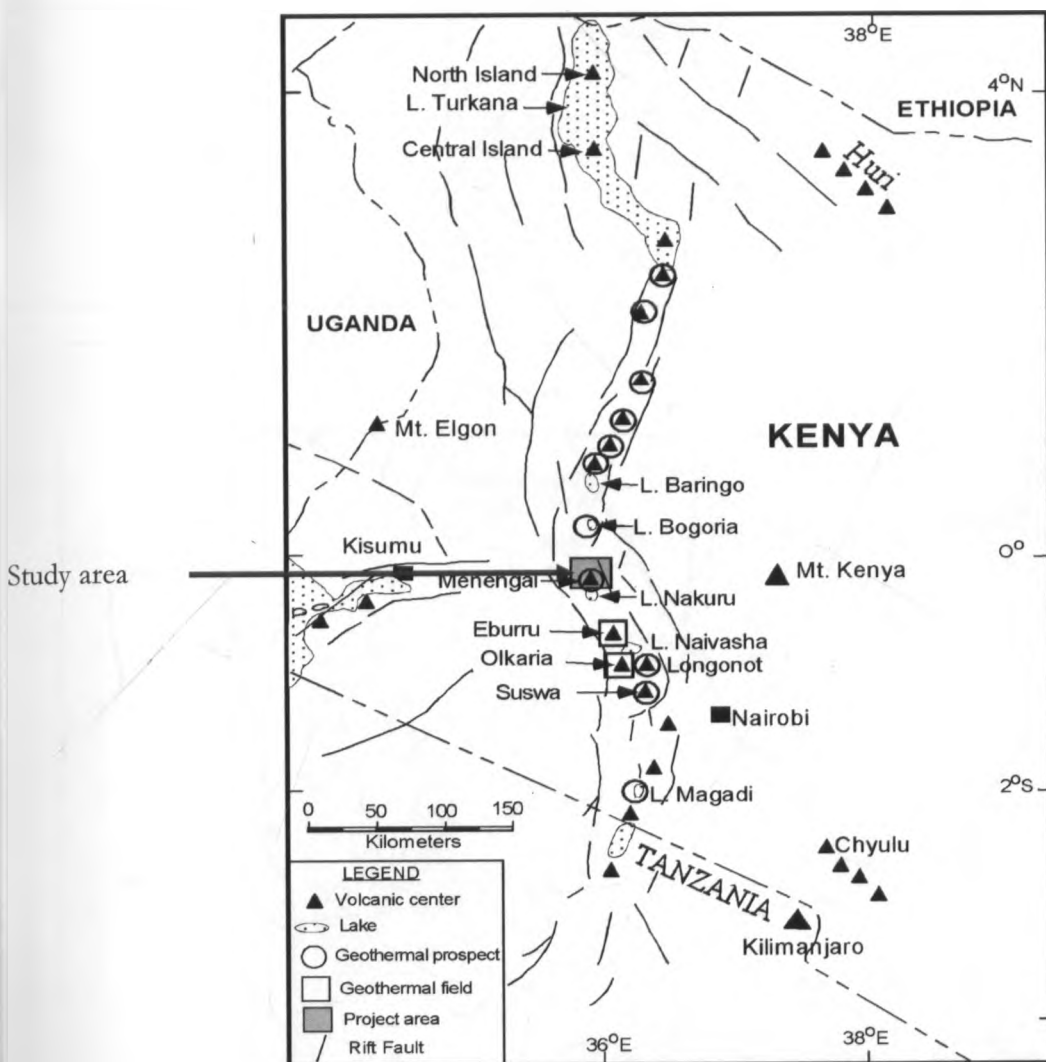


Figure 1.1 The central Kenya Rift with the study area shown in a square.

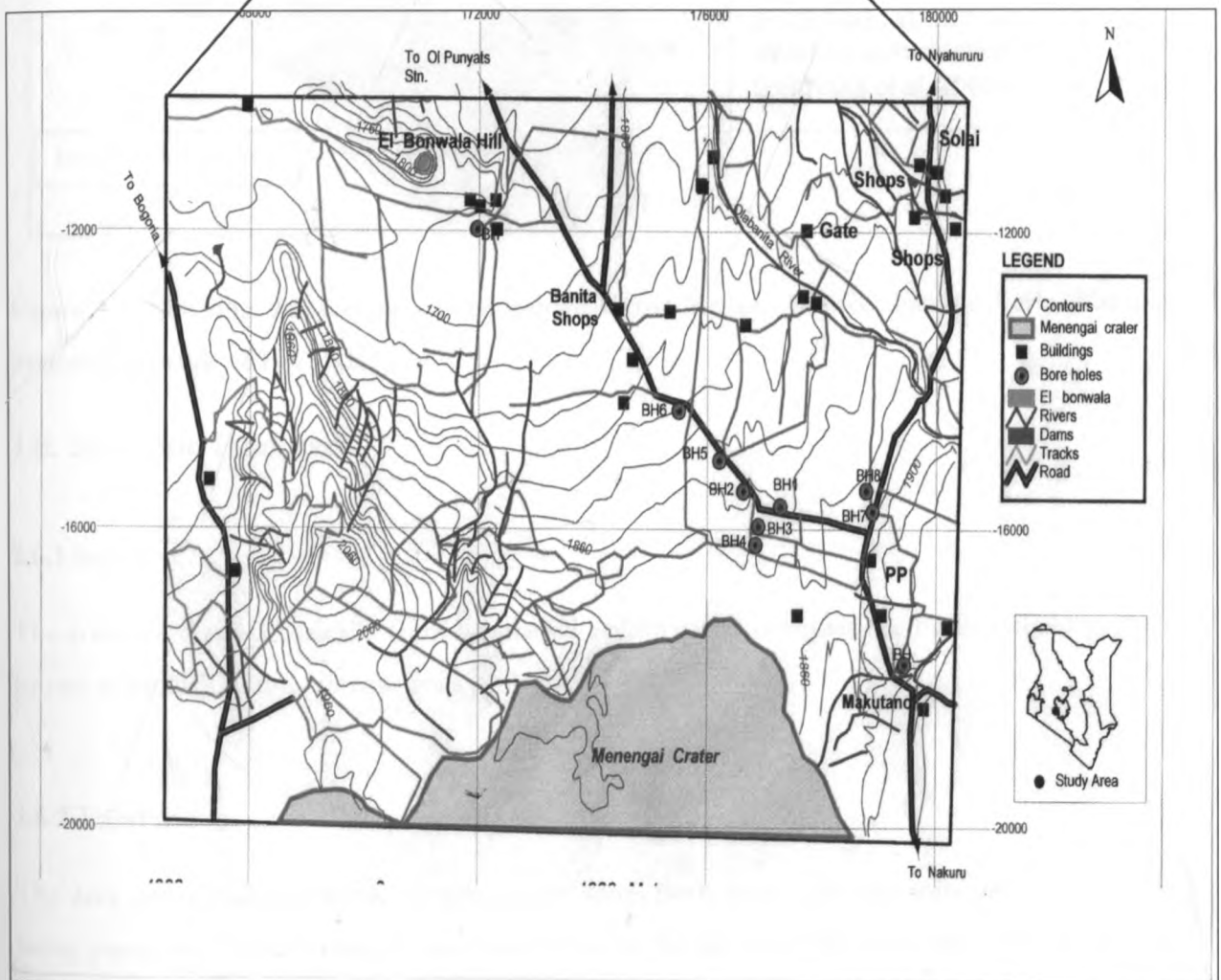


Figure 1.2 Map showing the Olobanita well field within the Lower Baringo Basin, Central Kenya Rift (After Barongo, 2008).

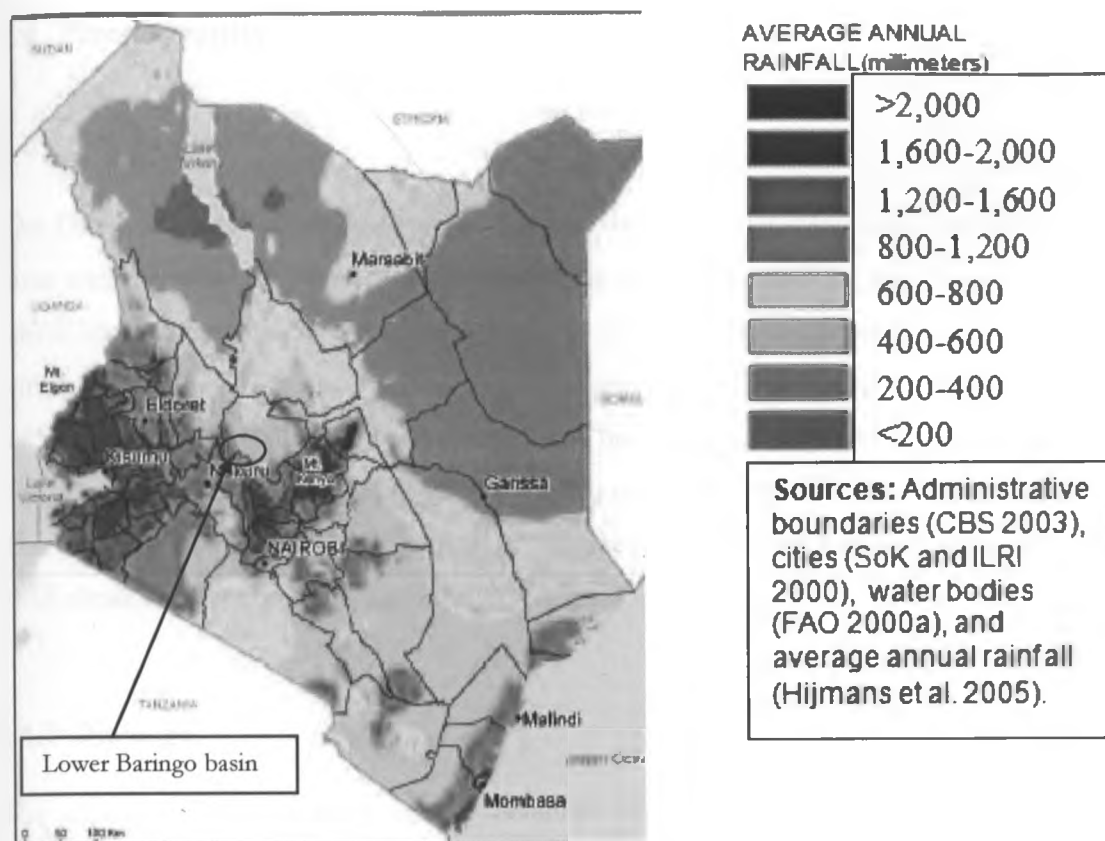


Figure 1.3. Showing the average annual rainfall across Kenya. Source: Famine Early Warning Systems Network (FEWSNET) 2009.

## 1.6. Soils and land use

### 1.6.1 Soils

The soils are derived basically from weathered volcanic and occupies the basin as light grey or brown to pinkish non-calcareous soils.

### 1.6.2 Land use

The area under study is mainly an agricultural zone. Both large scale and subsistence farming is being practiced. Coffee farming is the center stage in this area and almost entirely through private entrepreneurship.



## **1.4. Physiography**

### **1.4.1 Topography**

The Olobanita well-field is bordered by Bahati hills to the East, Menengai caldera to the South, Solai escarpment to the North and El Bonwala Hill to the North West (see Figure 1.2). The area where boreholes for supplying water to Nakuru are drilled is approximately 7.5 kilometers square within the study area. The vertical electrical sounding (VES) mapping covered an area of 0.25km<sup>2</sup>. The Rift Valley Water Services Board has drilled up to a total of ten boreholes where two are abandoned, two are capped and six are in use by Nakuru Water and Sewerage Company. The borehole X was abandoned because it collapsed and borehole 8 was abandoned because the yield obtained after drilling was uneconomical.

### **1.4.2 Drainage**

The drainage system consist of the perennial Olobanita river which flows off the Solai escarpment, draining high ground in the Bahati forest before reaching the Ol-Punyata swamp. The Watkins River also drains through the area to the north-east of Olobanita River and to the south-east drains the Crater stream.

## **1.5. Climate**

The dominant controls of weather and climate in the region and East Africa as a whole are:

(i) The Inter-tropical convergence Zone (ITCZ), (ii) Altitude and (iii) Latitude. The Lower Baringo basin experiences low and erratic annual rainfall which varies between 500 mm to 750 mm in most parts which is characteristic of semi-arid regions which are typical characteristics of the Rift Valley floor (see Figure 1.3). There are primarily two periods of rainfall per year, being seasonal and the pattern is similar to other parts of the country. The long rains come in the months of March to May and the short rains in the months of September to November. It is highly influenced by catchment areas like the adjoining escarpments of Mau to the West and Aberdares to the East, both highly forested. The temperature ranges between 35°C and 39°C for most of the year.

## **1.7. Vegetation**

The vegetation within this area has a semi-arid character and high potential rangeland for grazing purposes. This includes the acacia, bushes and savannah. The exceptional case is recognized in mountainous areas where tropical rain forests are prominent especially in Bahati area of Nakuru District.

## **1.8. Communication**

The Olobanita well-field is accessed from the Nakuru-Nyahururu road, at the Makutano junction, a feeder murram road connects to the well field which later form two other roads; one leading to Solai and another to Banita shops and beyond to Ol Punyats area. To the northwest of the project area passes a railway line.

## **1.9. Justification and significance**

### **1.9.1 Justification**

Nakuru town and its peri-urban areas face immense difficulties in trying to meet the water requirements for her rapidly growing population. The choice of the Olobanita well-field as study area was important, where regrettably, for the boreholes drilled; intended to supply water (about 15,000 m<sup>3</sup>/day) to the above mentioned town, are collapsing. In the process of trying to achieve production by drilling of new boreholes for groundwater abstraction, structural difficulties are encountered with either collapse of newly drilled boreholes or drying up of earlier drilled shallow boreholes or some boreholes with uneconomical yields as exhibited in the well-field. In view of the afore-mentioned problems, there is need to delineate the groundwater availability in Olobanita well field. This is achieved by checking and authenticating the resource and related geological and structural factors contributing to the availability and the causes of drill-hole collapse.

### **1.9.2 Significance**

The results achieved reveal the lithology and structures beneath the Olobanita well-field and their relation to groundwater occurrence. These results will help in advising on the best practice to be

employed in drilling operations to counter the problem of collapsing of boreholes. Further, they will also guide on the best points to drill to avoid the problem of siting uneconomical boreholes.

## **1.10. Aim and Objectives**

### **1.10.1 Aim**

The aim of the project is to determine the implications of various lithologies and structures on groundwater drilling operations in the Olobanita well field.

### **1.10.2 Objectives**

The specific objective is to use geophysical techniques to determine the relationship between geophysical parameters, mainly electrical resistivity and magnetic susceptibility to lithology and structures beneath the Olobanita basin and its impact on drilling operations.

## **1.11. Previous works**

Using geophysical tools during the initial characterization is an intuitive process offering rapid insight into subsurface physical properties. A geophysical survey is often the most cost-effective and rapid means of obtaining subsurface information, especially over large study areas (Sirles, 2006). Geophysics can be used to select borehole locations and can provide reliable information about the nature and variability of the subsurface between existing boreholes. Geophysical tools are designed to measure specific parameters, and are generally used to measure spatial variation in these specific parameters within a study area of interest and have given excellent results previously.

Despite the number of surveys that have been conducted in the Nakuru and Baringo basins, Central Kenya-Rift in connection with groundwater exploration, no comprehensive investigation has embraced the present study area. According to existing literature, some groundwater exploration works have been carried out in the area in a regional nature, but can be used as reference in the present study.

McCall, et al. (1965) investigated the general geology of the Nakuru –Kamasian basin. Their conclusion were that groundwater resources are found within the sedimentary formations of the Nakuru basin which they concluded that were of late Tertiary and Quaternary of age, arguments which are agreeable with those drawn by Mooney and Wetzel (1956). In addition, McCall (1957) published a detailed survey of geology and groundwater conditions of the Nakuru area.

According to Kuria, 1999, geophysical investigations were carried out in the area from mid 1960's. These were mainly done in search of groundwater, and in the 1970's in search of geothermal reservoirs within the Rift Valley by various groups and firms. The first sounding (Wenner) was done between lakes Nakuru and Bogoria which also covers the Menengai area, with the aim of establishing the structural geology of the geothermal area. According to Nyambok, et al. (1993), there is immense amount of groundwater in the floor of the Rift Valley, but its abstraction is influenced by the existence of a system of faults and fractures. Consequently, they unfolded that the main water aquifers are controlled by secondary permeability zones such as faults and fractures.

## CHAPTER TWO

### 2.0 GEOLOGY AND HYDROGEOLOGY

#### 2.1. Geology

##### 2.1.1 Regional geology

The Rift Valley where the study area lies is a rift system within the abardare detachment (Kuria, 1999). The geology of the Rift is implicitly represented by rocks which are exposed representing lava flows, superficial sediments and soils. Lava flow rocks whose origin is related to fissures and faulting within the rift valley covers the greater area in the region. Consequently, the lava sheets in the study area are associated with the eruption of Menengai volcano, and thus the subsequent pumaceous tuffs and sediments.

##### 2.1.2 Geology of the study area

The Olobanita well-field is a volcano-sedimentary basin located in the Central Kenya Rift, Nakuru district. The area is characterized by rhythmic successions of volcanic activity that was accompanied by major episodes of faulting. The geology predominantly consists of Tertiary to Quaternary volcanic suite, intercalated with thin successions of lake beds. The study area lies to the north, of Menengai Crater. A report on geology and groundwater by McCall, 1957, gives a thorough description of the geology and the characteristics of the rocks encountered in the area. A simplified geological succession of the area is presented in Table 2.1 (Kuria, 2006). The history of the evolution of the Rift Valley, certainly the study area is extremely complex with no rock exposures older than the Tertiary era. Firstly, the continental surface planed by the erosion cycle which moulded the sub-Miocene erosion surface, was apparently warped down prior to the first eruptions, along a zone roughly corresponding with the present Rift Valley trend.

The first volcanic eruptions were the Samburu series of thin basalt and picrite lava flows, and subordinate pumice showers. These in part erupted from swarms of dykes and in part from central sources. This phase of eruption was followed by earth movements, which led to unconformity between the Samburu volcanics and the overlying plateau phonolites. The plateau

phonolites form an extensive series of flows with no pyroclastic horizons intervening. A continuous succession of more than 600 metres of these phonolites is exposed on Ngelesha. However, they thin out rapidly towards the median line of the rift and away from the rift shoulder to the east.

Table 2.1. Stratigraphic Table

PERIOD	VOLCANIC ROCKS & SEDIMENTS	IGNEOUS INTRUSIVE	TECTONIC EPISODES
Recent	Superficial deposits, soils and alluvium. Upper Menengai Volcanics		
Pleistocene	Tuffs and sediments - Nakuru Basin, Tuffs and fluviatile sediments, Pumice Tuffs, welded tuff 'Ignimbrite' and sediments forming unconformable outliers on the Kinangop and Bahati tuffs.	Syenite boulders on Menengai slopes	Minor Faulting - Solai, Marigat, and West of Nakuru Major Faulting.  Unconformity
Tertiary	<b>Pliocene:</b> Kwaibus basalt, Kisanana sediments, Mau Tuffs, Bahati Tuffs, Kinangop Tuffs, Lower Menengai Volcanic Series. <b>Miocene:</b> Rumuruti phonolite, Samburu Series, Simbara Series.		Major Faulting  Major Faulting Warping Unconformity
Precambrian	Basement System		Precambrian Orogenic movements

These eruptive series were followed by major faulting in the north of the area. The vertical displacement on these earlier faults, now represented by dissected scarps, may have been as much as 1370 metres in the Lake Bogoria sector.

After a long erosional interval, there followed a second series of volcanic eruptions. These were initiated by basalt eruptions, e.g., Kwaibus basalts which outcrop in the area and consist of cinder cones marking old vents and numerous successive thin flows of lava. These basalts were followed by phonolite eruptions from centres in Menengai and Kiplombe and from fissure sources away from the volcanic centres. The eruptives included pumice tuff, lava and ignimbrites. These eruptions were followed by major faulting which roughed out the Rift Valley as known today to the south.

Following these fault movements, an erosional period formed an unconformity between outliers of late pumice tuff, welded tuff 'ignimbrite', sediments and the Kinangop and Bahati Tuffs. A third major faulting episode succeeded, forming Menengai caldera. A minor volcanicity in Menengai followed with the eruption of trachyte cinder cones and lava flows. This was followed by the deposition of Solai tuffs associated pumiceous sediments and Tuffs and fluvial sediments of Mugurin. Minor faulting followed creating new fractures and renewing the older ones in Solai area. The geological map (see Figure 2.1) indicates the geological formations found in the study area. The geological formations are discussed as follows;

### **Basement**

The oldest rocks in the study area are the quartzites and the gneisses forming part of the Kenya's Basement System. The Basement System metamorphic rocks, of presumed Precambrian age in the area are concealed by Tertiary and Pleistocene volcanic rocks. These rocks are subdivided into; quartzites and micaceous quartzites, feldspathic biotite gneisses and pegmatites. Absolute age determinations carried out on Basement system rocks from other parts of the country show that regional metamorphism took place in the late precambrian times but the age of the sediments is unknown.

### **Basalt**

These rocks are noted in the Stratigraphic column of the study area and they are exposed in the Bahati Escarpment to the east of the Olobanita well field. Minor intercalations of pumiceous

tuffs, interlaid with diatomite beds are dominantly noted within the basalt and these are part of the Older Miocene formation.

### **Phonolite and Trachyte**

According to Kuria, 1999, the phonolitic and trachytic lava flows and sheets are overlying the basalt. These lava sheets have their origin from the eruption of Menengai volcano.

### **Tuffs**

Overlying the phonolites and trachytes are the tuffs in the succession within Pliocene Period. These rocks are found around Menengai crater in form of welded pyroclastics. There are two types of tuffs: agglomeratic tuffs and graded tuffs as later shown in the geologic log from the study area.

### **Sediments**

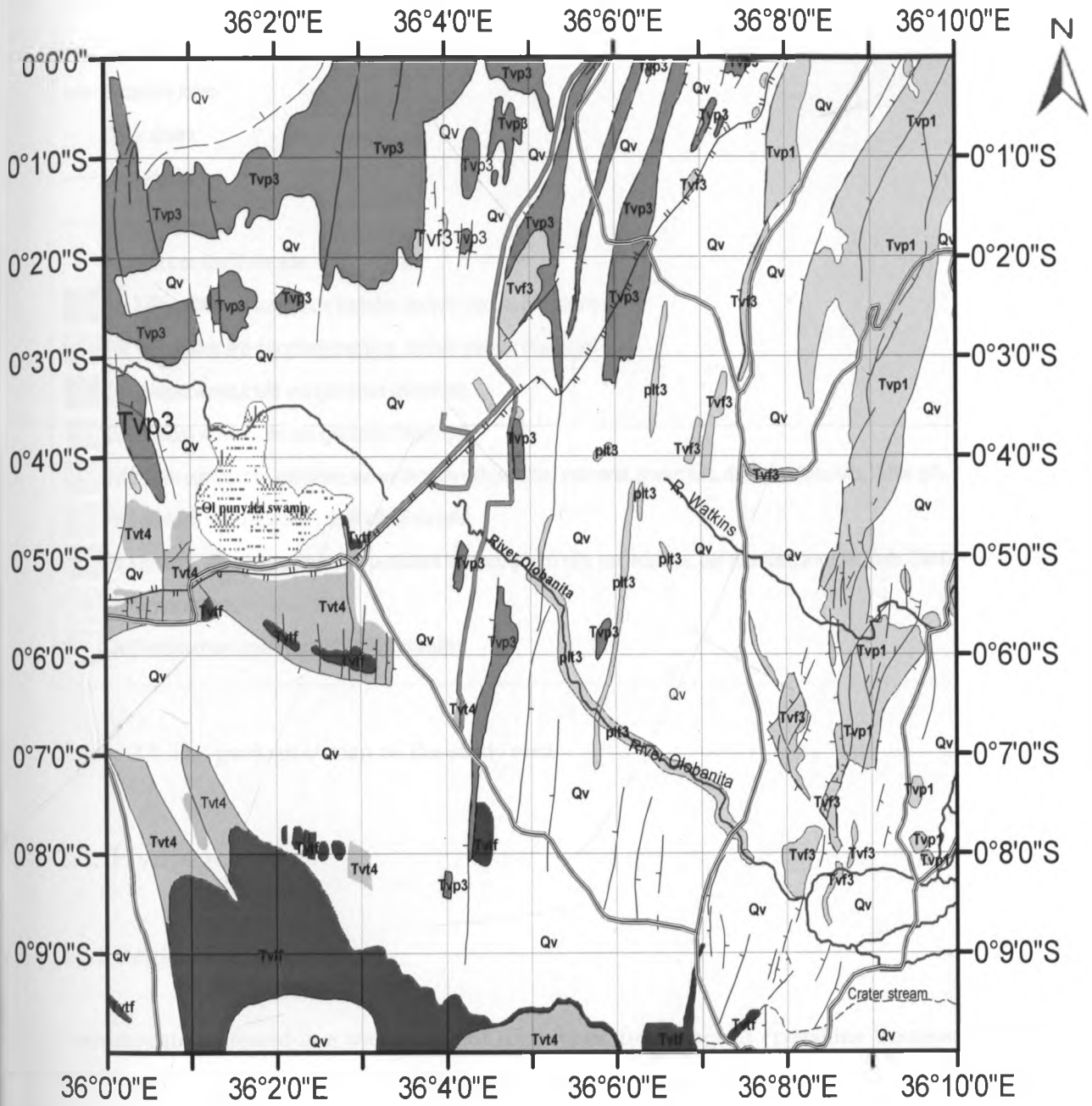
Overlying the tuffs are the stratified tuff ash deposits and diatomaceous silts and sands. These sediments, were probably deposited during the eruptive period of the Menengai volcano and thus deposited as ashes. The characteristic features distinguishing these rocks from underlying and overlying harder tuffs are their common coarse-grained and their porous nature and the rare incidence of collapsed pumice blocks and lapilli. Colours are also frequently distinctive, many of the agglomeratic rocks being marked by yellowish tints. These ashes are predominantly unconsolidated, non-eutaxitic, ash-fall types.

### **Superficial deposits**

Superficial deposits in the area are mainly clayey derived from deep weathering of volcanic ashes in a region of moderate to high rainfall. Dark brown soils give way to reddish varieties in the more densely forested parts of the area.



# GEOLOGICAL MAP OF THE STUDY AREA



Scale 1 centimeter = 1.25 Kilometers



## EXPLANATION















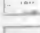

	Main roads-
	Railway-
	Secondary roads-
	Crater stream
	River Watkins
	River Olobanita
	Faults, tick on downthrow side
	Tvp 3 (Phonolites and subordinate trachytes, trachyte breccias (Koishiram)
	Tvp 1 (Phonolites and subordinate trachytes, trachyte breccias (Koishiram)
	Tvtf (Welded vitreous tuffs and ignimbrites (Menengai)
	Tvt4 (Welded vitreous tuffs and ignimbrites (Menengai)
	Tvt 3 (Vitric pumice tuffs, ignimbrites and welded tuffs with lacustrine sediments, graded tuffs, diatomites (Mau tuffs, Bahati tuffs, Kinangop tuffs)
	Pt 3 (Reddish-brown unstratified lapilli tuffs (Solai tuffs)
	Pt 3 (Gravels, silts, diatomaceous silts, pumiceous beds and graded tuffs, part lacustrine, part fluvatile (Larmudiac Beds, Gamblian silts of Kariandusi)
	O1 Punyata swamp
	Qv (Reddish-brown unstratified lapilli tuffs (Solai tuffs)

Figure 2.1 The geological map of the study area

## 2.2. Hydrogeology

### 2.2.1 Regional hydrogeology

Groundwater is found in a wide range of rock types, from ancient crystalline basement rocks that store minor quantities of water in shallow weathered and jointed layers, weathered and /or fractured zones in the volcanic rocks and sediments interbedded between volcanic rocks, to alluvial plain sediments that may extend to depths of several hundred metres and contain enormous volumes of groundwater. Groundwater in the Rift Valley more so in the Lower Baringo Basin occur in volcanic rocks and at varying depths and several aquifers may exist top of one another. The aquifers in these areas are confined and the depths to the aquifers and piezometric levels within them vary widely (IEA, 2007). Groundwater is an important contributor to sustaining the water balance in the Rift Valley lakes (Clarke, *et al.* 1990;

Robert and David 2002). The existence of complex geological and geomorphic features associated with the volcano–tectonic evolution of the rift makes hydrogeological studies more complicated, ( Clarke, *et al.* 1990). The movement of groundwater in the basin is heavily dependant on regional and local geology. The groundwater flow pattern in the basin is less complicated, with the groundwater flow often following the topographical slope. Groundwater flow in the basin is controlled by geological structures, either directly via flows in the tensional faults, or through fluvial and lacustrine deposits whose occurrence is influenced by tectonism. The major groundwater conduits are faults lying parallel and subparallel to the Rift axis.

On a regional scale, the evidence suggests that the structural features divert substantial quantities of groundwater in the Rift Valley interfluves system, which comes from elevated recharge areas to low-lying discharge areas. The flow occurs both laterally and longitudinally, according to the Rift fault systems. The longitudinal flow always dominates, and governs the interconnection of the lakes in the subsurface. The structure of the Rift Valley and particularly the major marginal faults and the system of grid faulting on the Rift floor have a substantial effect on the groundwater flow system in the basin. The high hydraulic gradient developed across the Rift Valley escarpments extending to the east and west is a clear manifestation of axial faults acting as a zone of low permeability, thereby inhibiting flows from the escarpments towards the lakes. It is speculated that, at depth, groundwater flows away from the Lake Nakuru–Elementeita basin beneath Menengai Crater into the Lake Baringo catchment far to the north (Ayenew and Becht, 2008). Groundwater generally flows towards the lakes, predominantly from the eastern and western highlands.

The prevailing geological and climatological conditions in the lower Baringo basin, favour groundwater occurrence in:

- Lacustrine sediments,
- Weathered and /or fractured zones in the volcanic rocks, and
- Sediments interbedded between volcanic rocks.

The groundwater system in the basin is locally recharged by infiltration of rainwater through the permeable volcanic soils, whose percolation into the deep lying aquifers is facilitated by the open fault and fissure zones acting as groundwater conduits. However, ample recharge takes place along the high lying areas of Bahati Forest and Kiplombe Hill located to the east and west of the

of Nakuru area, respectively. Maximum mean annual rainfall in these recharge areas is approximately 1200 millimeters.

### 2.2.1.1 Groundwater Conditions of Lower Baringo Basin

The groundwater conditions have been discussed in detail according to Kuria, 2006, and thus the argument is presented as follows:

#### **Aquifer Piezometry**

**Menengai Crater – North:** Groundwater elevations adjacent to the Menengai Crater are high, indicating significant groundwater flow towards Olobanita area. Groundwater elevations vary between 1901 – 1623 metres indicating significant flow in a northwest direction. Confining pressures are generally low; hence the aquifer encountered in this area may result from permeable horizons within the Menengai volcanic deposits, rather than the Bahati tuffs.

**Bahati Escarpment:** In the area north of the Crater, groundwater elevations show a fairly even gradient from east to west down the escarpment. In Solai area the groundwater flow occurs towards a small lake Solai and further west of the region. The groundwater elevations range between 2143-1509 metres. Confining pressures are low indicating the possibility of unconfined or semi-confined conditions occurring, if the local groundwater levels are lowered by borehole abstraction.

From the results it is inferred that groundwater from the Crater flows in the northwest direction, augmenting the flow from the Bahati Forest. The combined flow moves towards Olobanita swamp. In the central part of the zone, crater and Solai groundwater flow occurs in an east-west direction towards Kisanana. The groundwater elevations range between 2143 -1496 metres at Solai and Legisianan, respectively.

**Rongai area:** Groundwater level conditions in this area are not clearly understood because boreholes drilled in this area are either dry or produce steam. The groundwater elevations range between 1919-1739 metres above mean sea level: this indicates a flow in North-North-East direction towards Mogotio and Lomolo area. The confining pressures are low indicating unconfined conditions.

**Lomolo-Mogotio area:** Groundwater elevation in this area is low ranging between 1425-1417metres; this indicates groundwater inflow from other areas. This receives inflow from: Rongai to the southwest, Olobanita to the southeast, Solai to the west and Kiplombe to the east. In the northern part towards Chemogoch area, the flow occurs in a northwest direction. From the groundwater results, it can be postulated that the groundwater of Lomolo-Mogotio area escapes through the fault systems forming a part of the flow towards Lake Baringo. The confining pressures are high indicating confined conditions resulting in high yields for the boreholes in the area.

### **Aquifer Geometry and Aquifer parameters**

The boreholes drilled in the area have revealed that the aquifers within either the volcanic or the sediments are confined. Even though the area has been affected by intense faulting, it supports a regional aquifer system. Three aquifers exist in the area identified on the basis of borehole specific capacities, groundwater flow map and isochure map.

- Lomolo-Mogotio and Olobanita aquifer
- North Solai aquifer
- Rongai aquifer

### **Lomolo-Olobanita Aquifer**

This is where the study area falls; an area which has been developed for groundwater supply to Nakuru town. The regional aquifer system in Lomolo-Olobanita area is composed of weathered volcanic rocks, fractured volcanic rocks, fractured and weathered volcanic rocks, and Lacustrine sediments. The weathered tuffs underlying the Wasagess flows (phonolites and trachytes) of the Rumuruti group and overlying the Samburu basalts form the best aquifers in Lomolo-Olobanita area. This system is recharged locally by rainwater and also by rivers flowing along fault zones; e.g. Molo and Rongai Rivers and other streams to the west of the area and Olobanita River to the east. From the western side, this zone is further recharged by high rainfall occurring in the area of Kiplombe hill and Bahati forest.

### **North Solai aquifer**

The regional aquifer system of this zone is composed of weathered volcanic rocks, fractured volcanic rocks, fractured and weathered volcanic rocks, sediments, and old land surfaces with sediments forming the best aquifers. However, these sediments have mainly been deposited in

grabens, hence the aquifers are localised. This system is recharged locally along the fault and fissure zones by both rainwater and rivers. Several streams flow off the Solai escarpment and disappear underground in the area around Milton's sidings. The zone is further recharged regionally from the south in Bahati forest.

### **Rongai aquifer**

The regional aquifer system is composed of weathered volcanic rocks, fractured volcanic rocks, fractured and weathered volcanic rocks, and old land surfaces. This system is recharged locally and from the south in the areas of Njoro.

## CHAPTER THREE

### 3.0 BASIC THEORY

#### 3.1. Introduction

The field data were collected by use of electrical resistivity methods (VES and Electrical Resistivity Tomography (ERT)) and magnetic method. These geophysical tools are designed to measure specific parameters, and are generally used to measure spatial variation in these specific parameters within a study area of interest (refer to Table 3.1).

Table 3.1. Geophysical tools and the specific parameters they measure

<b>Geophysical Method</b>	<b>Measured Parameter(s)</b>	<b>Physical Property or Properties</b>	<b>Physical Property Model (Geotechnical Application)</b>	<b>Typical Site Model (Geotechnical Applications)</b>
Electrical resistivity	Potential differences in response to induced current	Electrical resistivity	Resistivity–depth model often with interpreted layer boundaries	Geologic–hydrologic profile
Magnetics	Spatial variations in the strength of the geomagnetic field	Magnetic susceptibility and remanent magnetization	spatial variations in magnetic susceptibility of subsurface	Geologic profile or map (location of faults, variable depth to bedrock, etc.)

The specific parameters measured by geophysical tools shown in Table 3.1, are functions of the physical properties of the Earth's subsurface. Properly acquired and processed geophysical survey data can generally be transformed into a physical property model.

## 3.2 Basic Principles

### 3.2.1 Vertical Electrical Sounding

#### THE SCHLUMBERGER ARRAY

The Schlumberger array has been used for VES throughout this study. An outline of its theory is given below.

#### Theory

In the Schlumberger array (see Figure 3.1), A and B are current electrodes, and M and N are potential electrodes. Let the current I enter the ground at A and return at B.

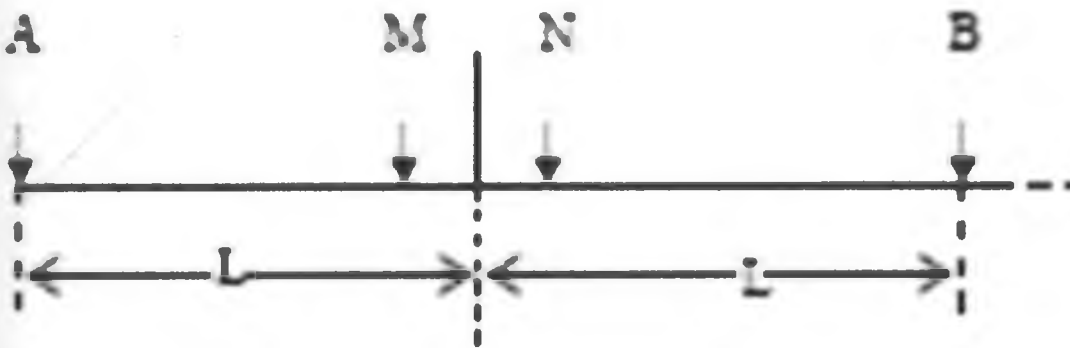


Figure 3.1. Showing the current and potential electrode arrangement in the field.

Assuming the medium below the sub-surface of the earth to be homogeneous and isotropic of resistivity  $\rho$ , the potentials  $V_M$  and  $V_N$  as measured at M and N, respectively, are given by:

$$V_M = \frac{\rho l}{27r} \left[ \frac{1}{(a - b/2)} - \frac{1}{(a + b/2)} \right], \quad (3.1)$$

$$V_N = \frac{\rho l}{27r} \left[ \frac{1}{(a + b/2)} - \frac{1}{(a - b/2)} \right], \quad (3.2)$$

from which  $\rho = 7r(a^2/b - b/4) (V_M - V_N / I)$ . Denoting  $(V_M - V_N)$  by  $\Delta V$ , and acknowledging the fact that, in reality, the medium is anisotropic, the apparent resistivity  $\rho_a$  as measured by the Schlumberger array is given by:



$$\rho_a = \frac{7r(a^2/b - b/4)AV}{I} \quad (3.3)$$

If  $a$  and  $b$  are measured in meters, and  $\rho$  in ohm-meters and  $I$  in milliamperes respectively,  $\rho_a$  would be in ohm-meters.

Equation (3) may be written as:

$$\rho_a = K/I AV, \quad (3.4)$$

where  $K = (a^2/b - b/4)$  is the geometric factor for the Schlumberger array. It can be shown (Keller and Frischknecht, 1966, p. 96) that by keeping the distance  $b$  less than 40% of  $a$ , the electric field  $E$  at the center of the spread is what is being measured by the Schlumberger array with an error of 5%.

The electric field that will be measured by the Schlumberger array (AMNB) over an earth made of  $n$  homogeneous and isotropic layers of resistivities  $[p_1, p_2 \dots p_n]$  and thicknesses  $[h_1, h_2, \dots, h_n]$  can be calculated by the following formula:

$$E = -\frac{p_1 I}{7r} \sum_{m=1}^n F_n(m) J_1(ma) m dm, \quad (3.5)$$

where  $p_1$  = resistivity of uppermost layer,

$I$  = current,

$a$  = distance from center of spread to current electrode

$m$  = dummy variable,

$J_1(ma)$  = first order Bessel function,

$F_n(m)$  = a kernel function of depth to the lower boundary of each layer and the reflection coefficients.

The derivation of the above equation is rather complex. It is given by Keller and Frischknecht (1966, p. 144). Since  $E = -AV/b$ , substitution in equation (5) yields:

$$\rho_a = \frac{p_1 Kb}{7r} \sum_{m=1}^n F_n(m) J_1(ma) m dm \quad (3.6)$$

Several methods of evaluating equation (6), on a computer, have been devised. The computer program used in this work is Advanced Geosciences, Inc.(AGI) EarthImager one-dimension (1D) inversion and modeling software manufactured by AGI. AGI EarthImager 1D is a Windows 32-bit platform based computer program that interprets 1D electrical resistivity sounding data and produces a layered resistivity model that reveals subsurface geology. EarthImager 1D processes VES data collected with Schlumberger, Wenner, dipole-dipole, pole-pole and other arrays. The forward modeling calculation is based on a two dimension (2D) finite element method. Both smooth model inversion and damped least squares inversion methods were implemented in EarthImager 1D.

If external constraints are available, resistivity–depth models can be transformed into geologic models. According to Kuria, (2006), the ability of a rock to conduct electrical current depends primarily on the amount of open spaces between particles (porosity), the degree of interconnection between those open spaces and the volume and conductivity of the water in the pores. The presence of water and its chemical characters are the principal controls on the flow of the electric current because most rock particles offer high resistance to electrical flow. Thus resistivity decreases as porosity, hydraulic conductivity, water content, clay and water salinity increase. Fresh compact rocks have higher resistivities than saturated sand or gravel.

### **Limitations**

The interpretation of resistivity data is ambiguous. It is possible to find different combinations of thicknesses and resistivities which when substituted in equation [6] would yield the same theoretical resistivity sounding curve.

### **3.2.2 Electrical Resistivity Tomography**

This is an increasingly used geophysical survey technique in which vertical electrical resistivity sections are generated tomographically from measurements along a linear array of equally spaced electrodes inserted at the ground surface. ERT surveys map areas with complex subsurface geology where conventional resistivity sounding or profiling surveys are inadequate (Loke and Barker, 1996). Such surveys employ a number of electrodes laid out with consecutive address numbering. The array is multiplexed to a resistivity meter which gathers one set of all possible independent apparent resistivity measurements. A computer-controlled system in the meter

selects automatically the active electrodes used for each measurement. Two different pairs of electrodes are selected for the next measurement and so on until the survey is completed. The software then uses complex processing algorithms to generate a geophysical section or profile (see Figure 3.2). The closer the electrode spacing, the more detailed the image of the subsurface can be generated, but at the expense of a lower penetration depth.

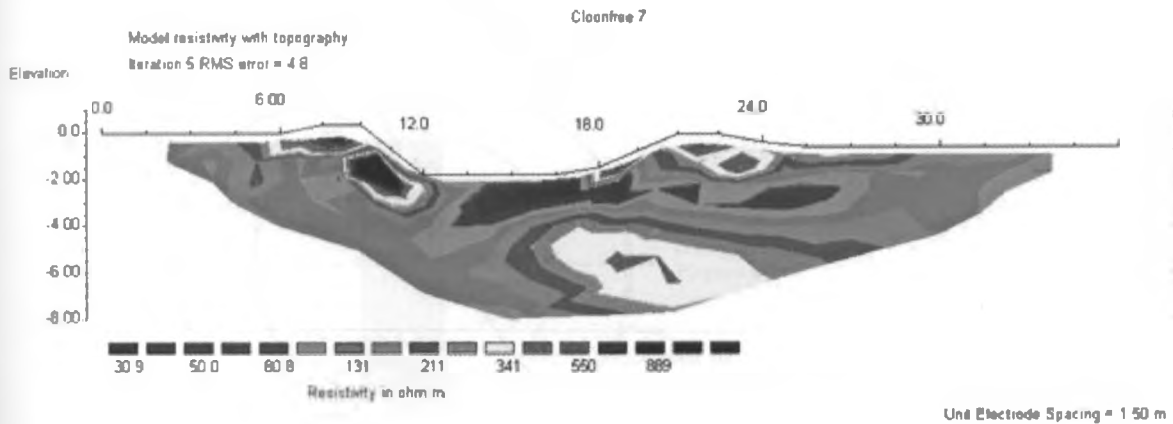


Figure 3.2 ERT geophysical section or profile

### Limitations

Limitations of imaging using ERT arise because of the difficulty of quantifying the reliability of tomographic images. A major source of uncertainty in tomographic inversion is data error. Data error due to electrode mislocations is characterized by the sensitivity of electrical potential to both source and receiver positions. This sensitivity is described by a scattering-type equation and, therefore, depends not only on source–receiver separation, but also on the location and magnitude of contrasts in electrical conductivity. At the overlapping scales of near-surface environmental and engineering geophysical surveys, for which electrodes may be close to the target and experiment dimensions may be on the same order as those of the target, errors associated with electrode mislocations can significantly contaminate the ERT data and the reconstructed electrical conductivity. For synthetic experiments, variations in the data due to electrode mislocation are comparable, in magnitude to typical experimental noise levels and, in some cases, may overwhelm variations in the data due to changes in material properties. Furthermore, the statistical distribution of electrode mislocation errors can be complicated and multimodal such that bias may be introduced into the ERT data. The resulting perturbations of the reconstructed electrical conductivity field due to electrode mislocations can be significant in magnitude with complex spatial distributions that are dependent both on the model and the experiment.

### 3.2.3 Magnetic Method

The theory behind the applied magnetic method can be explained by a magnetic dipole in which the basic elements can be seen in a simple bar magnetic (see Figure 3.3).

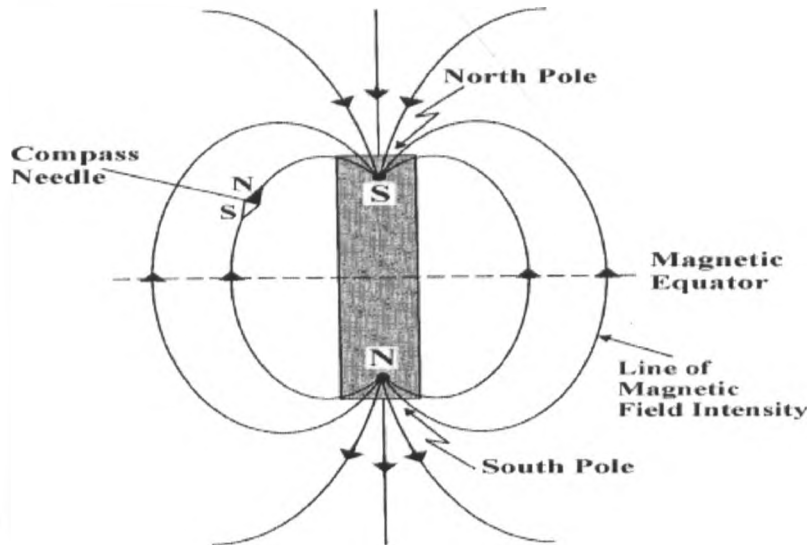


Figure 3.3 Magnetic fields due to a simple bar magnetic (adapted from Reynolds, 1998).

The bar magnetic consists of two poles (dipolar), a positive north-seeking pole and a negative south-seeking pole, and these poles always exist as pairs. These two poles produce a magnetic field called the magnetic field intensity ( $H$ ). If a magnetizable body (e.g., iron or magnetite) is placed in an external magnetic field (e.g., the earth's magnetic field), it will become magnetized and produce a secondary magnetic field, determined by the material's magnetic polarization ( $M$ ). For low external magnetic fields (e.g., the earth's), the degree in which the body is magnetized is determined by its magnetic susceptibility,  $k$ , and is defined as

$$M = kH. \quad (3.7)$$

Magnetic susceptibility is a nondimensional quantity and is the fundamental physical property used in the magnetic method. The measurement of the total magnetic field, (which includes the external magnetic field and the magnetization) is called the magnetic induction ( $B$ ) and is written as

$$B = \mu_0 (1 + k) H \quad (3.8)$$

Where,  $\mu_0$  is the magnetic permeability of free space. The units of  $B$  are teslas, which is generally too large a number for applied magnetic work, so gammas ( $10^{-9}$  teslas) are more commonly used. Also, note that  $B$  is a vector quantity and in most magnetic work today, the amplitude of  $B$  is measured and it is called the total magnetic field.

Magnetometers are designed to measure variations in the magnetic field of the Earth. These are usually caused by the presence of magnetically susceptible material of natural or human origin (typically magnetite or iron, respectively). In certain instances, magnetic data can be interpreted quantitatively, and transformed into constrained geologic models. More typically, however, magnetic data are interpreted qualitatively, and simply used to verify the presence or absence of magnetically susceptible materials (Anderson, 2006).

## CHAPTER FOUR

### 4.0 DATA ACQUISITION

#### 4.1 Introduction

In order to achieve the expected results, necessary data was collected. These data included both primary and secondary data. The secondary data was obtained from archives and primary data collected from the field. The steps used to obtain the relevant data has been subsequently discussed.

#### 4.2 Aquisition of Pleriminary Data

In the view of the aim and the objectives of the study pleriminary data was considered necessary to give the introductory knowledge about the study area and the Lower Baringo sub-basin at large. The following data was considered necessary and thus collected to aid in the study.

- Geological (Drilling operations) data.
- Geologic logging (borehole logging) data.
- Borehole data ( including water rest levels, water stike levels, yield and total depths of the boreholes) in the study area.
- Geological map of Nakuru area which covers the study area.
- Hydrogeological data (groundwater potential map of Kenya).
- Rainfall data.
- Literature on geology and hydrogeology.

The methods that were employed in the collection of the afore mentioned data included reviewing of existing groundwater data from the MOWI and its sub-ordinate institutions, geological maps and reports from the Ministry of Environment and Natural Resources, Mines Department, and topographic maps from the Survey of Kenya. The data was useful in desktop studies that led to further understanding the outlined study problem in Olobanita well field.

#### 4.2.1 Drilling operations data

According to Yujie Shi, 2008, the drilling of borehole 1 encountered geological formations dominated by trachytic tuff rock type, which range in lithology from typical trachytic tuffs, tuff, to phonolitic trachytes and trachytes. Similarly, borehole X (BHX), previously BH2, was to be drilled to the anticipated depth of 300 metres deep. The encountered formations were dominantly trachytic tuff rock types. The stratigraphy largely consists of harmonic alterations of trachytic tuffs and lava flows. The individual thickness of these flows typically ranges from 20 to 50 metres.

The walls of borehole 1 were largely stable. However, in the course of drilling, lithologic material collapsed and dropped into the hole from weakly consolidated layers at 8-22, 110 metres below the ground(see appendix B). The drilling operations of BHX was hampered by collapsing difficulties which culminated in the abandonment of the borehole. Below a depth of 220 metres, air circulation was lost: as a result, it was not possible to obtain reliable yield estimates of individual aquifers.

#### 4.2.2 Geologic Logging Data

Though most of the geological data from existing boreholes were not available, information was obtained from the available lithologic logs; Figure 6.1 from BH2 (previously BH1), Figure 6.3 from abandoned BHX and Figure 6.5 from BH6. The BH2 log shows that the subsurface materials are basically divided into loose volcanic clastic sediments which ranges from zero metres to a depth of 120 metres. These includes; sand silts, gravel sand silts, volcanic sands with few gravels, volcanic ashes with tuff fragments, volcanic ash with welded tuff and trachyte fragments, loose sediments with rounded fragments and tuff fragments(an erosional horizon), mud with imbedded rock fragments(erosional horizon), ash horizon with tuff and trachyte fragments, silt, ash and sand(loose sediment) with pumice fragments, ash/tuff horizon with trachyte fragments. The second division is tough volcanic rocks with few bands of loose sediments and this ranges from 120 metres to 210 metres depth. These includes; tough aphanitic trachyte rock, tough trachyte with some tuff, loose volcanic ash horizon, tough phonolitic trachyte horizon, horizon of alternated weathered gravel and mud(erosional horizon) and weathered trachyte horizon with pumice. The third division penetrated by the borehole is

loose volcanic sand from a depth of 210 metre to 271 metres. These comprises of gravels and sands(loose sediments) some reddish due to weathering, and loose volcanic sands.

The subsurface materials as shows in abandoned BHX are sediments to adepth of 20metres which overlies welded tuff that is underlain by pumice and gravel. A hard rock of welded tuff overlies an erosional surface at a depth of 76 metres which subsequently overlies trachytic rock. Loose sediments of gravels and sands and occassionally silty covers the depth of 98 metres to the total depth of the borehole at 262 metres. In the arguement the subsurface materials as found in BH6 are loose sediments from top to a depth of 16 metres underlain by a hard rock rock to a depth of 72 metres in the order of trachyte, pumice and tuff and trachyte respectively. These overlies an erosional surface of gravels in in turn overlies a hard rock of welded tuff which lies on an erosional surface. From a depth of 104 to 140 metres is a hard welded tuff underlain by loose sediments of sands and gravels. These sediments sits on a hard trachyte rock at a depth of 226 metres. From tghe depth of 226 metres to the total depth of the borehole at 260 metre are sediments silt, fine to coarse sands and gravels.

### **4.3 Aquistion of Field Data**

#### **4.3.1 Instrumentation**

The integrated geophysical surveys involving VES, electrical resistivity imaging (ERI) and ground magnetic measurements were carried out in the study area. The VES was done using the SYSCAL R2 equipment from IRIS instruments of France in the Schlumberger electrode configuration, electrical resistivity imaging involved the SYSCAL R1 switch 72 resistivity equipment from IRIS instruments of France and the magnetic measurements utilized the SINTREX Total Field Proton Precession Magnetometer from SINTREX Ltd of Canada.

#### **SYSCAL R2**

The SYSCAL R2(Fig. 4.1) is a powerful resistivity system for sounding and profiling. This is a fully automated high power resistivity meter designed for direct current electrical resistivity surveys in either horizontal electrical profiling mode or VES mode.





Figure 4.1 SYSCAL R2 electrical resistivity equipment which was employed in data collection.

The instrument is powered by a 12V car battery connected to a direct current(DC) –direct current (DC) converter. It generates a DC current which is delivered into the ground through two current electrodes and measures the voltage drop between two receiving potential electrodes and displays the apparent resistivity value. It carries out fully automated measurements through the control of a microprocessor which performs automatic self potential correction, automatic ranging, and digital stacking for signal enhancement and error display in case of any procedure problems. It computes and displays the apparent resistivity automatically for the most common electrode arrays. This tool has high reliability in a large range of weary field conditions.

#### **SYSCAL R1 Plus switch 72 resistivity meter**

The SYSCAL R1 plus resistivity meter (Fig. 4.2) is the most powerful, internally powered, transmitter/receiver unit available for DC resistivity applications. It features 200W output and may be powered from internal rechargeable battery, or external 12 V. Surveys to depths of 65 meters can be achieved with confidence. The unique two channel design of the Syscal resistivity meters permits measurement of voltage and current simultaneously. This results in an instrument with very high accuracy and freedom from noise. Noise rejection is better than 120 db at power line frequencies. A 20 bit A/D converter provides excellent resolution and data quality. The case

is fully watertight, with the only access through the top keypad, which is protected by O ring seals.



Figure 4.2 Field data collection using SYSCAL R1 switch 72 ERT meter.

### **Proton Precession Magnetometer**

For land-based magnetic surveys, the most commonly used magnetometer is the proton precession magnetometer. The equipment used during the field data acquisition is SINTREX Total Field Proton Precession Magnetometer from SINTREX Ltd of Canada (Fig. 4.3). Unlike the fluxgate magnetometer, the proton precession magnetometer only measures the total amplitude (size) of the Earth's magnetic field. These types of measurements are usually referred to as total field measurements. A schematic of the proton precession magnetometer is shown in Figure 4.4.



Figure 4.3. SINTREX Total Field Proton Precession Magnetometer used in the field.

The sensor component of the proton precession magnetometer is a cylindrical container filled with a liquid rich in hydrogen atoms surrounded by a coil. Commonly used liquids include water, kerosene, and alcohol. The sensor is connected by a cable to a small unit in which is housed a power supply, an electronic switch, an amplifier, and a frequency counter as shown in Figure 4.3.

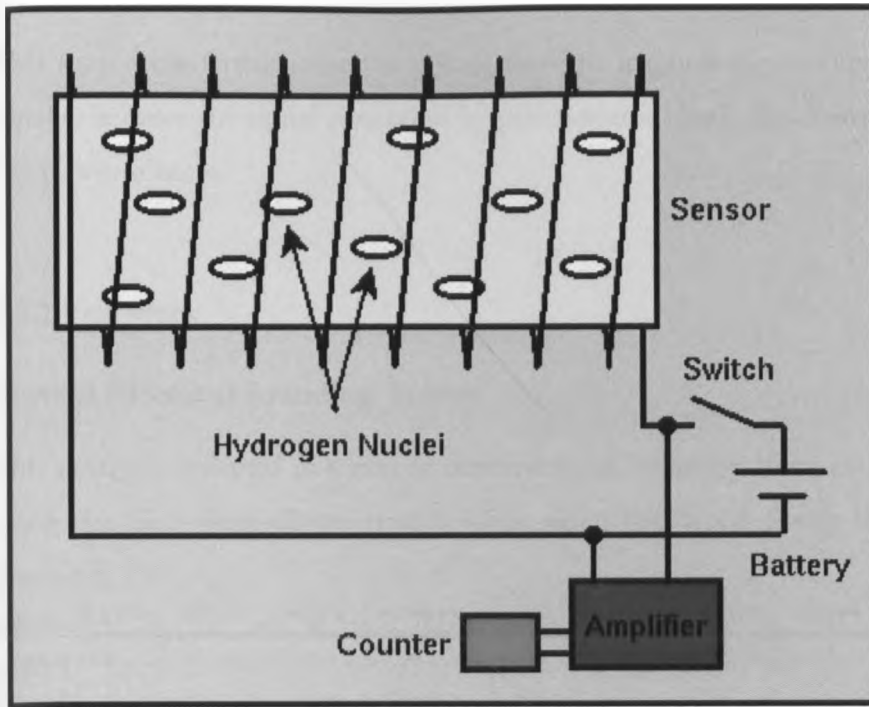


Figure 4.4 A schematic of the proton precession magnetometer. (After Serson, 1962).

When the switch is closed, a DC current delivered by a battery is directed through the coil, producing a relatively strong magnetic field in the fluid-filled cylinder. The hydrogen nuclei (protons), which behave like minute spinning dipole magnets, become aligned along the direction of the applied field (i.e., along the axis of the cylinder). Power is then cut to the coil by opening the switch. Because the Earth's magnetic field generates a torque on the aligned, spinning hydrogen nuclei, they begin to precess around the direction of the Earth's total field. This precession produces a time-varying magnetic field which induces a small alternating current in the coil. The frequency of the alternating current (AC) current is equal to the frequency of precession of the nuclei. Because the frequency of precession is proportional to the strength of the total field and because the constant of proportionality is well known, the total field strength can be determined quite accurately.

One of the important advantages of the proton precession magnetometer is its ease of use and reliability. Sensor orientation need only be set to a high angle with respect to the Earth's magnetic field. No precise leveling or orientation is needed. If, however, the magnetic field changes rapidly from place to place (larger than about 600 NT/m), different portions of the cylindrical sensor will be influenced by magnetic fields of various magnitudes, and readings will be seriously degraded.

This may occur if the sensor is placed close to magnetically-susceptible material, for instance. Finally, because the signal generated by precession is small, this instrument cannot be used near AC power sources.

### 4.3.2 Fieldwork

#### Vertical Electrical Sounding Survey

This data was collected in a grid of dimensions of 100m by 100m and covering an area of 600m along the East-West direction and 300m along the North-South directions as shown in the figure.4.5.

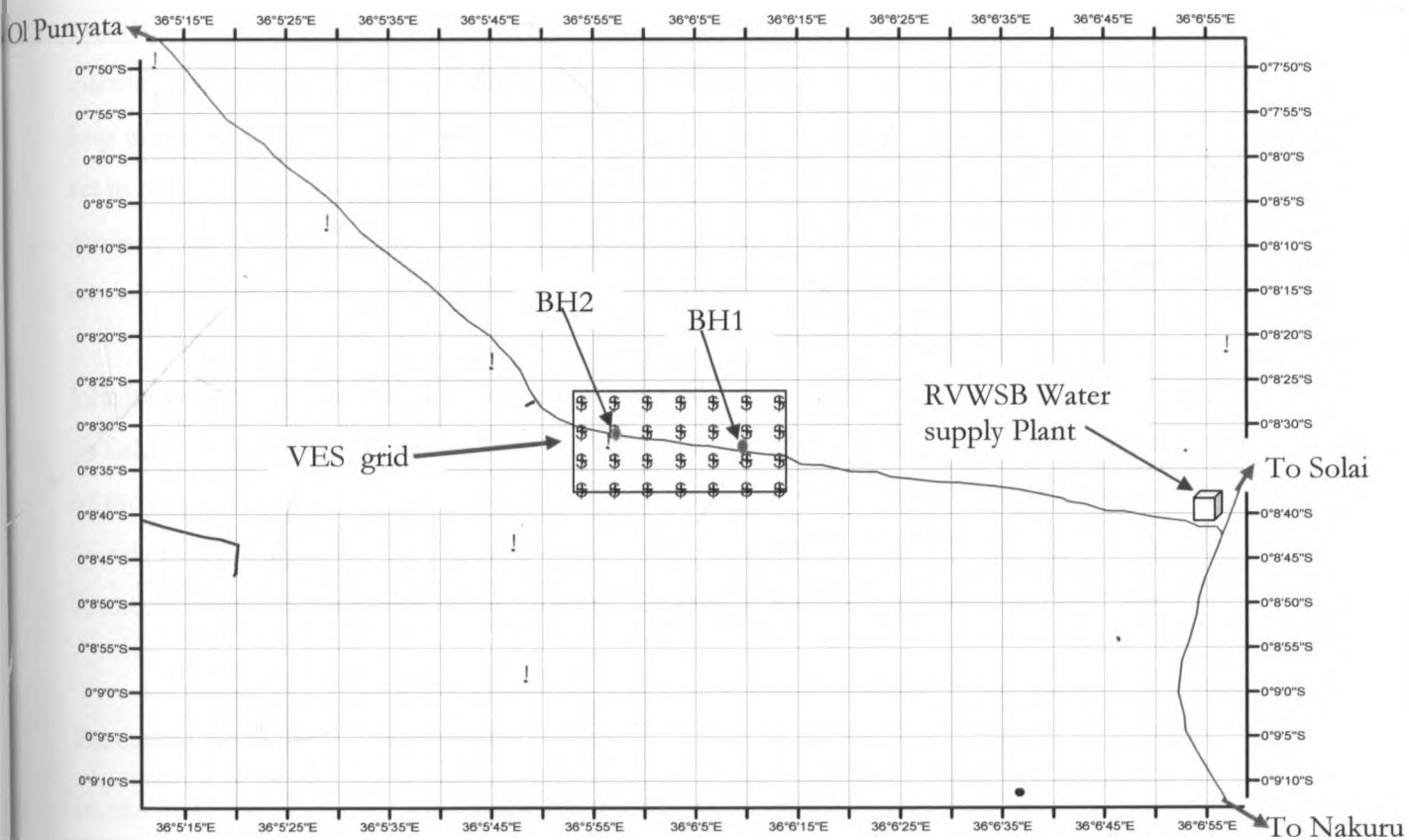


Figure 4.5. The grid within the study area where the VES data was collected.

The VES is a four electrode system. Thus it offers a meter that performs surveys in the traditional manner of placing four electrodes, taking a reading, and then moving the electrodes for the next reading. Various configurations are available: Schlumberger, Wenner, gradient, pole-dipole, dipole-dipole, etc. In this study, the VES method using the SYSCAL R2 electrical

resistivity equipment based on the Schlumberger configuration was used to probe the subsurface geological conditions of the study area. The VES were conducted on sounding points located 100 metres apart with a linear AB/2 spread of up to a maximum of 350 m.

Schlumberger configuration provides both VES and profiling, which is most successful in the exploration of ground water. Thus from this method, the thickness and depth of the various geoelectrical layers were obtained by interpreting the field resistivity data using EarthImager 1D V. 2.0.0 (AGI, 2008).

#### **Precautions taken to realize quality data**

The data collected using SYSCAL R2 is in form of apparent resistivity. The field equipment uses internal dry cells which are put when working and removed immediately after work. These cells help in the running of the machine. The right settings on spacing were adopted in the machine as set in the field. On the ground always in every reading AB/2 was the same in both directions and similarly this was applied to MN/2. Good contacts are also a recipe that was ensured to get correct readings.

#### **Limitations encountered when using the method**

In field surveys the line of survey where AB/2 runs ought to be straight. In some areas, because of the existence of a busy road the straight line could not be achieved. At times more time could be taken in checking on the contacts and even the equipment could not transmit current thus forced to check on the source of the problem. Despite all these the fieldwork was a success.

#### **Electrical Resistivity Tomography Survey**

In the field, SYSCAL R1 Plus resistivity meter, was used to collect field data for resistivity imaging. Two command files were created to record "Wenner-Schlumberger" data at a 5m electrode separation within the user mode option of the equipment. The two command files were designed to measure different parts of the profile line. The first spread begins with cable1 followed by cable2 with electrodes 1-36 and 37-72 respectively. This survey employs a number of electrodes laid out with consecutive address numbering. In the field, the data collection always started with placing the stainless steel electrode stakes into the ground at intervals of 5m along selected lines. The swift cables were then laid out on the ground and a connection clipped wires were used to connect the electrode to its electrode stake, making sure that there was an electrical

contact between them. The switching on and off of the electrodes are controlled automatically by the electronics in the swift box. The cables of electrodes 36 and 37 were then connected to the equipment and the details of the traverse from which data is to be collected were entered into the equipment and made ready for data collection.

A contact resistance test was run to check for poorly connected electrodes or abnormally high contact resistance reading. The total length of electrical tomography profiles in 2D was 360 meters. A computer-controlled system selects automatically the active electrodes used for each measurement. Two different pairs of electrodes are selected for the next measurement and so on until the survey is completed. The actual measurement was carried out after the contact resistance test output gave good results, otherwise, the causative electrode(s) were checked and properly connected or watered. It took between 30 to 45 minutes to complete one spread, so during the data collection period a new survey section was prepared for the next spread. The start and end locations of survey lines were mapped with a Global Positioning System (GPS). After a successful collection of data from a particular spread, the measured apparent resistivity data was downloaded to a Laptop. Negative data are automatically removed during this process.

According to Pipan et al., 1996, electrical tomography is a high-resolution technique as opposed to conventional geophysical methods like resistivity sounding. Thus, electrical tomography surveys map areas with complex subsurface geology where conventional resistivity sounding or profiling surveys are inadequate (Loke and Barker, 1996). Consequently, this helped in achieving the determination, with high resolution the various lithology and structures and hence their implications on groundwater drilling operations in the Olobanita well field. A 2D model for the subsurface gave reasonably accurate results in areas with elongated geological structures.

#### **Precautions taken to realize quality data**

In the field before the measurements commenced the field team ensured that all the electrodes were at equal distances of 5m. Equally it was ascertained that the electrodes and the cables were all in a straight line. To form a more unique image of the subsurface electrical conductivity distribution, the apparent resistivity was measured through many electrode combinations and interpreted simultaneously. Thus to ensure that the measurement was achieved using this method the the contacts at the electrodes were okey. The settings were procedurally done as per the array employed in the data collection.

## Magnetic Survey

The magnetic data was collected in a grid of of dimensions of 20m along the East-West profile by 100m along the North-South profile and covering an area of 300m along the East-West direction and 600m along the North-South directions as shown in the figure.4.6.

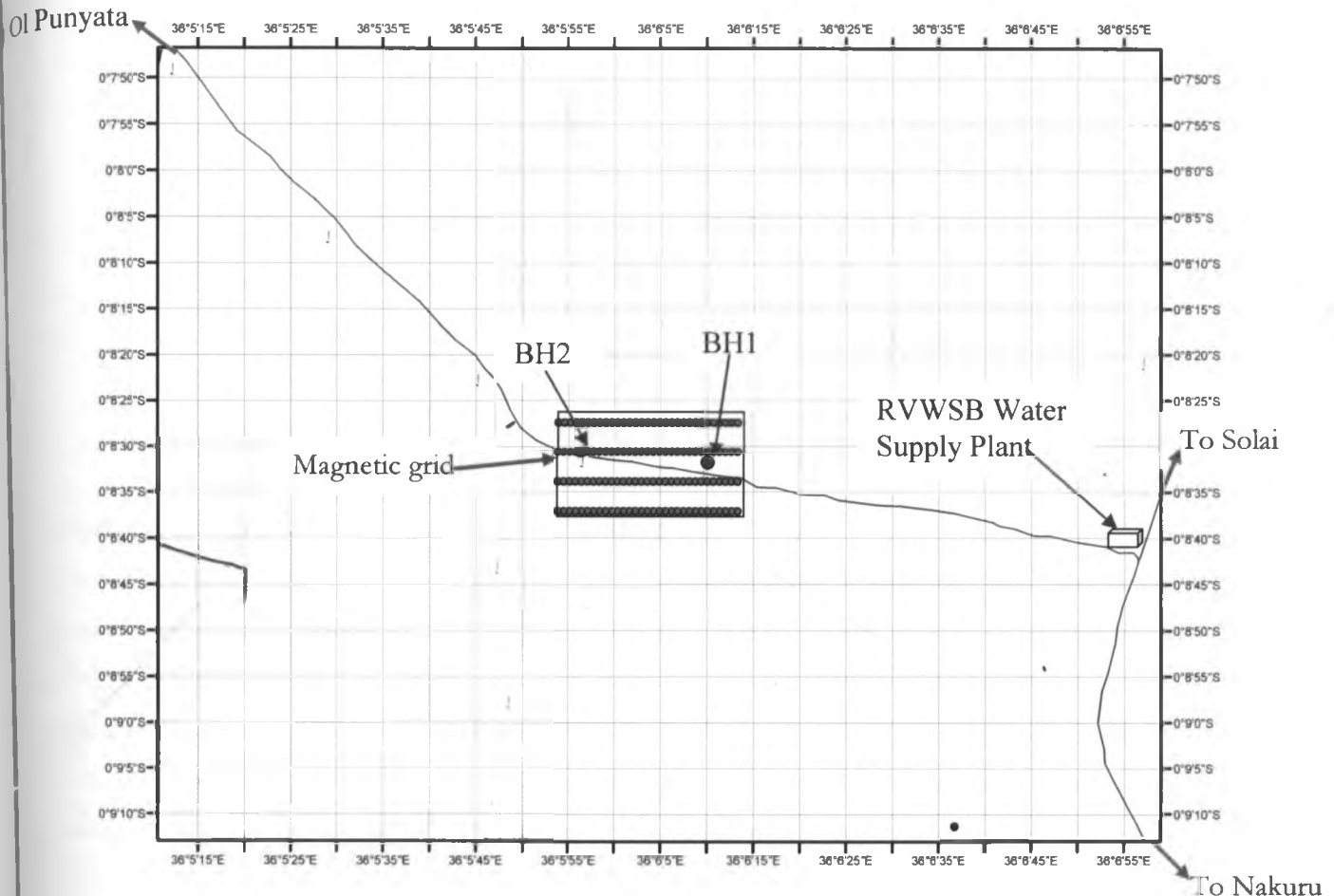


Figure 4.6. The grid within the study area where the magnetic data was collected.

In the field the same area where VES survey was done, a grid was designed of profiles done at a spacing of 100 metres and 20 metres from one measuring point to another. Consequently, a base station was decided on where the least noise was expected in the field area. The other data that used was collected in a greater grid of 100 metres by 100 metres with profiles running East to West within which most of the boreholes serving Nakuru town from the well field lies. When using the equipment, the North-South orientation was used for effective and correct measurements. Concurrently, the time of data recording, the coordinates including the altitudes was taken. At an interval of between 30 minutes to one hour base station reading was taken and then back to taking data in the field.



### **Precautions taken to realize quality data**

The following steps were taken to ensure correct data was obtained from the field.

1. As a general operation all metallic objects were removed from near the sensor.
2. The orientation effect was always checked and having the sensor in the same the same direction (N-S) in all stations.
3. Measurements were taken consistently.
4. Magnetic storms were always monitored by checking on the readings. These storms are as a result of large amount of electrons emitted by the sun and taking measurements should be avoided in the event of their happening.
5. The base station readings were recorded at intervals to monitor diurnal activity or perform drift corrections.
6. Measurements were done during the day.

### **Limitations encountered when using the method**

During the field work it was hard to avoid working near metallic installations and even below power lines. Thus the Magnetic data acquired is having a corresponding subsurface interpretation that is theoretically accurate (consistent with field data), but not likely geologically consistent. Therefore, necessary data corrections were done before using the data for interpretation. Of the numerous theoretical interpretations that was generated for the collected magnetic data set, the most reasonable model was the one most consistent with all other geophysical data sets (VES and ERT data) and available ground truth.

# CHAPTER FIVE

## 5.0 DATA PROCESSING AND INTERPRETATION

### 5.1 Introduction

The raw data collected from the field was processed in order to be utilised in interpretation. The processing considered; the kind of data, the software to be used in the interpretation and the conditions surrounding the collection of data in the field, among other factors. The subsequent discussions have given details on the processing and interpretation of different kinds of data that was obtained from the field.

### 5.2 Vertical Electrical Sounding

#### 5.2.1 Data Processing

The data collected from the field was not in the format that is readily used by the software utilised in the interpretation. Thus raw VES data was processed in consideration of the software that was to be used for interpretation. Among the many available softwares for interpretation of VES data, the AGI EarthImager 1D inversion and modeling software was used. Thus the software required that data be processed in the order shown in the figure 5.1.

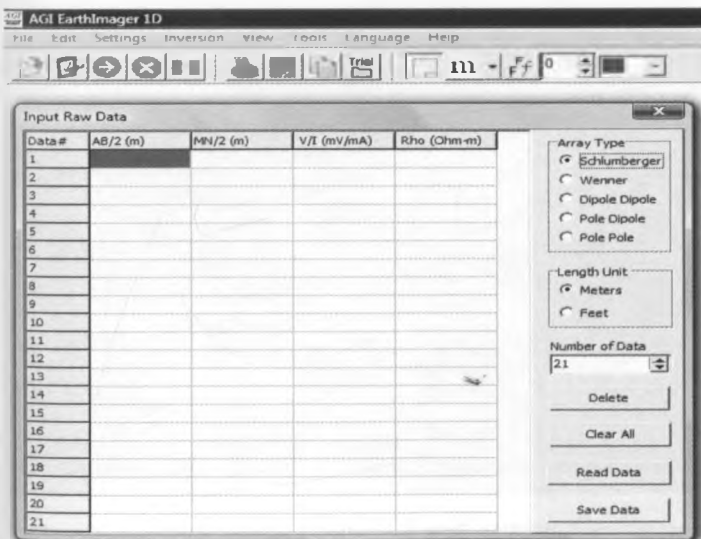


Figure 5.1. Format of inputting raw Ves data to be interpreted by use of the AGI EarthImager 1D inversion and modeling software.

The raw data from the field is entered into the notepad in order AB/2, MN/2 and resistivity as collected from the field, see figure 5.2. Using a program resist. For (figure 5.3) installed in the data working folder, the data is processed to give ab2, xmn2, xk, rho and ohms as shown in figure 5.4.

File	Edit	Format	View	Help
22				
1	0.5	250		
2	0.5	232.3		
3	0.5	171		
3	1	156.3		
5	1	65.1		
7	1	55.4		
10	1	61.5		
10	3	61.1		
15	1	68.6		
15	3	66.4		
20	3	76.5		
30	3	95.7		
50	3	128.6		
50	10	123		
70	3	142.8		
70	10	137.6		
100	10	143.4		
150	10	131.7		
200	10	127.9		
250	10	98.3		
300	10	76.1		
350	10	58.6		

Figure 5.2. Raw data from the field in an input American Standard Code for Information Interchange(ASCII).

```

Microsoft Windows [Version 6.0.6002]
Copyright (c) 2006 Microsoft Corporation. All rights reserved.

C:\Users\Mogaka>cd c:/
c:\>cd olobanitaves
c:\Olobanitaves>resist

+-----+
| 32-bit Power for Lahey Computer Systems |
| Phar Lap's 386;DOS-Extender(tm) Version 8.02 |
| Copyright (C) 1986-96 Phar Lap Software, Inc. |
| Available Memory = 32684 Kb |
+-----+

Enter filename for input > stn17.dat
Enter filename for output > stn17out.dat_
  
```

Figure 5.3. Input file in figure 5.2 and output file for processed results entered in the Resist.for.

```

c:\ Command Prompt
Enter filename for output > stn17out.dat
3.14159      79.5775      250.000      250.000
12.5664      18.4858      232.300      232.300
28.2743      6.04789      171.000      171.000
14.1372      11.0560      156.300      156.300
39.2699      1.65776      65.1000      65.1000
76.9690      0.719770     55.4000      55.4000
157.080      0.391521     61.5000      61.5000
52.3599      1.16692      61.1000      61.1000
353.429      0.194098     68.6000      68.6000
117.810      0.563621     66.4000      66.4000
209.440      0.365261     76.5000      76.5000
471.239      0.203082     95.7000      95.7000
1309.00      0.982432E-01 128.600      128.600
392.699      0.313217     123.000      123.000
2565.63      0.556588E-01 142.800      142.800
769.690      0.178773     137.600      137.600
1570.80      0.912913E-01 143.400      143.400
3534.29      0.372635E-01 131.700      131.700
6283.19      0.203559E-01 127.900      127.900
9817.48      0.100128E-01 98.3000      98.3000
14137.2      0.538297E-02 76.1000      76.1000
19242.3      0.304538E-02 58.6000      58.6000

c:\>

```

Figure 5.4. Shows next stage of processed VES data.

```

c:\ Command Prompt - edit stn17out.dat
File Edit Search View Options Help
C:\Olobanitaves\STN17OUT.DAT
1      1.00      0.50      79.577468900
2      2.00      0.50      18.485845600
3      3.00      0.50      6.047887800
4      3.00      1.00      11.055963500
5      5.00      1.00      1.657757760
6      7.00      1.00      0.719770133
7      10.00     1.00      0.391521156
8      10.00     3.00      1.166924000
9      15.00     1.00      0.194098279
10     15.00     3.00      0.563620687
11     20.00     3.00      0.365260571
12     30.00     3.00      0.203081697
13     50.00     3.00      0.098243162
14     50.00     10.00     0.313216925
15     70.00     3.00      0.055658758
16     70.00     10.00     0.178773224
17     100.00    10.00     0.091291271
18     150.00    10.00     0.037263475
19     200.00    10.00     0.020355918
20     250.00    10.00     0.010012756
21     300.00    10.00     0.005382974
22     350.00    10.00     0.003045381

F1=Help | Line:1 Col:1

```

Figure 5.5. Shows final stage of processed VES data ready for entry to AGI Earthimager software(Fig. 5.1).

The data in the above format was read by the program which in turn gave the log-log plot of the data and the initial model as shown in figure 5.6.

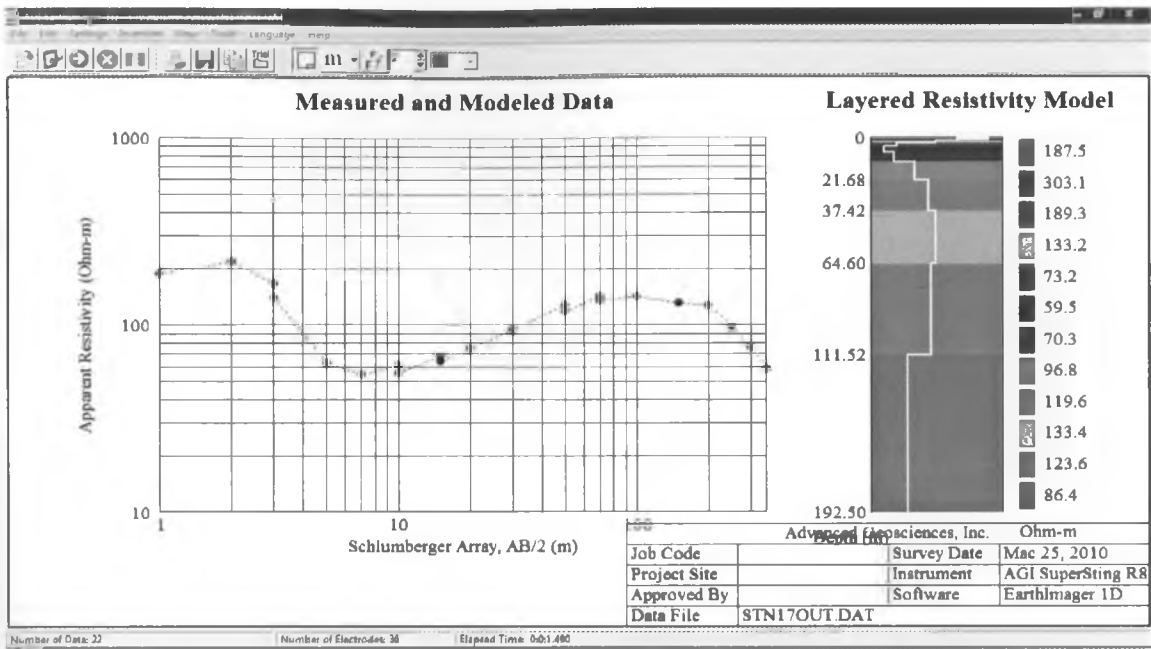


Figure 5.6. Measured and modeled data as read by AGI EarthImager 1D software.

## 5.2.2 Interpretation of the data

### Inversion of VES data

The interpretation of each VES curve was obtained through the use of an automatic interpretation computer program AGI EarthImager 1D inversion and modeling software by AGI of the United States of America. The steps used in interpretation are as follows.

- The processed data (Fig. 5.5) were entered into the AGI EarthImager 1D software which fits an initial model and automatically presents the results (Fig. 5.6).
- Inversion of the measured and modeled data was automatically carried out by opening the drop down menu labelled inversion and clicking the mouse on the start inversion. This gave the results as shown in Figure 5.7, where the red line with red dots show the calculated data, the black dots show the observed data with the blue line shows the geo-electric layer resistivity with depth.
- The initial model was modified until a very close match between the calculated and the measured resistivity curves was obtained. This takes into consideration the root mean square (RMS) which should be not more than 5%.
- This in turn gave the best interpreted model shown in Figure 5.8. and others, later used in the discussion.

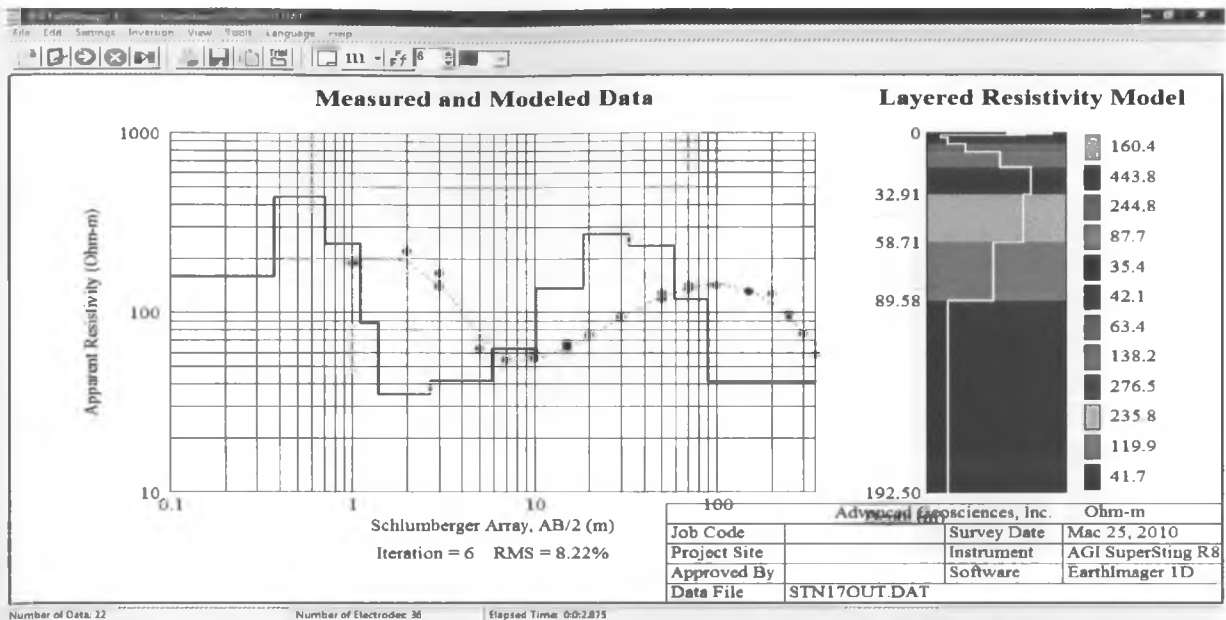


Figure 5.7. Inverted measured data of station 17.

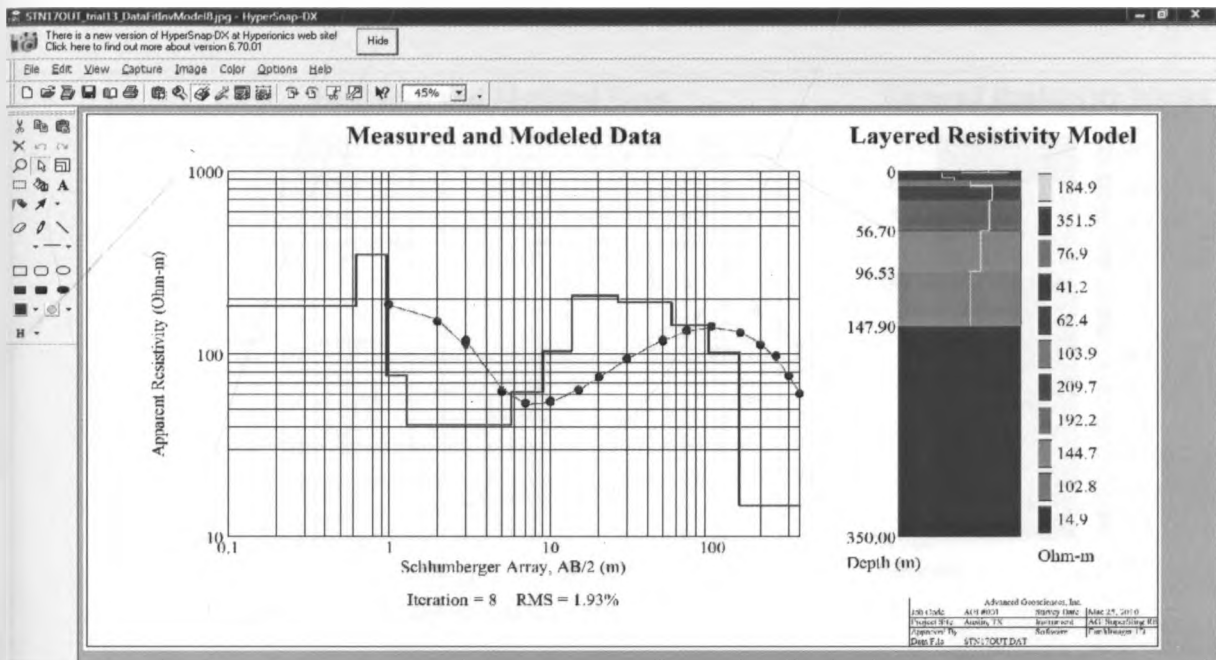


Figure 5.8. An interpreted model showing the subsurface of the station 17 in the study area.

Based on these interpretations, apparent resistivities and thicknesses of a geoelectric models, thought to be closer to reality, were estimated, and modified by trial and error until a very close match was attained between the calculated and observed resistivity curves. The best models for stations 13 (at BH2) and 16 (at BH1) are shown in Figures 5.9 and 5.10 respectively. Consequently, all the models in the study area are given in the Figures 6.8i-xxviii, together with the measured VES curve and layered resistivity model at each site.

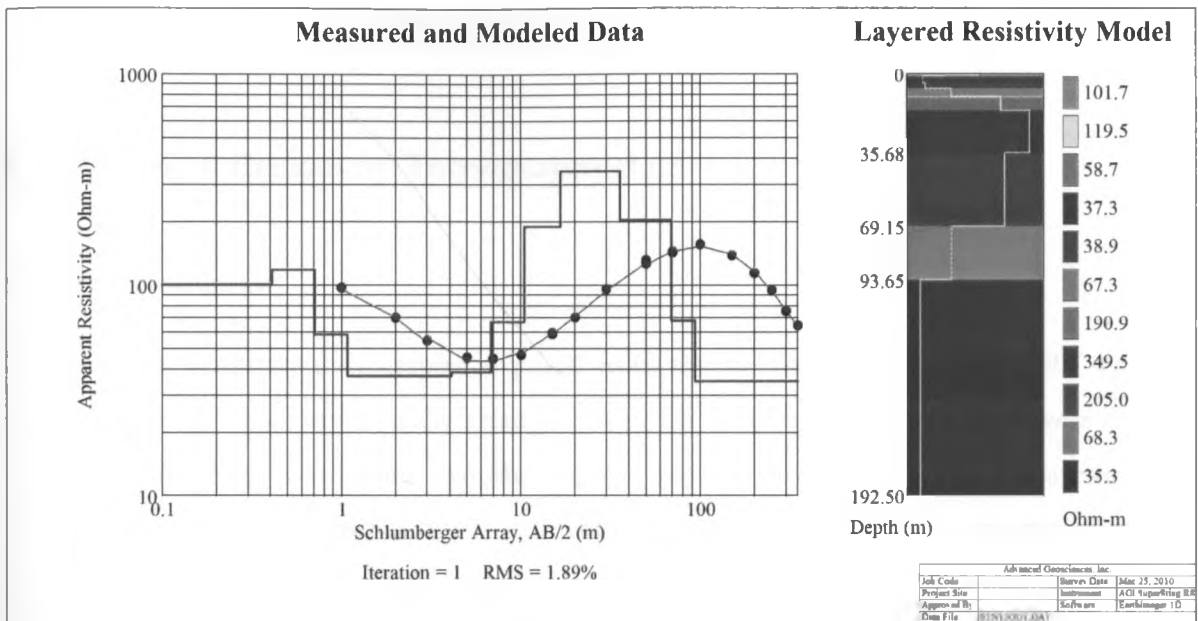


Figure 5.9. Interpreted model (station 13 at BH2) showing curve and layered resistivity model.

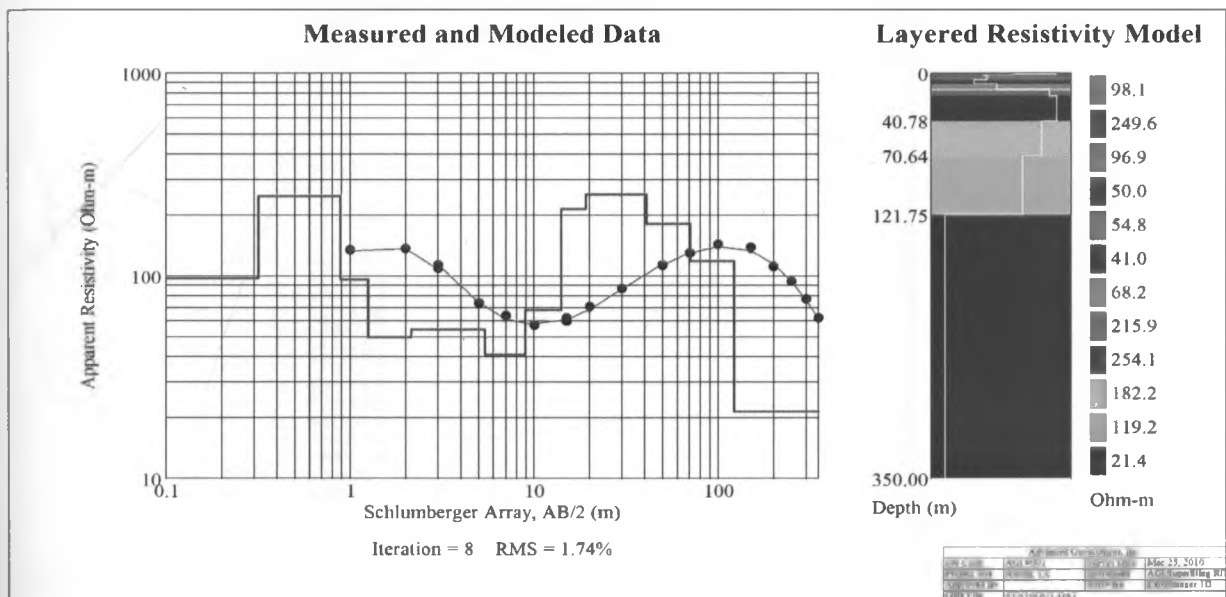


Figure 5.10. Interpreted model (station 16 at BH1) showing curve and layered resistivity model.

The automatic curve-matching computer program results in a geoelectric model the calculated apparent resistivity of which matches the given field curve almost exactly. Thus, the interpretation as determined by the program is mathematically correct but may not necessarily correspond to reality. The number of layers as determined by the program is twelve for station 16. The resistivities of some of these layers are sometimes unrealistically small or large, while their

thicknesses are too small to be detected by the VES method. In other words, the results may, on some occasions, tend to exceed the limitations of the VES method.

### 5.3. Electrical Resistivity Tomography data

#### 5.3.1 Processing raw

The electrical resistivity tomography acquired from the field are stored in the ERT system in internal memory which automatically arranges them. To be able to use them, they were imported to the laptop. They were then exported to the format acceptable by the Resistivity Two-Dimensional Inversion (RES2DINV) software which was used in the interpretation. The RES2DINV software by Geotomo software of Singapore and Figure 5.11 shows the acceptable format for Wenner-Schlumberger configuration.

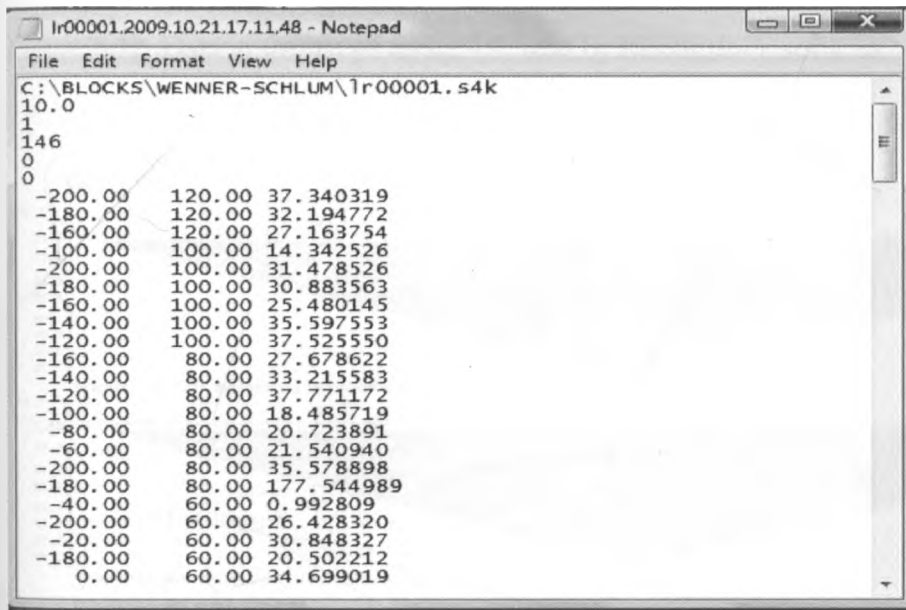


Figure 5.11. Data in a format as imported from the field machine for interpretation by RES2DINV software.

#### 5.3.2 Interpretation

The ERT data was interpreted using RES2DINV software. The data was read by the software as shown in Figure 5.12. After reading the data least squares inversion was used in interpretation which resulted in the images shown in figures 5.13 and 5.14. These images reveals variation in lithologies and faultzones as exhibited by the resistivity values.



C:\SAS4000\Projects\lr00012.s4k  
 Electrode spacing is 10.000.  
 Wenner array  
 Measurements are in apparent resistivity.  
 Total number of datum points is 104.  
 Position of first electrode in array is given.  
 104 150.000 10.000 11.5  
 Minimum electrode location is -200.0.  
 Minimum electrode spacing is 10.0.  
 Total number of data levels is 0.  
 Total number of electrodes is 41.  
 First electrode is located at -200.00.  
 Last electrode is located at 200.00.

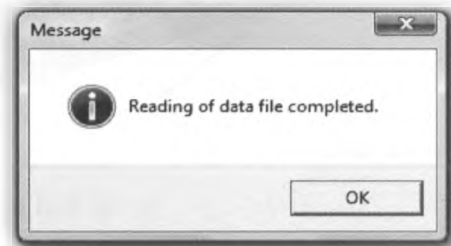


Figure 5.12. Data in format of figure 4.8. read by RES2DINV software.

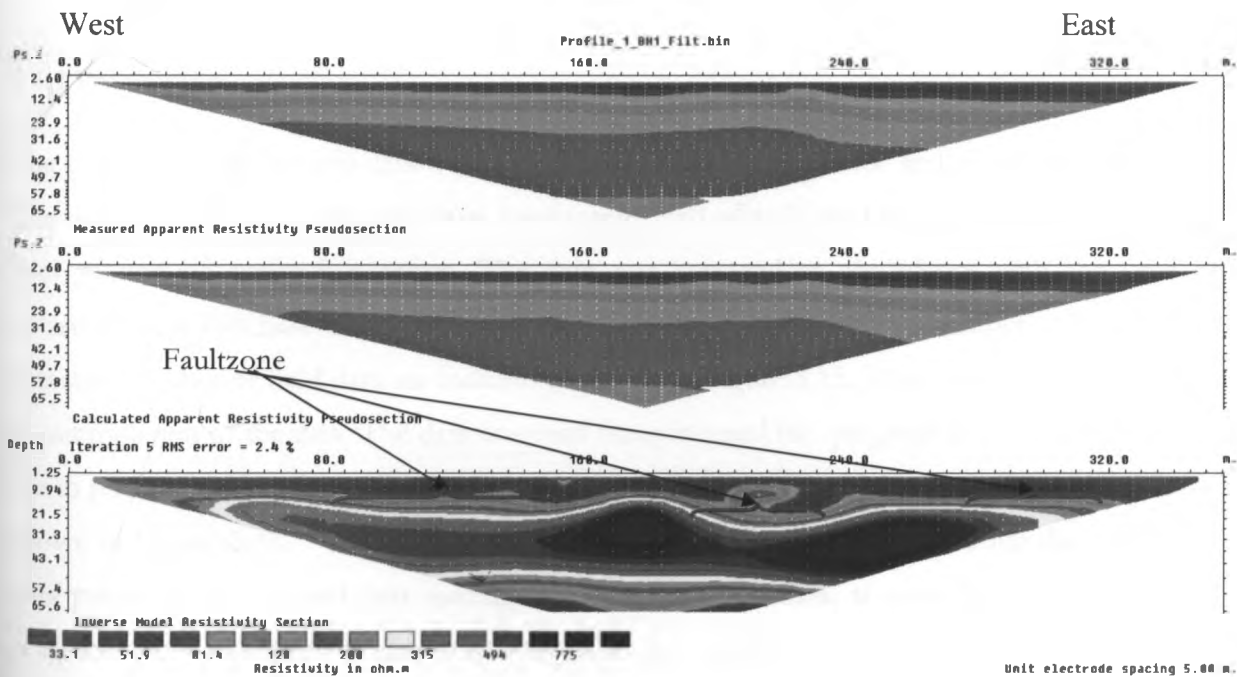


Figure 5.13. Profile 1 showing the vertical slice obtained from borehole 2.

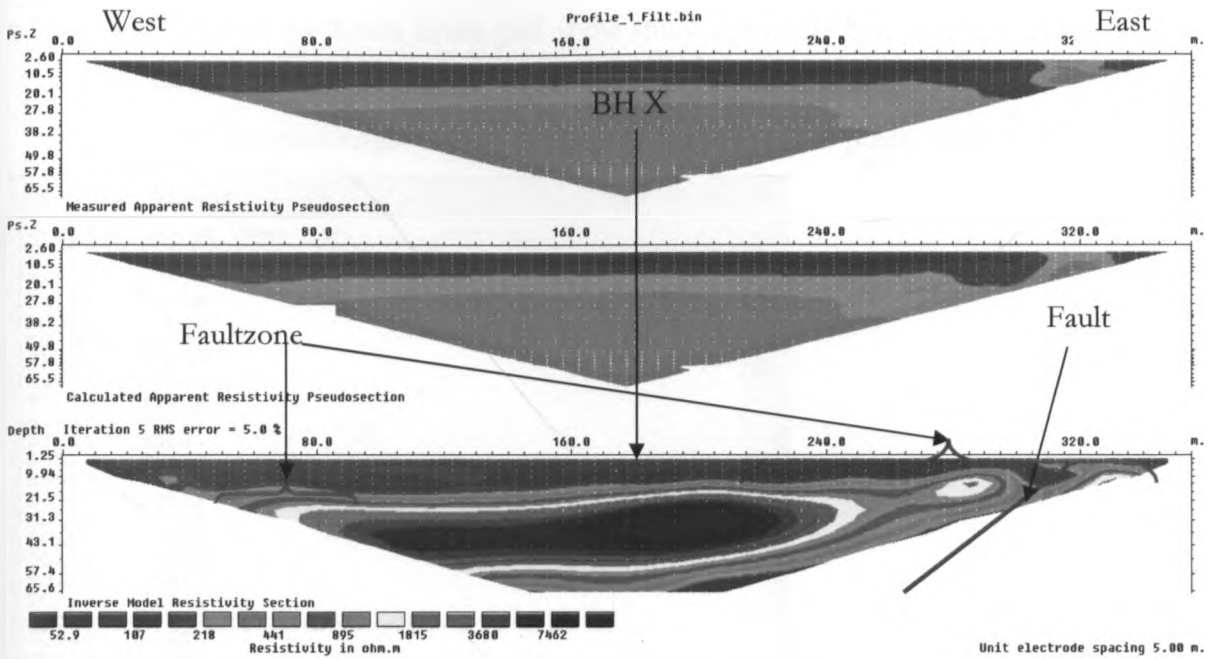


Figure 5.14. Profile 1 showing the vertical slice acquired from BH X.

## 5.4 Magnetic data

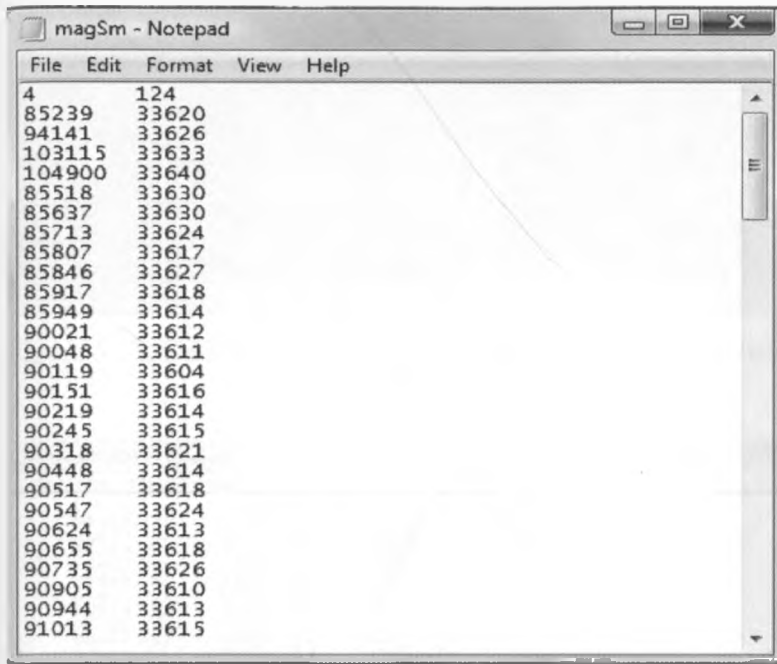
### 5.4.1 Processing

The processing of magnetic data was done by use of both `interpol.for` and `correct.for` softwares. The processed magnetic data was then been interpreted using Euler Deconvolution Program and later plotted by `surfer 8` program. The data was arranged in accordance with the time of measurements with base station data first then field data, on the top the number of base station data and number of field data are indicate as shown in Figure 5.15. This is format that was used in interpolation of the data. The data was read using `interpol.for` program (Fig. 5.16) by entering the in put and output files. Clicking on enter key and then editing the output file gave results as shown in Figure. 5.17. The interpolated data shown in Figure 5.18, by entering the number of data points at the top and first reading of the base station data, is corrected using `correct.for` software. The correction of data is done by use of `correct.for` program( Fig. 5.19). By entering the input file and output file and clicking enter key, then editing output file the following results were obtained as shown in Figure 5.20, in columns; time and corrected data. The correction is done with the aim of removing diurnal variations. Consequently, the data is arranged ready for interpretation by Euler Deconvolution software and plotting using `surfer` in X, Y, Z format as shown in figures 5.21 and 5.22, respectively;

where: X-distance in the X-axis in the grid of the study area in the field

Y- distance in the Y-axis in the grid of the study area in the field

Z-is the corrected magnetic data corresponding to the X-Y points in the field



```
magSm - Notepad
File Edit Format View Help
4      124
85239  33620
94141  33626
103115 33633
104900 33640
85518  33630
85637  33630
85713  33624
85807  33617
85846  33627
85917  33618
85949  33614
90021  33612
90048  33611
90119  33604
90151  33616
90219  33614
90245  33615
90318  33621
90448  33614
90517  33618
90547  33624
90624  33613
90655  33618
90735  33626
90905  33610
90944  33613
91013  33615
```

Figure 5.15. Format of magnetic field data to be interpolated.



```
Command Prompt - interpol
c:\PROFILES>cd c:\
c:\>cd olobanitaves
c:\0lobanitaves>interpol

-----
| 32-bit Power for Lahey Computer Systems |
| Phar Lap's 386 iDOS-Extender(tm) Version 8.02 |
| Copyright (C) 1986-96 Phar Lap Software, Inc. |
| Available Memory = 32684 Kb |
-----

ENTER FILENAME FOR INPUT:mag.dat
ENTER FILENAME FOR OUTPUT:magout.dat_
```

Figure 5.16. Reading data using interpol.for program.

```

Command Prompt - edit magout.dat
File Edit Search View Options Help
C:\Olobanitaves\MAGOUT.DAT
85518.00 33620.28 33630.00
85637.00 33620.40 33630.00
85713.00 33620.48 33624.00
85807.00 33620.57 33617.00
85846.00 33620.61 33627.00
85917.00 33620.68 33618.00
85949.00 33620.71 33614.00
90021.00 33624.36 33612.00
90048.00 33624.38 33611.00
90119.00 33624.43 33604.00
90151.00 33624.45 33616.00
90219.00 33624.50 33614.00
90245.00 33624.52 33615.00
90318.00 33624.57 33621.00
90448.00 33624.66 33614.00
90517.00 33624.70 33618.00
90547.00 33624.72 33624.00
90624.00 33624.77 33613.00
90655.00 33624.79 33618.00
90735.00 33624.84 33626.00
90905.00 33624.95 33610.00
90944.00 33624.97 33613.00
F1=Help Line:1 Col:1

```

Figure 5.17. Data resulting from interpolation of magnetic field data.

```

MAGSMOT - Notepad
File Edit Format View Help
124 33620
85518.00 33620.28 33630.00
85637.00 33620.40 33630.00
85713.00 33620.48 33624.00
85807.00 33620.57 33617.00
85846.00 33620.61 33627.00
85917.00 33620.68 33618.00
85949.00 33620.71 33614.00
90021.00 33624.36 33612.00
90048.00 33624.38 33611.00
90119.00 33624.43 33604.00
90151.00 33624.45 33616.00
90219.00 33624.50 33614.00
90245.00 33624.52 33615.00
90318.00 33624.57 33621.00
90448.00 33624.66 33614.00
90517.00 33624.70 33618.00
90547.00 33624.72 33624.00
90624.00 33624.77 33613.00
90655.00 33624.79 33618.00
90735.00 33624.84 33626.00
90905.00 33624.95 33610.00
90944.00 33624.97 33613.00
91013.00 33625.01 33615.00
91108.00 33625.07 33608.00
91224.00 33625.13 33618.00
91310.00 33625.18 33669.00
91423.00 33625.24 33617.00

```

Figure 5.18. Format of interpolated data used in correct.for program.

```

Command Prompt - correct
Microsoft Windows [Version 6.0.6002]
Copyright (c) 2006 Microsoft Corporation. All rights reserved.
C:\Users\Mogaka>cd c:/
c:\>cd olobanitaves
c:\Olobanitaves>correct

-----
32-bit Power for Lahey Computer Systems
Phar Lap's 386 iDOS-Extender(tm) Version 8.02
Copyright (C) 1986-96 Phar Lap Software, Inc.
Available Memory = 32684 Kb
-----

ENTER FILENAME FOR INPUT:MAGSMOT.DAT
ENTER FILENAME FOR OUTPUT:MAGCORR.DAT_

```

Figure 5.19. Reading data using correct.for program.

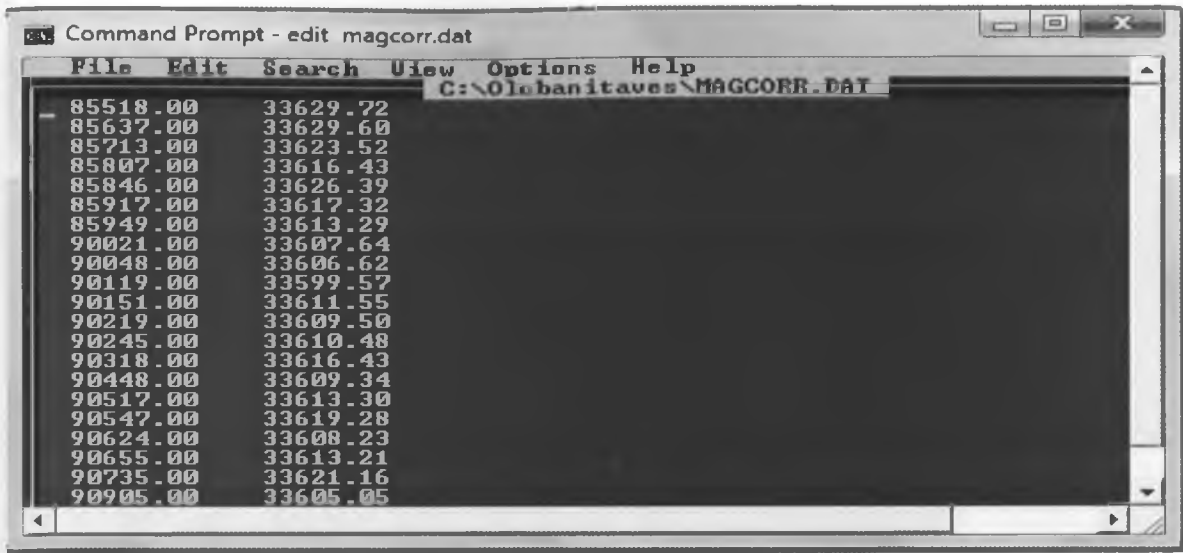


Figure 5.20. Corrected magnetic data.

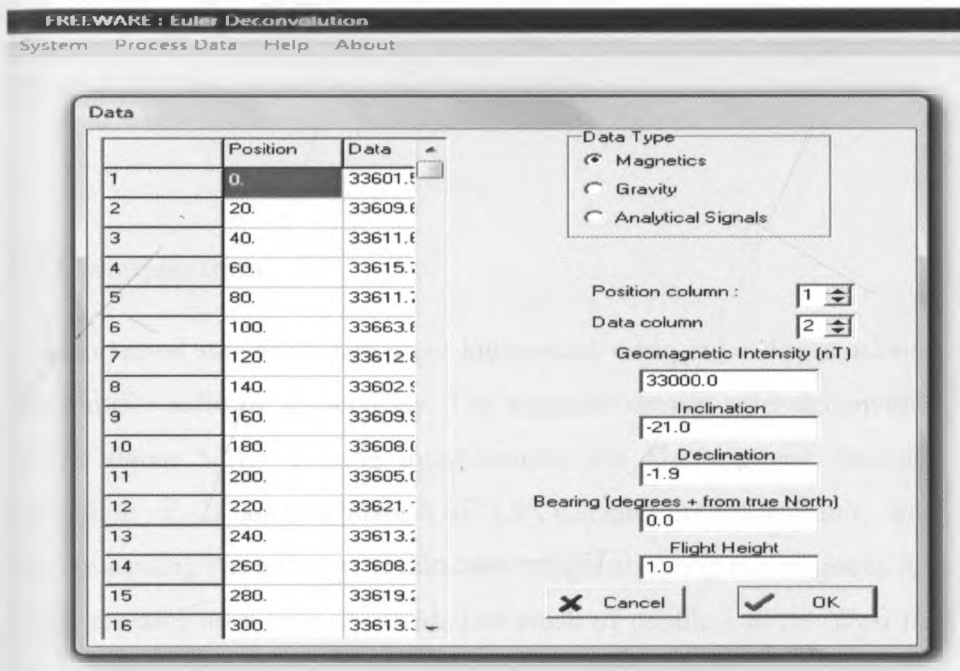


Figure 5.21. Data reading using euler deconvolution freeware.

	A	B	C	D	E	F	G	H	I	J	K	L	M	N	O	P
1		0	33601.69													
2	20	0	33609.62													
3	40	0	33611.68													
4	60	0	33616.72													
5	80	0	33611.78													
6	100	0	33603.82													
7	120	0	33612.87													
8	140	0	33602.93													
9	160	0	33608.99													
10	180	0	33608.03													
11	200	0	33605.05													
12	220	0	33621.16													
13	240	0	33613.21													
14	260	0	33618.27													
15	280	0	33618.28													
16	300	0	33613.3													
17	320	0	33605.34													
18	340	0	33618.43													
19	360	0	33610.48													
20	380	0	33609.52													
21	400	0	33611.55													
22	420	0	33608.57													
23	440	0	33608.62													
24	460	0	33607.64													
25	480	0	33613.29													
26	500	0	33617.32													
27	520	0	33628.39													
28	540	0	33618.43													
29	560	0	33623.5													
30	580	0	33629.8													
31	600	0	33629.72													
32	0	100	33622.38													
33	20	100	33604.33													
34	40	100	33608.31													
35	60	100	33617.28													
36	80	100	33614.25													
37	100	100	33612.23													

Figure 5.22. Data entered in surfer for plotting.

### 5.4.1 Interpretation

The corrected magnetic data were interpreted using euler deconvolution software and plotted using surfer software respectively. The magnetic data in euler deconvolution was read as shown in the figure 5.21. During interpretation the Geomagnetic intensity (nT) used is 33000, inclination of  $-21^{\circ}$  and declination of  $-1.9^{\circ}$ . Clicking the Ok window, the result is figure 5.23. on the processing dat window, results into images showing the magnetic material in the subsurface in the research area were obtained. The result of profile 1 in the West-East direction in th study area is shown in the Figure 5.24a. These magnetic results shows areas of faultzones as marked by red lines and the depths of the magnetic susceptible materials which ranges from about 10 metres to 50 metres depth. These materials are sands and gravels as further confirmed by the other methods (VES and ERT) used in the study. These materials are loose and dry sediments as confirmed by the geologic log obtained from BH2 in the study area.

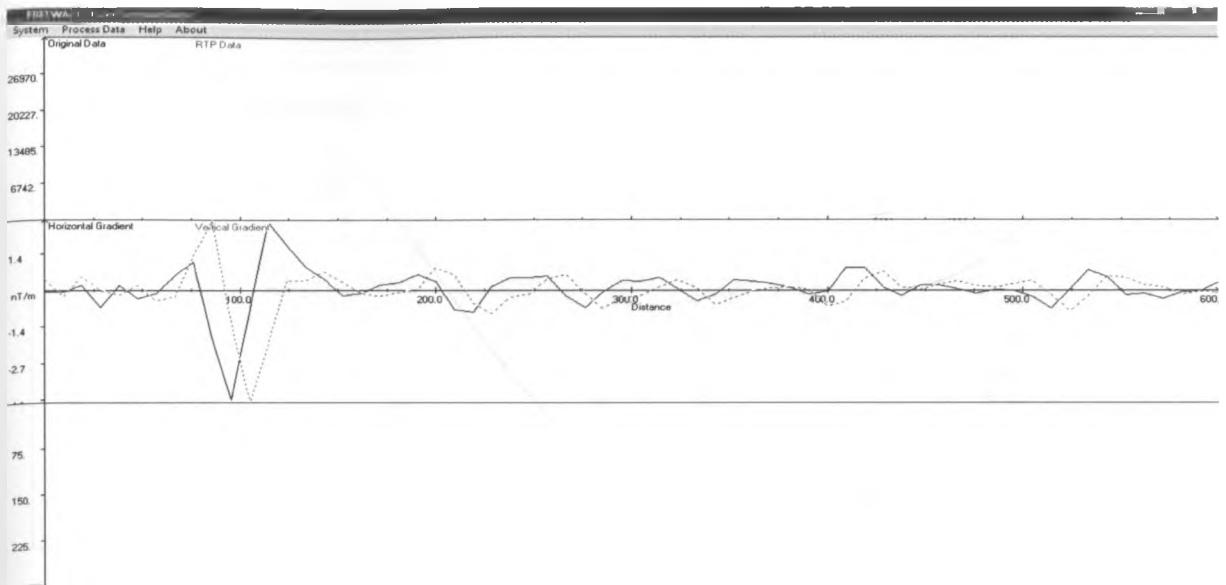


Figure 5.23. Initial plot of the processed magnetic data in interpretation.

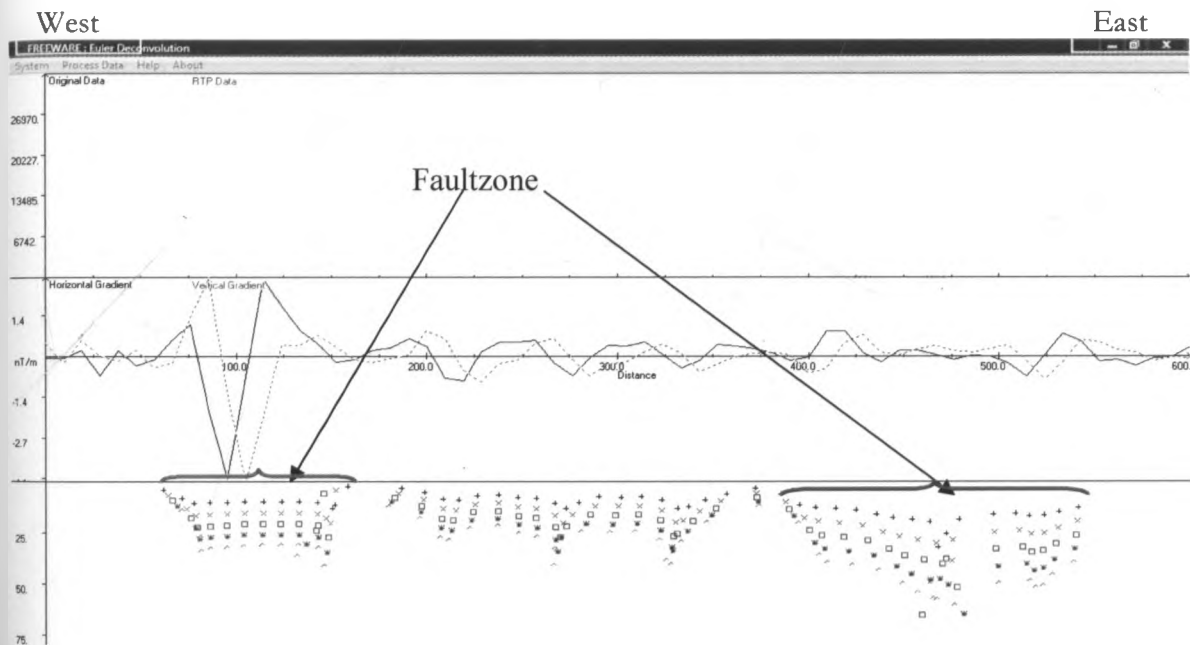


Figure 5.24a. Magnetic profile 1 about 100metres to the north of BH2.

The magnetic material shown in profile 1 (Figures 5.24a and 5.24b) occurs from a depth of about 10 m to about 50 m and generally spread at similar depths in the study area. The profile also shows three foremost fault zones. The system of faults which scuttle much deeper even in the rest of the Olobanita well field are a major impediment to the drilling operations given that it sets up heterogeneity.

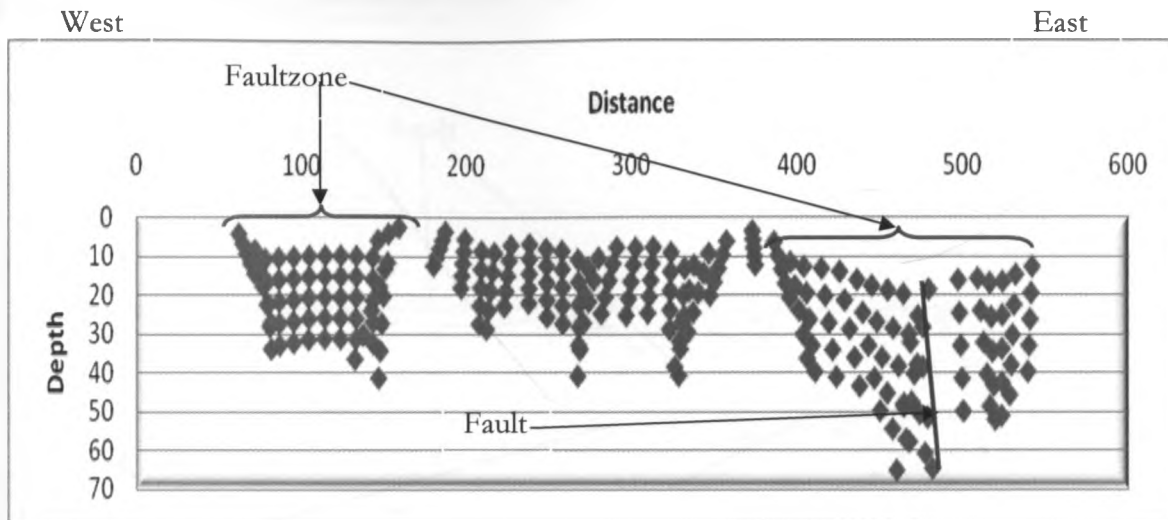


Figure 5.24b. Shows fault zones in magnetic profile 1 of the study area.

Similarly, profile 2 (10 m north of BH2) and profile 4 shows magnetic susceptible materials to a depth of about 50 metres as shown in figures 5.25a,b and 5.26a,b. With an exception is profile 3 which has the magnetic material between the depths of 20 m to 80 m as shown in figure 5.27a, b. These geologic materials have a horizontal resemblance across the profiles revealing the same depths. An exception is seen in areas disturbed by fault zones, where the material tends to go deeper.



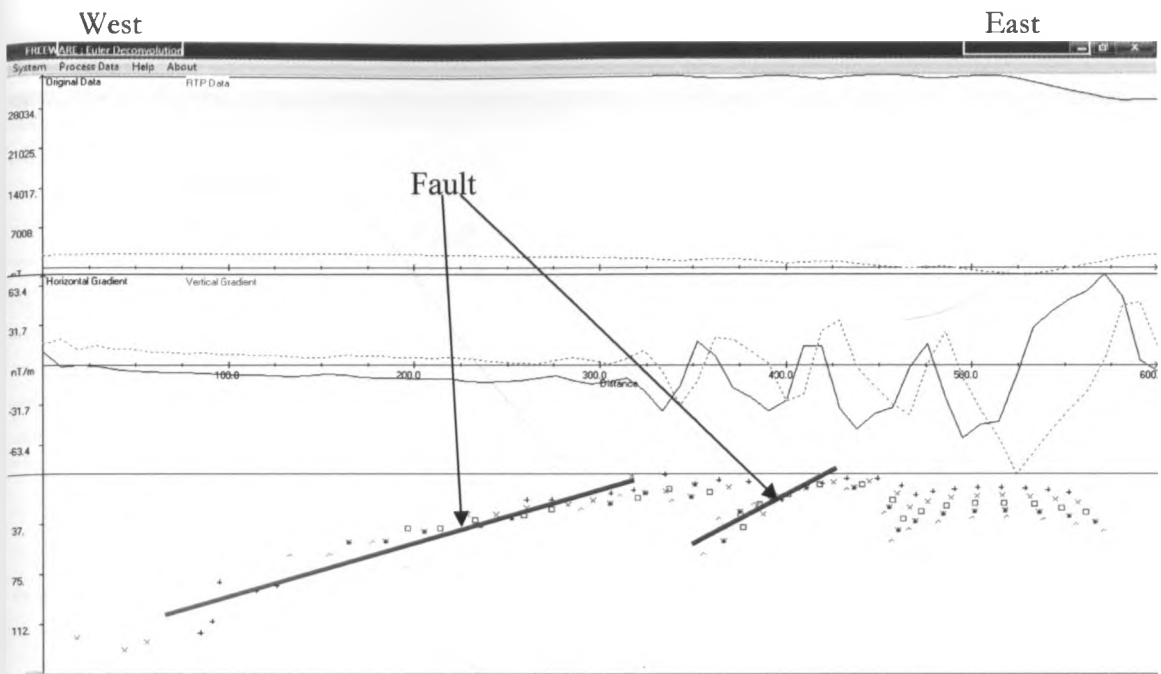


Figure 5.25a. Magnetic profile 1 about 10 metres to the north of BH2.

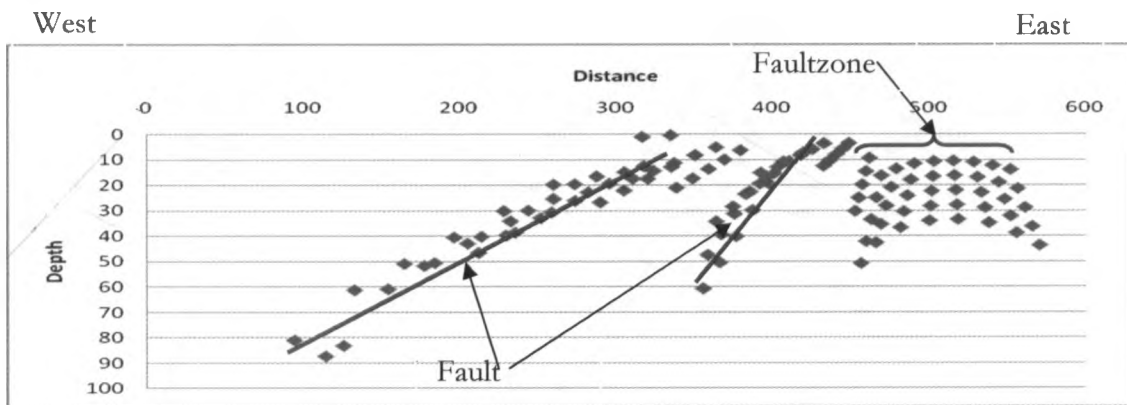


Figure 5.25b. Shows fault zones in magnetic profile 1 of the study area.

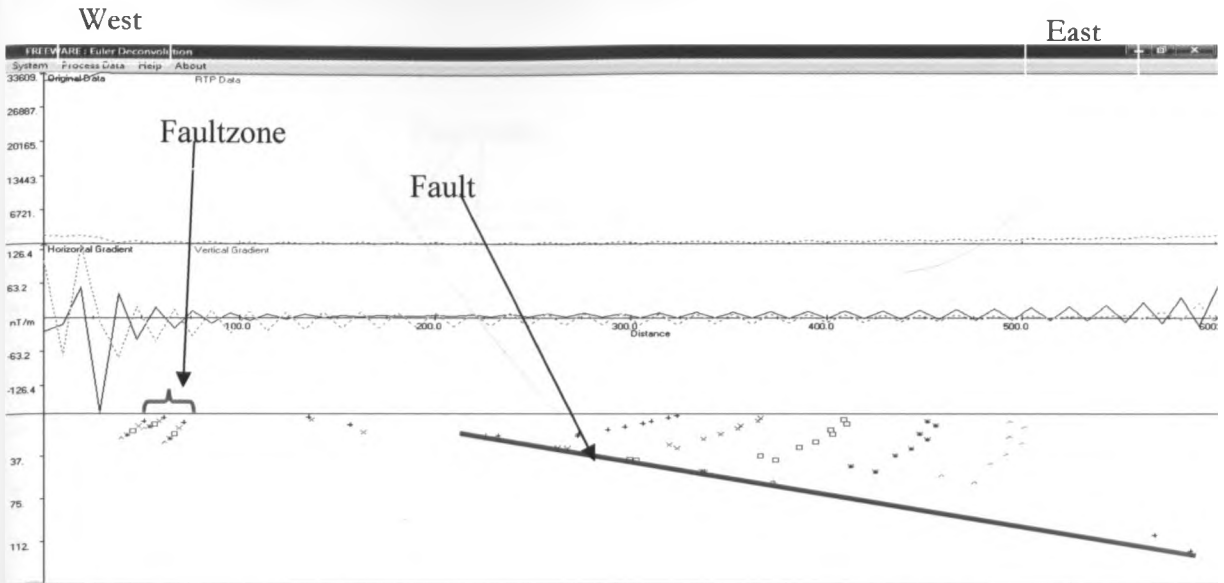


Figure 5.26a. Magnetic profile 4 about 200 metres to the south of BH2.

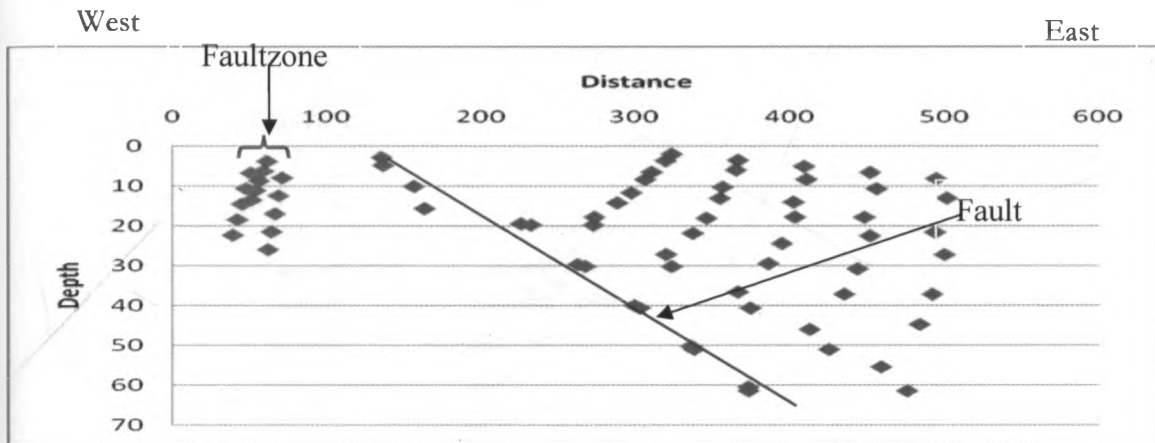


Figure 5.26b. Magnetic profile 4 showing fault zones.

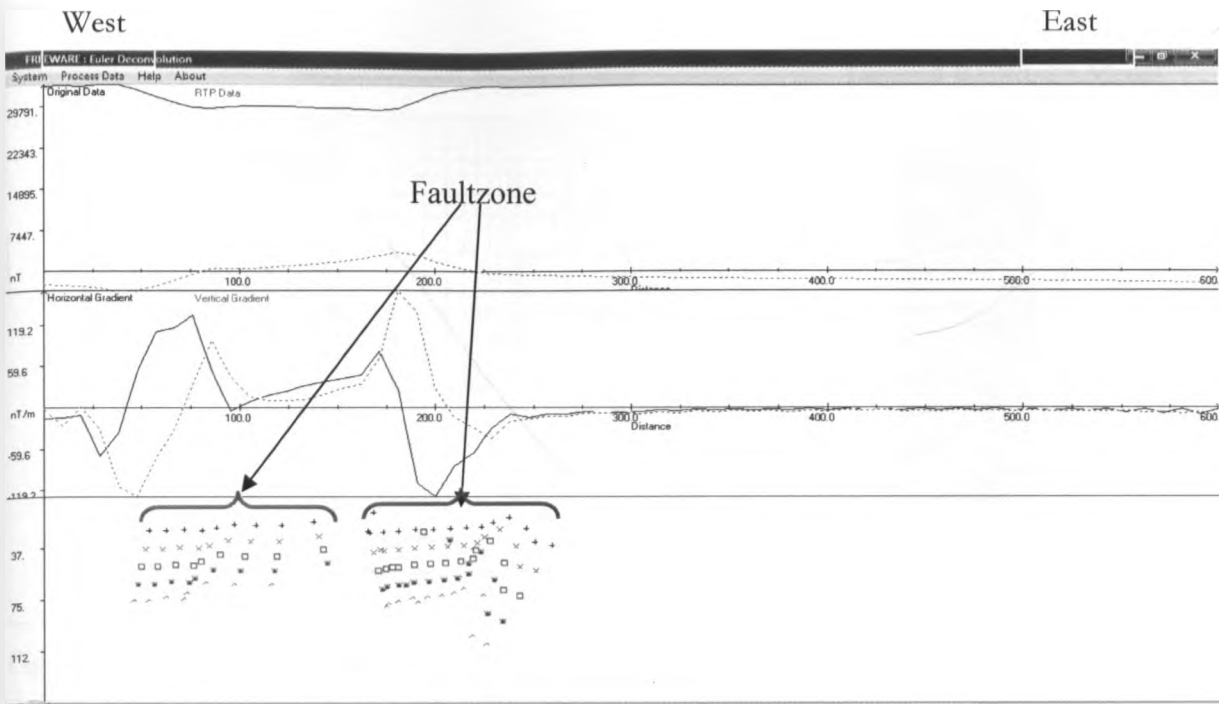


Figure 5.27a. Magnetic profile 3 about 200 metres to the south of BH2.

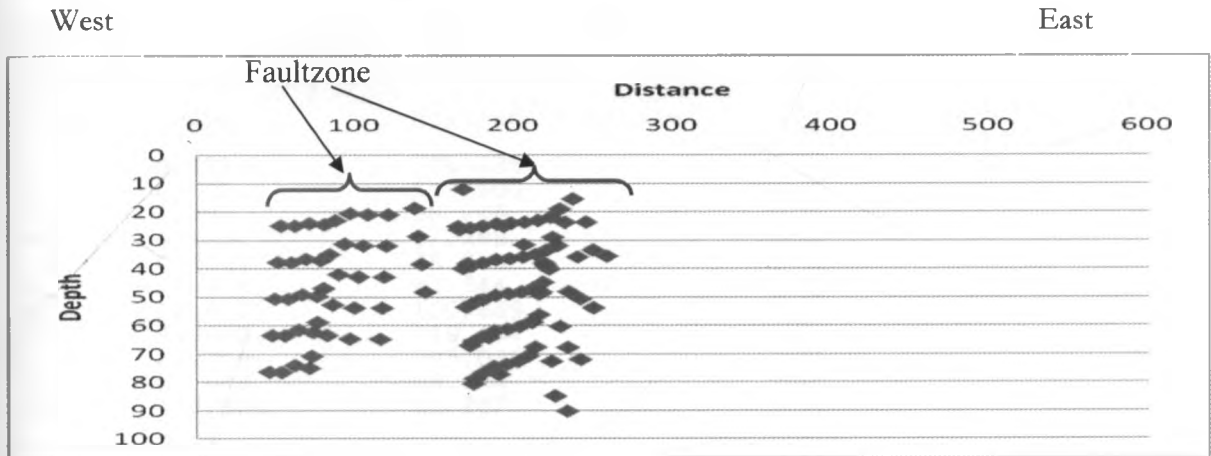


Figure 5.27b. Magnetic profile 3 showing fault zones.

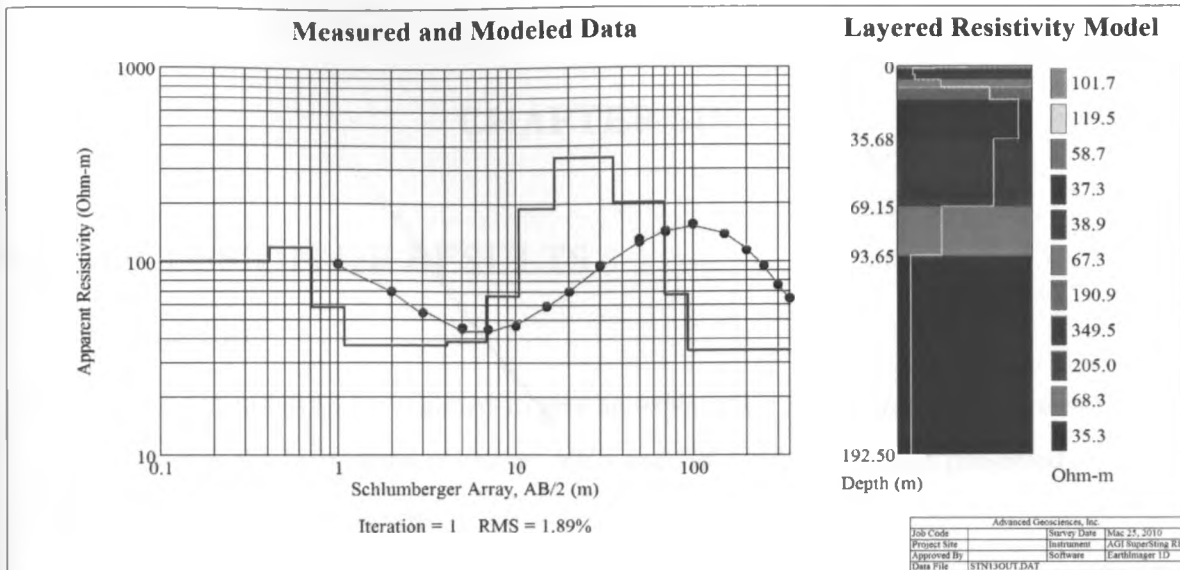


Figure 6.2. Interpreted model at station 13 (at BH2) showing curve and layered resistivity model.

Table 6.1. Formation resistivities from interpreted model of station 13.

Layer	Depth	Apparent resistivity
1,	0.411,	101.738
2,	0.711,	119.500
3,	1.081,	58.746
4,	4.112,	37.298
5,	6.835,	38.853
6,	10.438,	67.344
7,	16.631,	190.869
8,	35.683,	349.454
9,	69.149,	205.029
10,	93.648,	68.344
11,	192.500,	35.267

Table 6.2. General relationship between F and grain-sizes established in NW-Europe [Sporry, 2001]

F	Grain size
1	clays
1.5 -- 2	sandy clays
2 -- 2.5	silty and clayey Sands
3	fine sands
4 -- 5	medium coarse sands
6 -- 7	coarse sands
> 8	very coarse sands and pebbles

## CHAPTER SIX

### 6.0 DISCUSSION OF RESULTS

#### 6.1 Introduction

The interpreted data has to be qualified to give an explanation on the intended matter of study. In this discussion the interpreted magnetic, VES and ERT data have been presented and their geological meaning has been given.

#### 6.2 Relationship between borehole lithology/structure and collapsing of boreholes

The geologic log of BH2 (see figure 6.1) presents a lithology which includes loose volcanic sediments covering a depth of 120 metres; from 0-120 metres below the ground surface. These sediments are underlain by tough volcanic rocks with few bands of loose sediments at the depth of 121-210 metres below the ground surface. Subsequently, loose volcanic sands are the lithological materials covering the remaining part of the geologic log from the depth of 211- 271 metres below the ground. In the course of drilling of borehole 2, lithologic material collapsed and dropped into the hole from weakly consolidated layers at 22-24 metres as shown in appendix B (mostly of silts, gravel sand silts and volcanic sands with few gravels), 110-138 metres ( which records medium ash/tuff horizon with trachyte fragments at 110-120 metres) and 189-195 metres having horizon of alternated weathered gravel and mud(erosional horizon) and weathered trachyte horizon with pumice.

The geologic log of the abandoned BHX (see figure 6.3) gives sediments for a depth of 0-20 metres below the ground which overlies welded tuff that is underlain by pumice and gravel. A hard rock of welded tuff overlies an erosional surface at a depth of 76 metres which subsequently overlies trachytic rock. Loose sediments of gravels and sands and occasionally silty covers the depth of 98 metres to the total depth of the borehole at 262 metres. The drilling operations of BHX was hampered by collapsing difficulties which culminated in the abandonment of the borehole. At the depth of 42 metres below the ground there was intensive collapse of borehole wall lithologic materials and thus loss of drilling mud and water. This is the depth which lithologically has pumice gravels from a depth of 30-46 metres below the ground. The stratigraphic formation of over 50 metres thick collapsed beyond the depth of 200 metres below

the ground which eventually led to the closure of the borehole. Below a depth of 220 metres, air circulation was lost: as a result, it was not possible to obtain reliable yield estimates of individual aquifers. Structurally, borehole X was drilled near a faultzone ( see figure 5.14) which may have contributed to the intensity of collapsing of lithologic materials at depth.

### 6.3 Lithological interpretation of geophysical results

Resistivity is a fundamental electrical property of rocks, that is closely related to rock lithology of which the main controlling factors are bulk rock porosity, pore structure, amount and salinity of water, temperature and the presence of clays. To convert the resistivity results into geological meaning requires some knowledge of the typical resistivity values for the different types of subsurface materials and geology of the surveyed area. The geology of the area, the electrical conductivity (EC) of the borehole waters, the interpreted VES results in the identified boreholes have been used to come up with standard ranges of formation resistivities of geologic subsurface materials in the study area. These has been closely correlated with the borehole geologic logs as further discussed.

The EC of the waters in BH2 (previously BH1) is approximately 800 $\mu$ S/cm and therefore its mean resistivity,  $\rho_w$  (the reciprocal of EC) is 12.5 Ohm.m. The formation factor (F) has been calculated for this borehole which lies at VES point 13 of the survey grid which has a modelled image shown in Figure 6.2 and interpreted results of formation resistivities shown in table 6.1. Electrical F is given by the relation;

$$F = \frac{\rho_f}{\rho_w} \quad (6.1)$$

where  $\rho_f$  is the resistivity of formation and  $\rho_w$  is the resistivity of pore water. This relation is a derivation from Archie's Law (Keller and Frischknecht, 1966). Using the relationship in equation (1), the formation resistivity ranges for station 13 at BH2 have been calculated using results in table 6.1 and F ranges of table 6.2 and taking into account the geologic log of borehole 2 (see Figure 6.1), which correlates well with the geophysical results.

Vertical Scale: 1 cm represents 10m

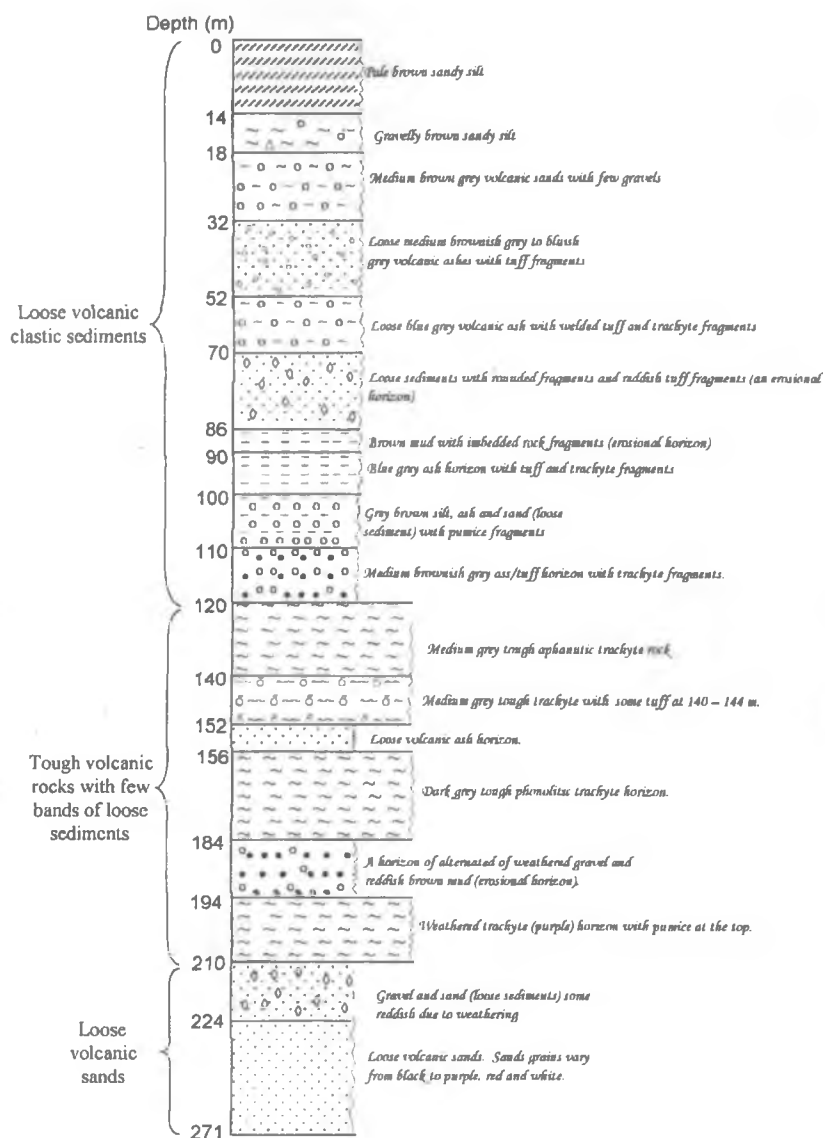


Figure 6.1. Geologic log of Olobanita Borehole no. 2 (After Mathu, 2008).

Table 6.3. Resistivity Ranges for Materials in BH2

Material type	Formation resistivity Range (Ohm.m)	Formation depth
Very coarse sand and gravels	>100	0-0.7
Medium to coarse sands	50-62.5	0.7-1.1
Fine sands	37.5-50	1.1-6.8
Medium to coarse sand	62.5-87.5	6.8-10.4
Very coarse sand and gravels	>100	10.4-69.1
Medium to coarse sand	62.5-87.5	69.1-93.6
silty clay sands to fine sands	31.25-37.5	93.6-192.5

The general relationship between F and grain-sizes established in NW-Europe (Sporry, 2001) shown in table 6.2. has been adopted as a rough guide, because it fitted well with borehole evidence and the calculated F values for BH2 are shown in table 6.3 (showing Resistivity Ranges for Materials in BH2).

The EC for waters in BH2 is  $850 \mu\text{S}/\text{cm}$  and thus the resistivity ( $\rho_w$ ) is  $((1/850) \mu\text{S}/\text{cm} * 10000)$  giving  $11.76 \text{ Ohm.m}$ . Using the F ranges given in table 6.2 and the  $\rho_w$  value, the formation resistivity ranges have been calculated for subsurface formation in BH2 (see table 6.5).

These values are correlated with values in table 6.4 showing Formation resistivities from interpreted model BH2 (Fig. 6.4). The interpreted subsurface lithologies, their resistivities and the geologic log equivalents are discussed in section 6.2.2.



Vertical Scale: 1 cm represents 10m

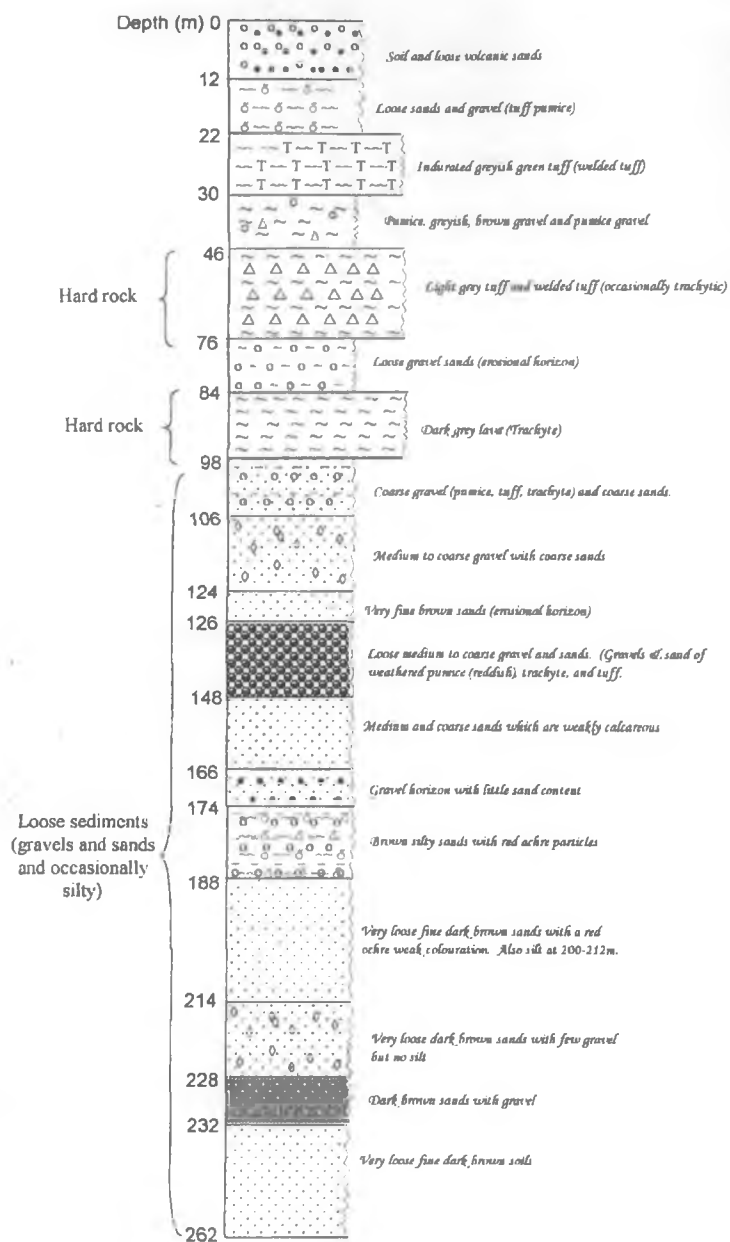


Figure 6.3. Geologic log of Olobanita abandoned Borehole X (After Mathu, 2008).

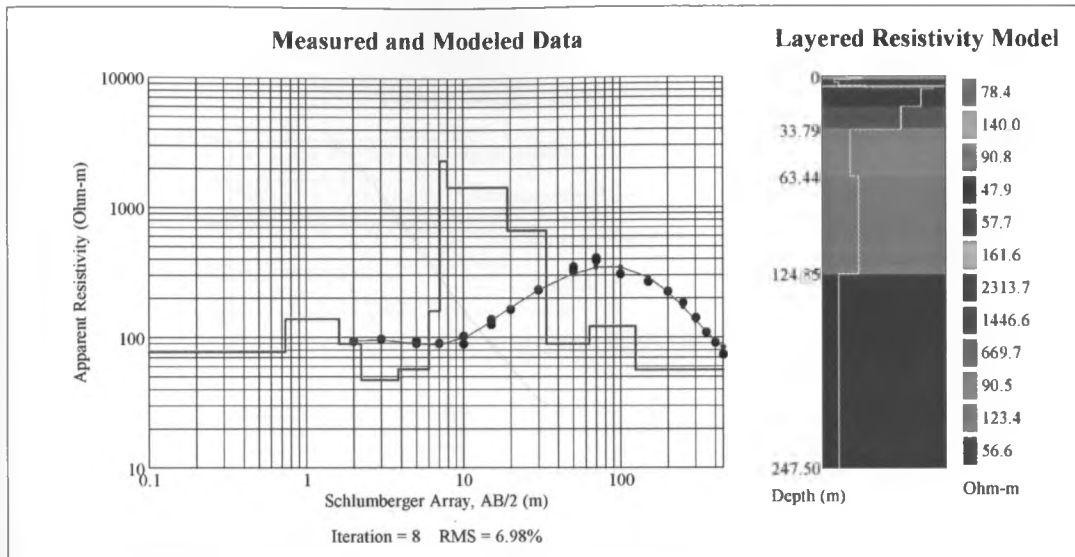


Figure 6.4. Interpreted model at the abandoned BHX showing curve and layered resistivity model.

Table 6.4. Formation resistivities from interpreted model of abandoned BHX.

Layers	Depth	Apparent resistivity
1	0.741	78.448
2	1.624	140.044
3	2.247	90.791
4	3.861	47.88
5	6.031	55.703
6	7.07	161.603
7	7.911	2313.679
8	19.115	1446.625
9	33.794	669.663
10	63.437	90.502
11	124.851	123.409
12	247.5	56.648

Table 6.5. Resistivity Ranges for geologic materials in BHX

Material type	Formation resistivity Range (Ohm.m)	Formation Depth (m)
Coarse sands	70 - 83	0-0.7
Very coarse sands and pebbles	>94	0.7-1.6
Very coarse sands	83 - 94	1.6-2.2
Medium coarse sands	47 - 59	2.2-6.0
Very coarse sands and pebbles	>94	6.0-33.8
Very coarse sands	83 - 94	33.8-63.4
Very coarse sands and pebbles	>94	63.4-124.9
Medium coarse sands	47 - 59	124.9-247.5

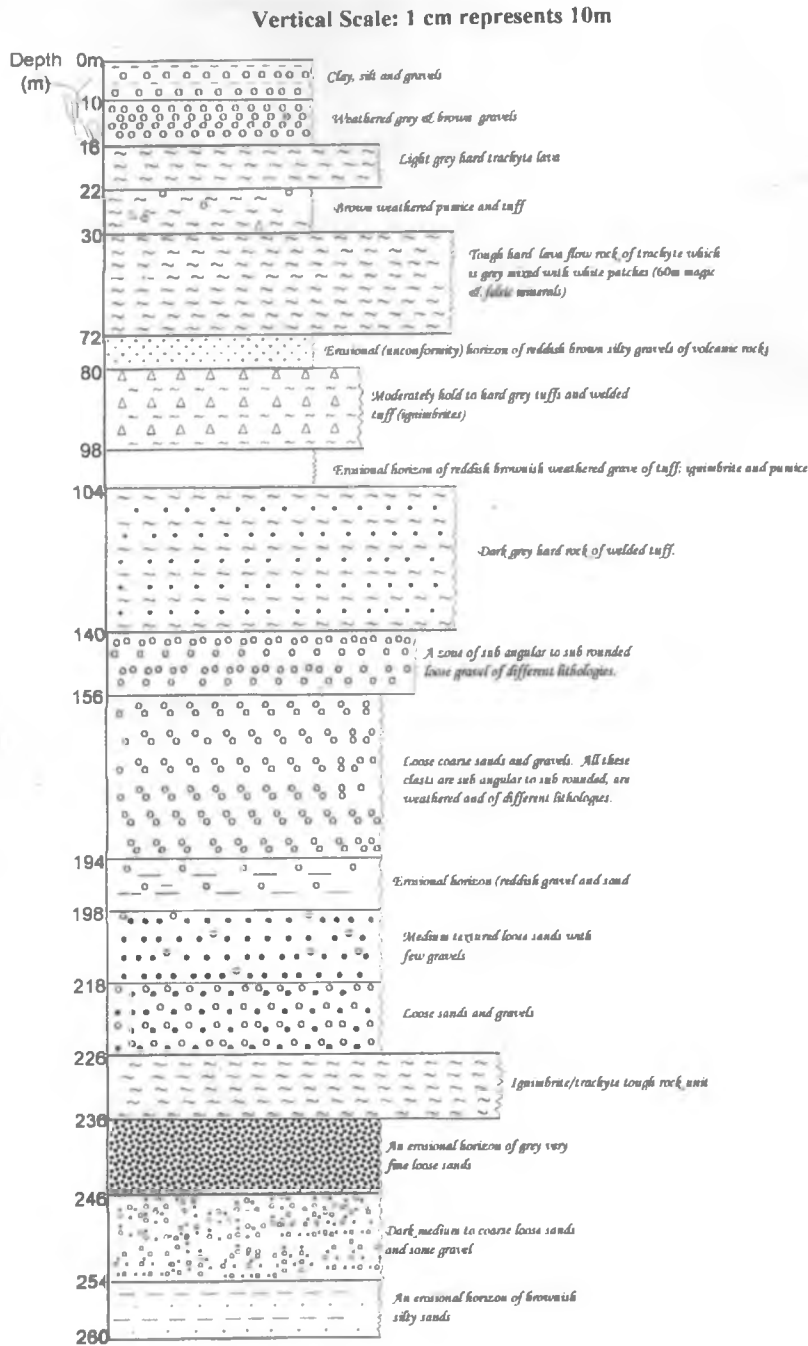


Figure 6.5. Geological log of Olobanita Borehole 6 (After Mathu, 2008).

The interpreted model for VES point at borehole 6 is shown in the Figure 6.6 and its equivalent formation resistivities in table 6.6.

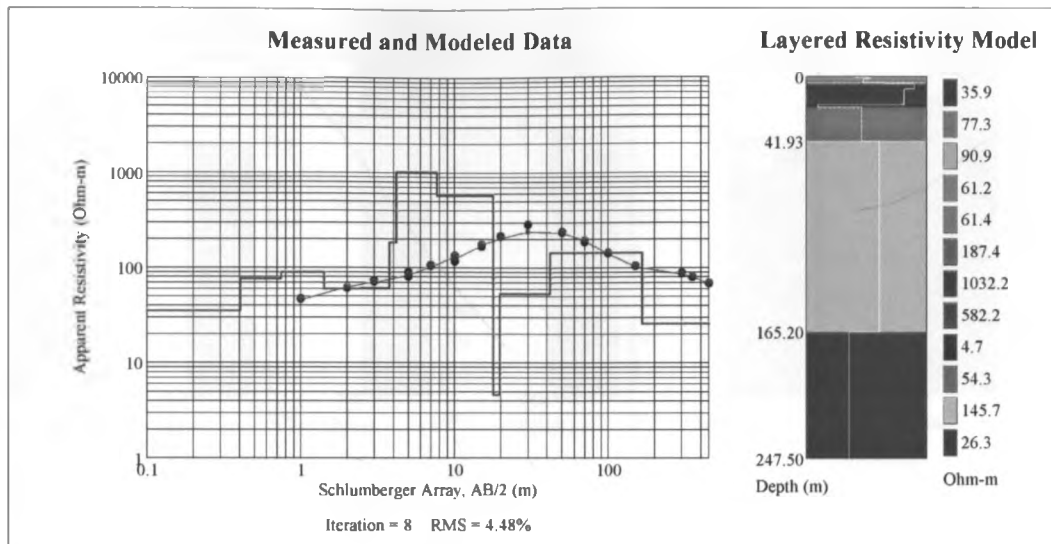


Figure 6.6. Interpreted model at the abandoned BH6 showing curve and layered resistivity

Table. 6.6. Formation resistivities from interpreted model of BH6.

Layer	Depth	Apparent resistivity
1	0.406	35.933
2	0.747	77.337
3	1.421	90.884
4	2.457	61.163
5	3.764	61.425
6	4.178	187.353
7	7.683	1032.191
8	17.783	582.172
9	19.671	4.669
10	41.935	54.29
11	165.197	145.734
12	247.5	26.302

The VES and 2D Resistivity gave similar subsurface distribution patterns of resistivity, and the magnetic data susceptibility profiles and hence the individual sections are discussed here together. Resistivity values of the lithologies in the study area varies from 10.2 to 949.8  $\Omega$  m (see Figures 6.7a-d and figures 6.8 i-xxviii).

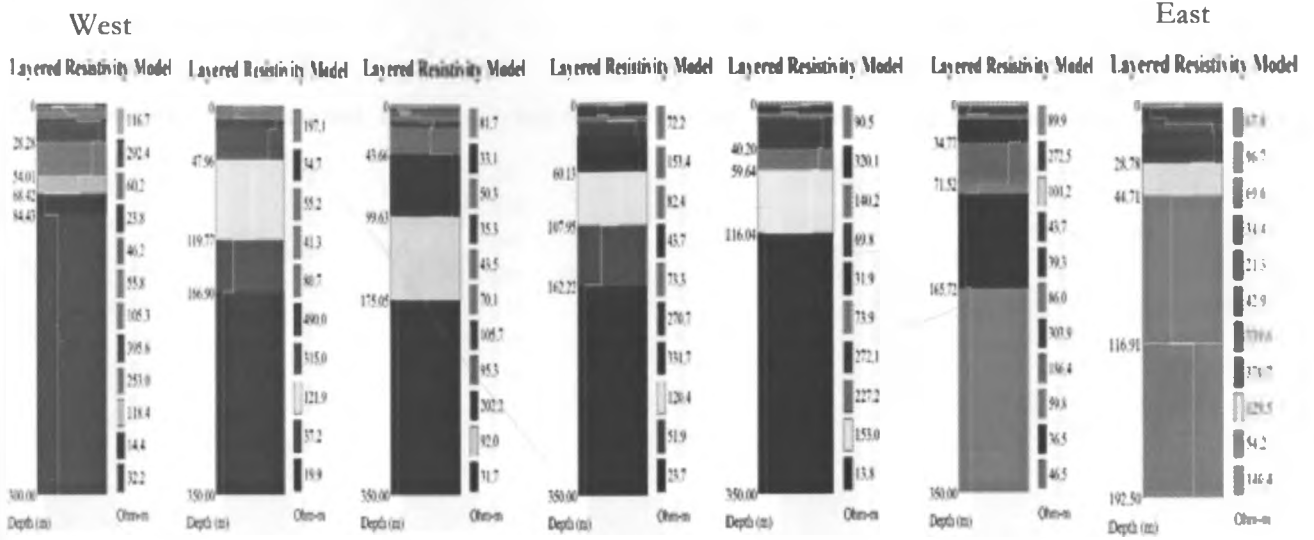


Figure 6.7a. VES interpreted models (profile 1 W-E).

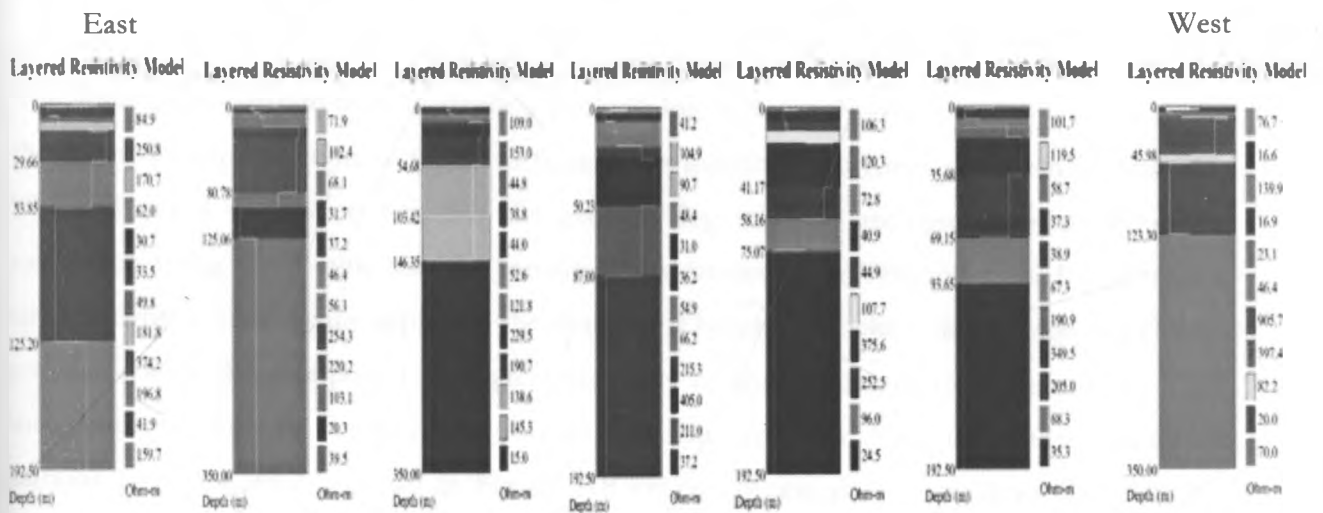


Figure 6.7b. VES interpreted models (profile 2 W-E).

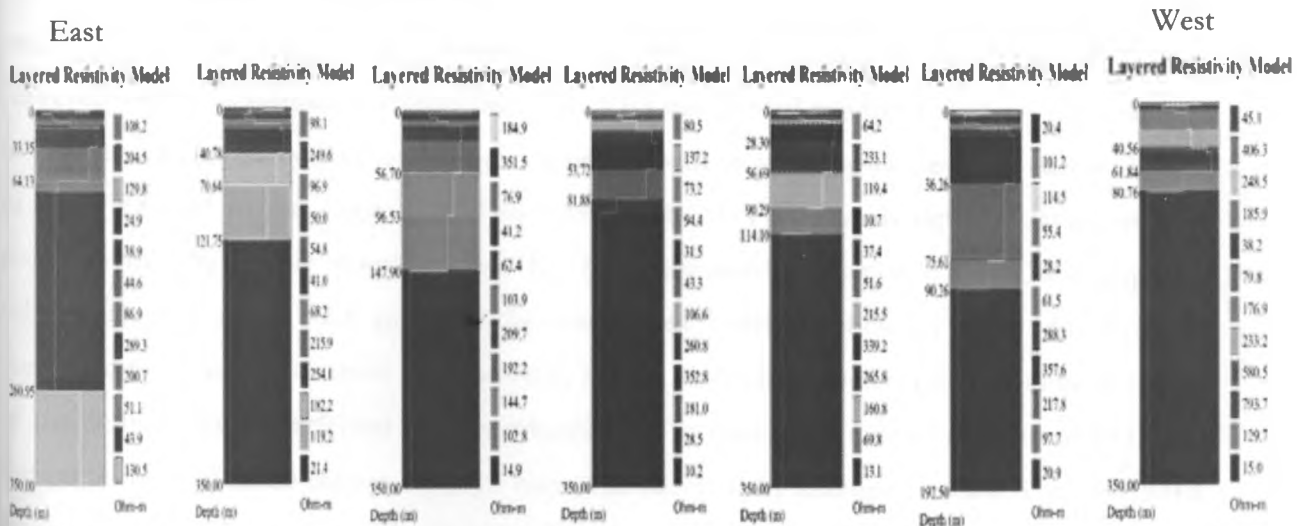


Figure 6.7c. VES interpreted models (profile 3 W-E).

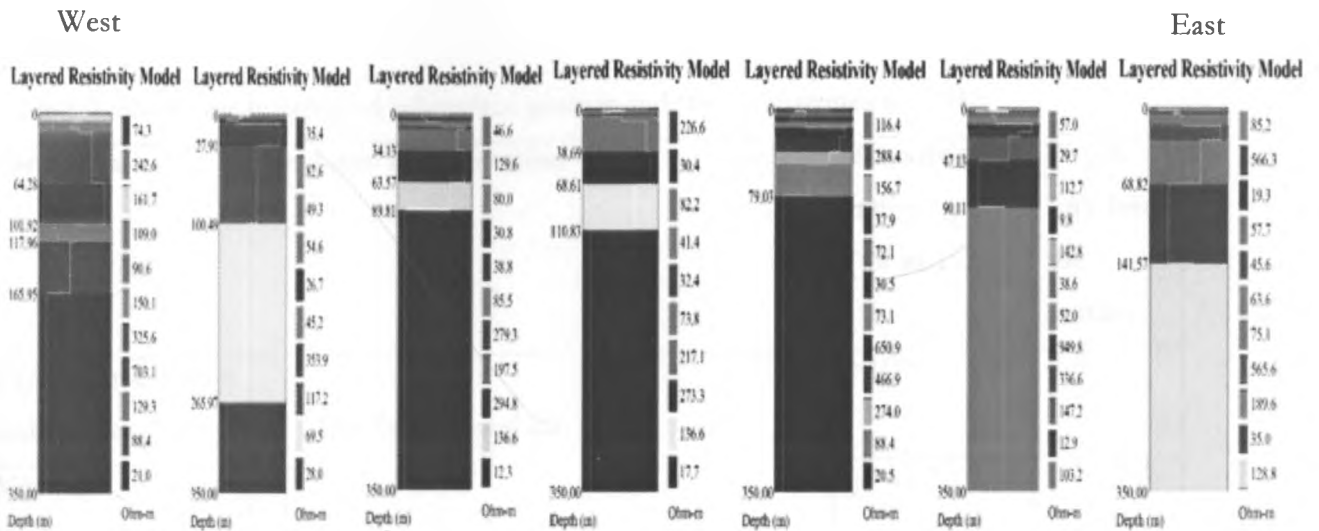


Figure 6.7d. VES interpreted models (profile 4 W-E).

The lithological variation from borehole 2 geologic log in the study area; when superimposed on the resistivity-depth section, is found to fit into the following categories as shown in table 6.7. These shows a correlation between the geologic log and the geologic materials from the calculation using the F table and the formation resistivities from VES interpreted results with specific depths. This equally applies to the abandoned borehole X where the geologic log closely correlates with the interpreted geologic image out of the formation resistivities from VES interpreted results and F table. The formation resistivities from VES interpreted results of stations 1-6, 9-14, 16-27, shown in Figures 6.8 i-vi, ix-xiv, xvi-xxvii, correlates well with the ranges established by using VES 13 interpreted results and the F table and thus with their relative depths correlating well with the geologic log in BH2. This shows a range of depths for high resistivity material from a depth of about 10 metres to 50-80 metres respectively across the VES surveyed area. The formation resistivities from VES interpreted results of stations 7,8,15 and 28 in Figures 6.8 vii, viii, xv and xxviii shows a similar pattern and they all are at the eastern border of the VES grid in the study area. This four points of VES reveals dipping nature of high resistivity materials. This unique pattern has been discussed in section 6.3. The interpreted subsurface geology of VES point at the abandoned borehole shows a slight difference as compared to results in borehole 2 as shown in table 6.8. the difference exhibited has been caused by the faulting that has affected the area whereby the formations in area of abandoned BHX has shifted to a depth of 20 metres from 10 metres as revealed by magnetic results. Thus the BHX area which lies in the western side of the study area is a down throw of the faultzone.

Table 6.7. Shows the interpreted subsurface geology and their resistivities for BH2

Formation	Geologic interpretation	Resistivity range ( $\Omega$ m.)	Depth (m) from the surface
Very coarse sands and pebbles	Pale brown sand silt	>100	0-0.7
Medium coarse sands		50-62.5	0.7-1.1
Fine sands		37.5-50	1.1-6.8
Medium coarse sands		62.5-87.5	6.8-10.4
Very coarse sand and pebbles	Gravelly brown sand silt, medium brown grey volcanic sands with few gravels	>100	10.4-69.1
Medium coarse rock material	Loose medium brownish grey to blackish volcanic ashes with tuff fragments	62.5-87.5	69.1-93.6
Fine rock material	Loose sediments with rounded fragments with reddish tuff fragments ( an erosional horizon), ash horizon with tuff and trachyte fragments, silt, ash and sand(loose sediment) with pumice fragments, ash/tuff horizon with trachyte fragments., tough aphanitic trachyte rock, tough trachyte with some tuff, loose volcanic ash horizon, tough phonolitic trachyte horizon, horizon of alternated weathered gravel and mud (erosional horizon) and weathered trachyte horizon with pumice.	31.25-37.5	>93.6

Table 6.8. Shows the interpreted subsurface geology and their resistivities for abandoned BHX

Formation	Geologic interpretation	Depth (m) of the geologic log	Resistivity range ( $\Omega$ m.)	Depth (m) of the formation resistivities
Coarse sands	Soil and loose volcanic sands	1-12	70 - 83	0-0.7
Very coarse sands and pebbles			>94	0.7-1.6
Very coarse sands			83 - 94	1.6-2.2
Medium coarse sands			47 - 59	2.2-6.0
Very coarse sands and pebbles	Loose sands and gravels (tuff pumice)	12-22	>94	6.0-33.8
	Welded tuff	22-30		
Very coarse sands	Pumice gravel	30-46	83 - 94	33.8-63.4
	Welded tuff (occasionally trachytic)	46-76		
Very coarse sands and pebbles	Loose gravel sands	76-84	>94	63.4-124.9
	Trachytic lava	84-98		
	Coarse gravel (pumice, tuff and trachyte) and coarse sands	98-106		
	Medium to coarse gravel with coarse sands	106-124		
Medium coarse sands	Very fine sands 2m (Erosional surface)	124-126	47 - 59	124.9-247.5
	Loose medium to coarse gravel and sands, trachyte and tuff	126-148		
	Medium and coarse sands which are weakly calcareous	148-166		
	Gravel horizon	166-174		



	Silty sands with red ochre particles	174-188		
	Very loose fine brown sands	188-214		
	Loose sands with few gravels	214-228		
	Dark brown sands with gravel	228-232		
	Very loose fine dark brown soils	232-262		

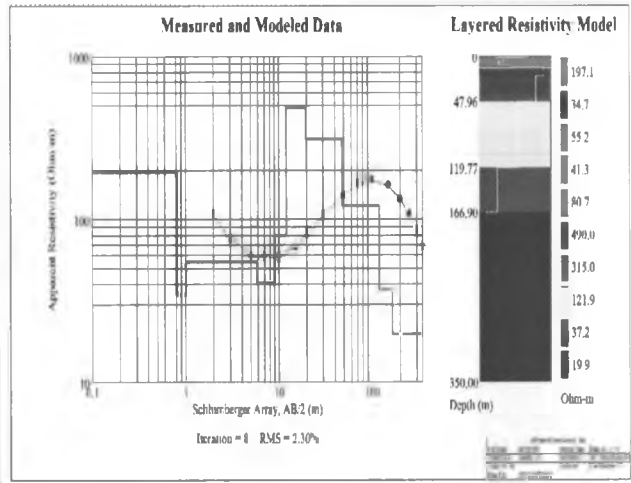
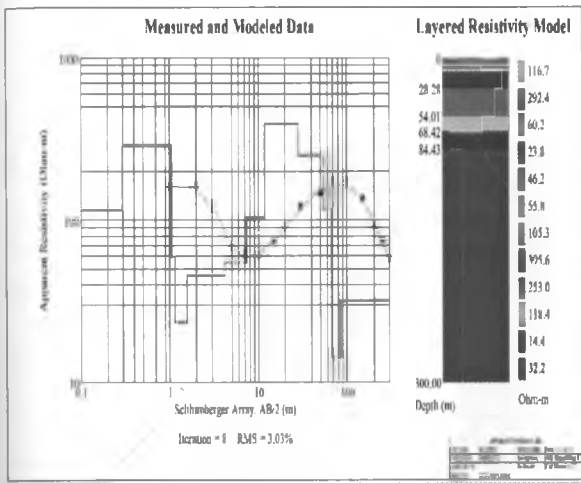


Figure 6.8i. Interpreted model at station 1.

Figure 6.8ii. Interpreted model at station 2.

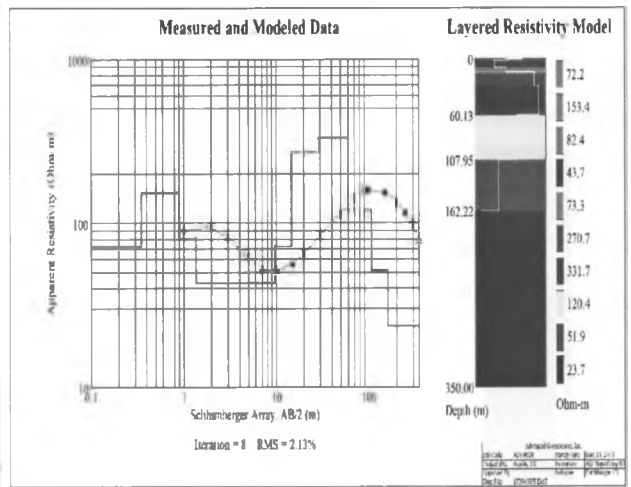
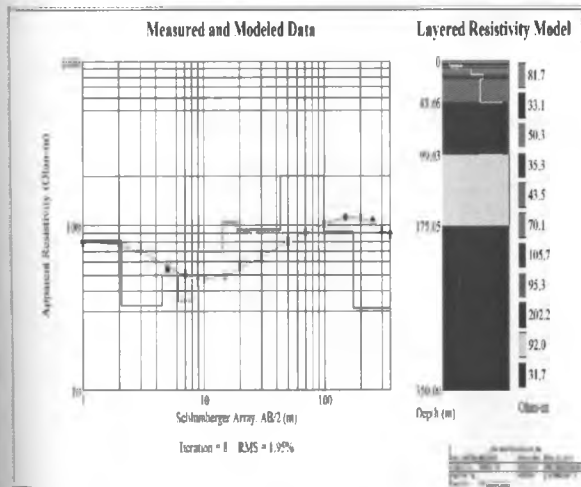


Figure 6.8iii. Interpreted model at station 3

Figure 6.8iv. Interpreted model at station 4

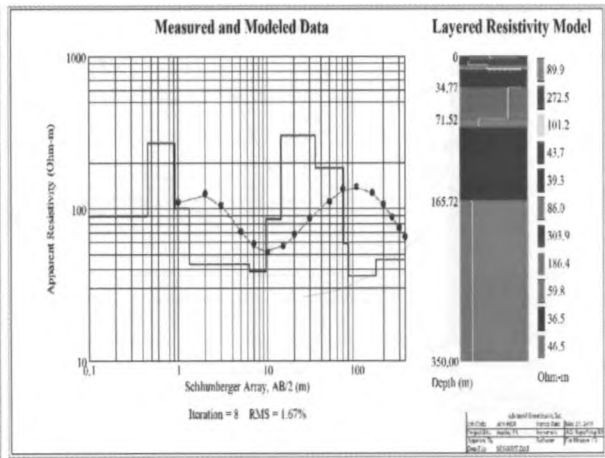
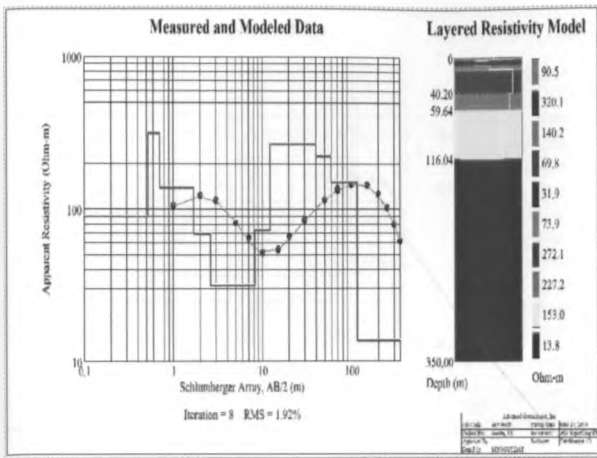


Figure 6.8v. Interpreted model at station 5

Figure 6.8vi. Interpreted model at station 6

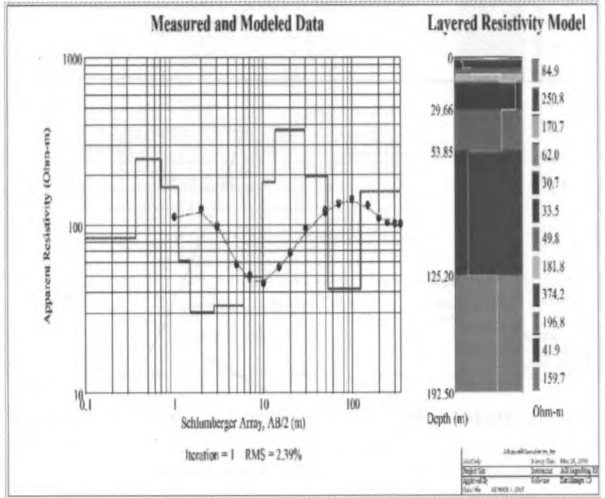
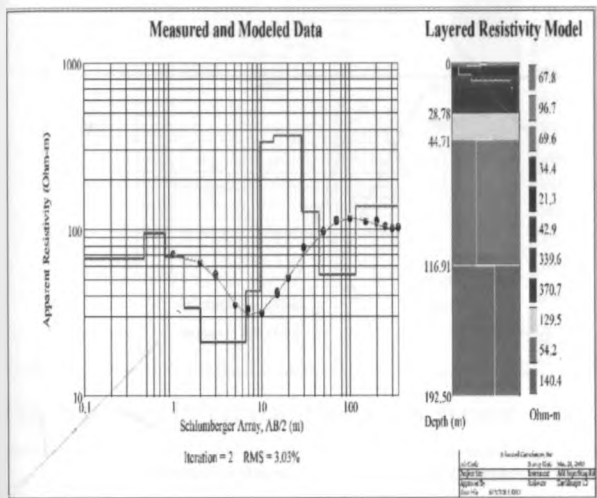


Figure 6.8vii. Interpreted model at station 7

Figure 6.8viii. Interpreted model at station 8

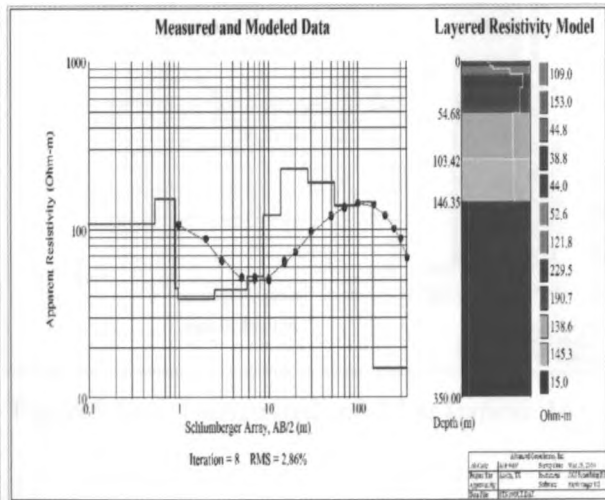
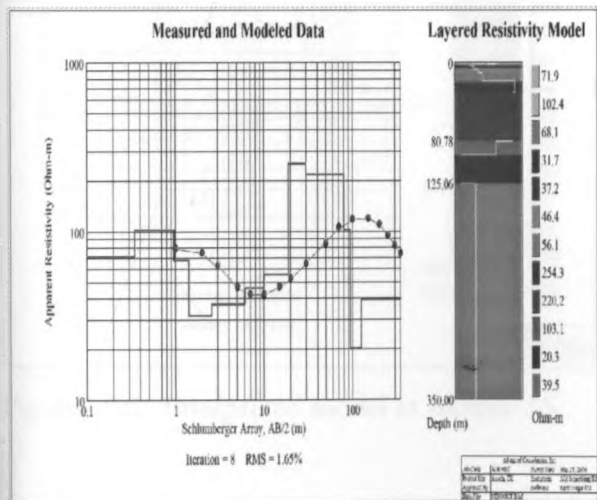


Figure 6.8ix. Interpreted model at station 9

Figure 6.8x. Interpreted model at station 10

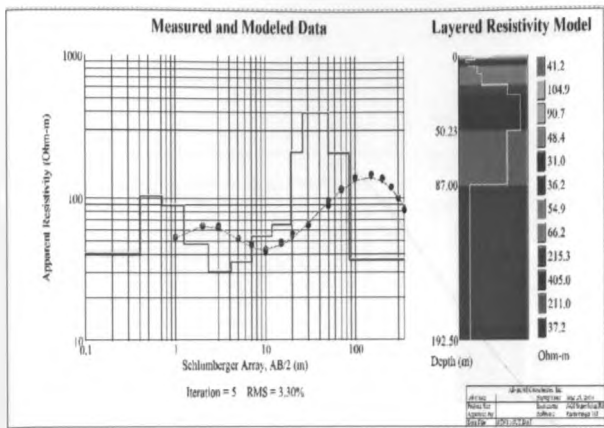


Figure 6.8xi. Interpreted model at station 11

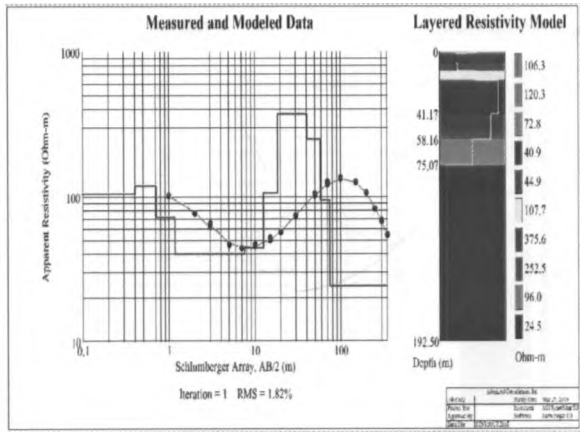


Figure 6.8xii. Interpreted model at station 12

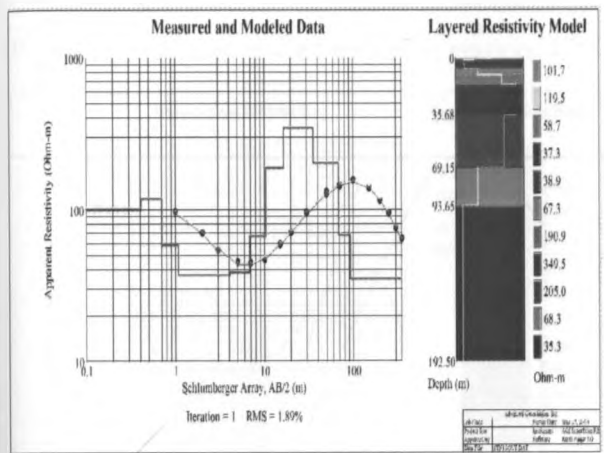


Figure 6.8xiii. Interpreted model at station 13.

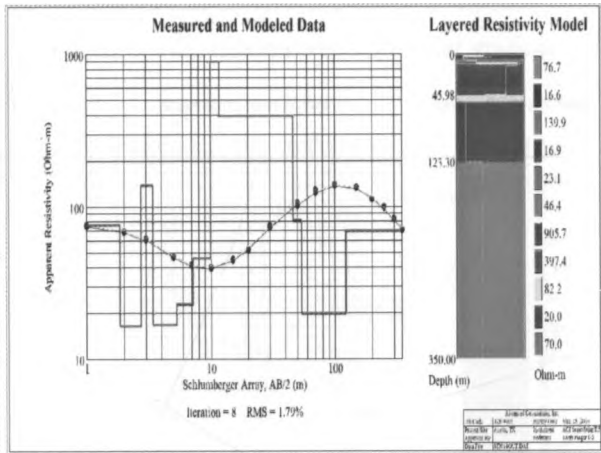


Figure 6.8xiv. Interpreted model at station 14.

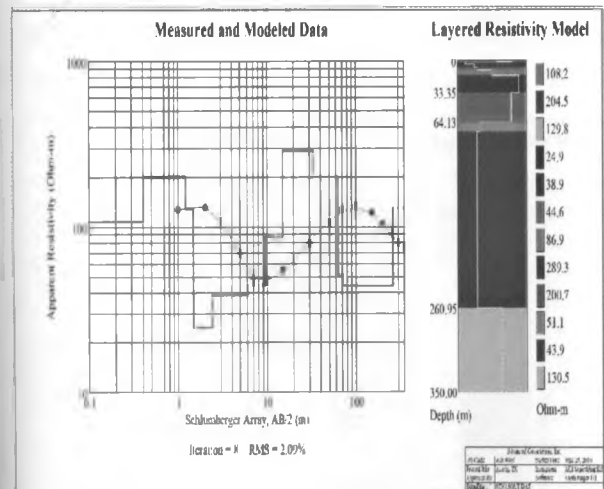


Figure 6.8xv. Interpreted model at station 15.

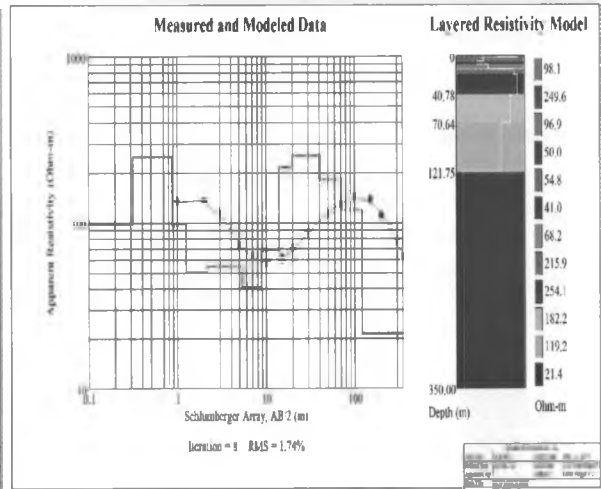


Figure 6.8xvi. Interpreted model at station 16.

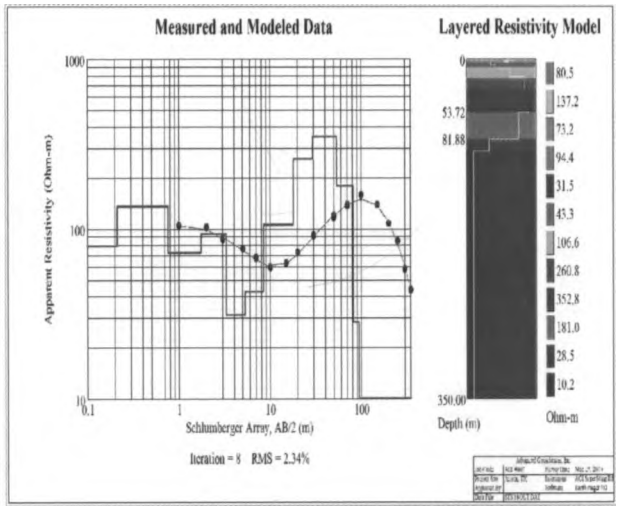
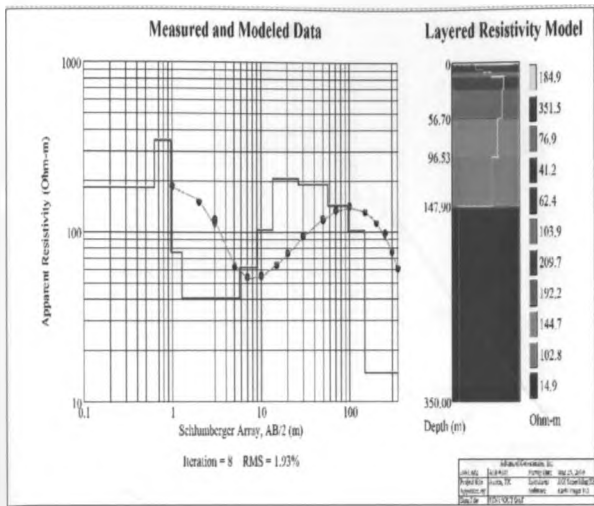


Figure 6.8xvii. Interpreted model at station 17.

Figure 6.8xviii. Interpreted model at station 18.

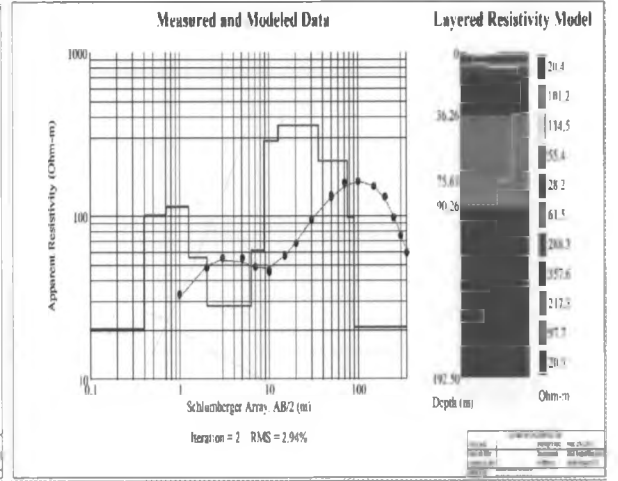
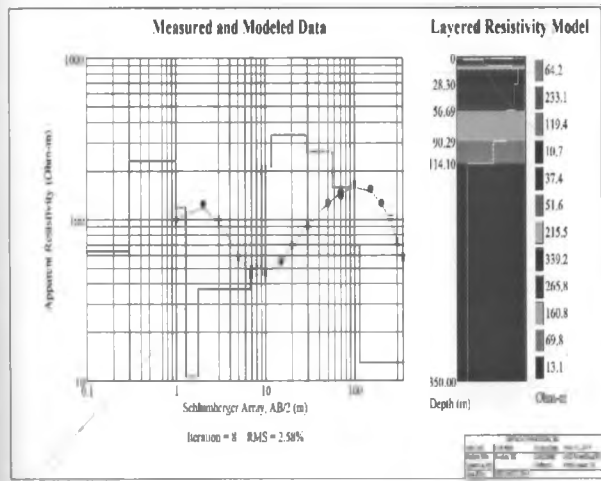


Figure 6.8xix. Interpreted model at station 19.

Figure 6.8xx. Interpreted model at station 20.

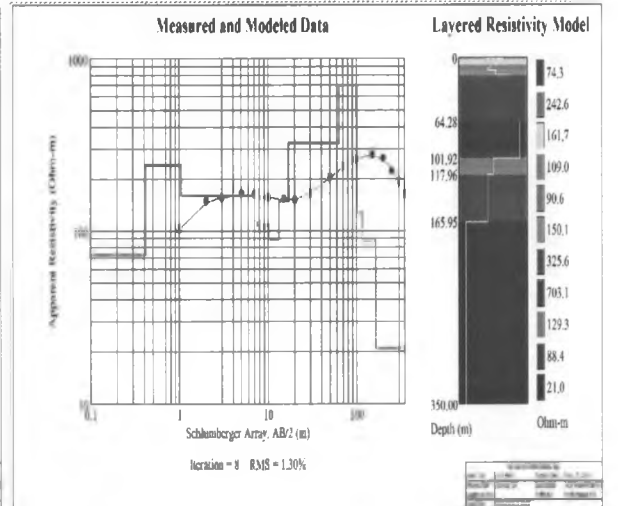
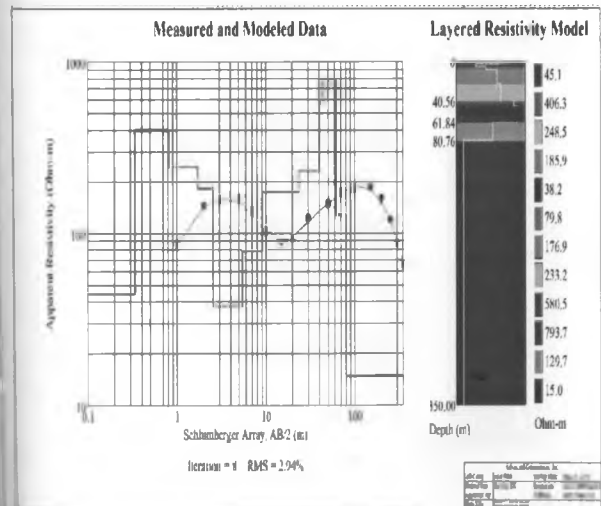


Figure 6.8xxi. Interpreted model at station 21.

Figure 6.8xxii. Interpreted model at station 22.

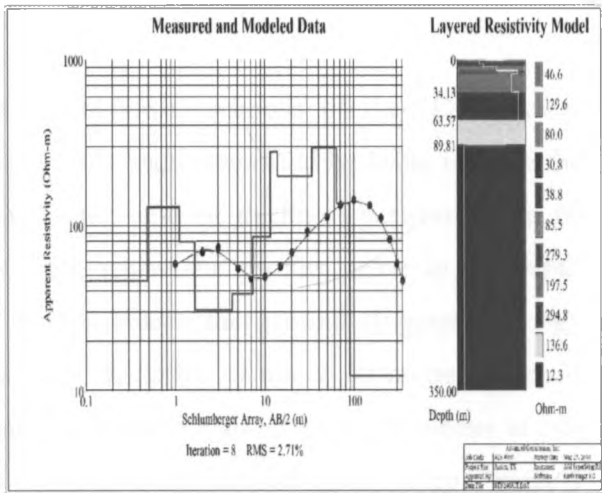
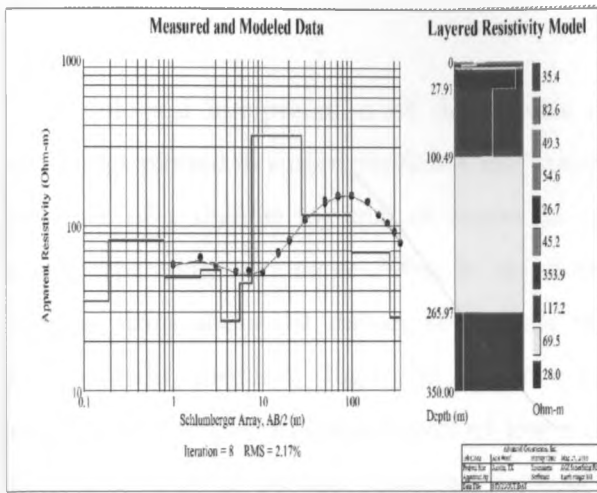


Figure 6.8xxiii. Interpreted model at station 23.

Figure 6.8xxiv. Interpreted model at station 24.

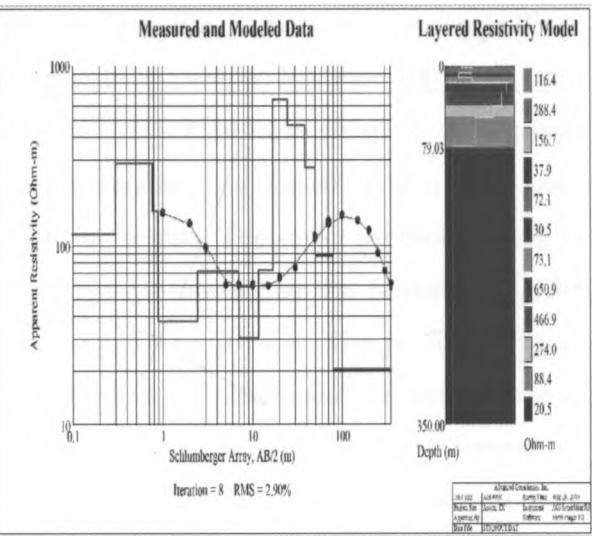
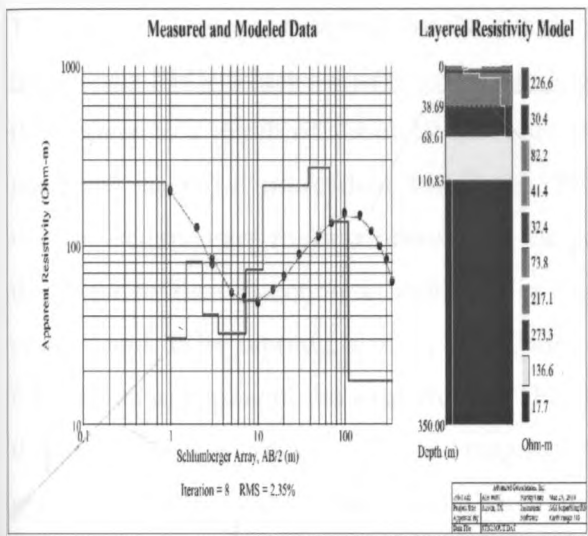


Figure 6.8xxv. Interpreted model at station 25.

Figure 6.8xxvi. Interpreted model at station 26.

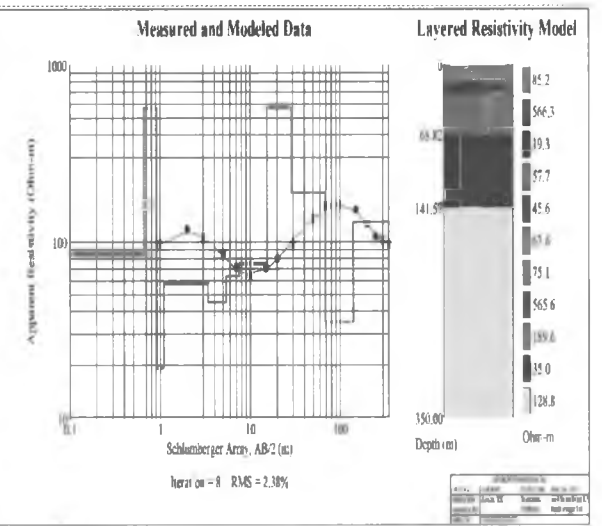
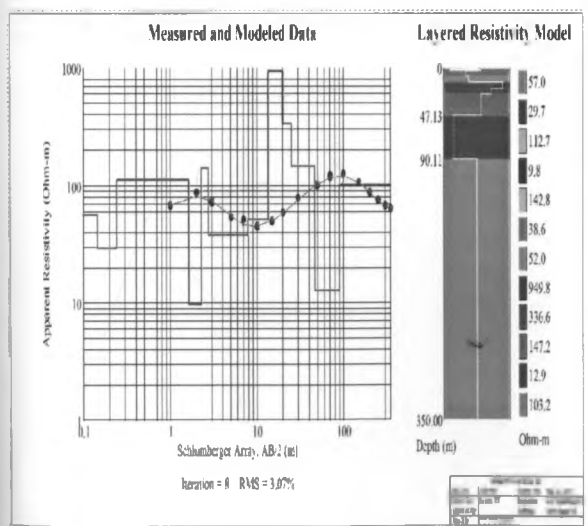


Figure 6.8xxvii. Interpreted model at station 27.

Figure 6.8xxviii. Interpreted model at station 28.

The geological interpretation of the models of the resistivity sections of the 1D resistivity soundings plotted in surfer; profiles 1 to 7 running North-South separated by 100m indicate the presence of a shallow material of coarse to very coarse sand of thickness between 45 to 60 metres spanning over some 300m in the north-south where the profiles cover in the depth ranging from about 10 metres to about 60 metres below the ground (Figures 6.9 a-g). Exceptionally, profile 7 (Fig. 6.9g) depicts a narrower thickness of about 50 metres which is slightly intruded by an intercalation of low resistivity material for about 45 to 90 metres at one point and then the previous materials continues to a depth beyond 300 metres deep. Profile 1 shows a change to the southern where the same material is noted from depth of 25 metres to 120 metres. This is confirmed by the tomography profile.1( Fig.5.13) running through BH 2 (previously BH1) where subsists an outstanding low resistivity layer(i.e. less than  $100 \Omega \text{ m}$ ) from the surface to a depth of about 10 m. From the depth of about 10 m to about 55 m, is a high resistivity layer (i.e. more than  $100 \Omega \text{ m}$ ). This is attributable to a similar layer of dry, loose volcano-sedimentary rocks confirmed by the geologic log results. The surfer profiles running in the West to East direction as indicated in Figures 6.10a-c, shows that the formations in the eastern end to be dipping, that is, considering the change of resistivities. The profile in Figure 6.11 shows a dipping in the western side. This faulting both in the eastern and the western side of the project area is confirmed by the magnetic profiles as subsequently discussed. Otherwise the general bedding of the formation is horizontal with the high resistivity ranges from about 10 metres to 50-80 metres below the ground. To the depth beyond 50-80 metres are low resistivity formations; revealing the approximate depth where the first groundwater rest level is expected.

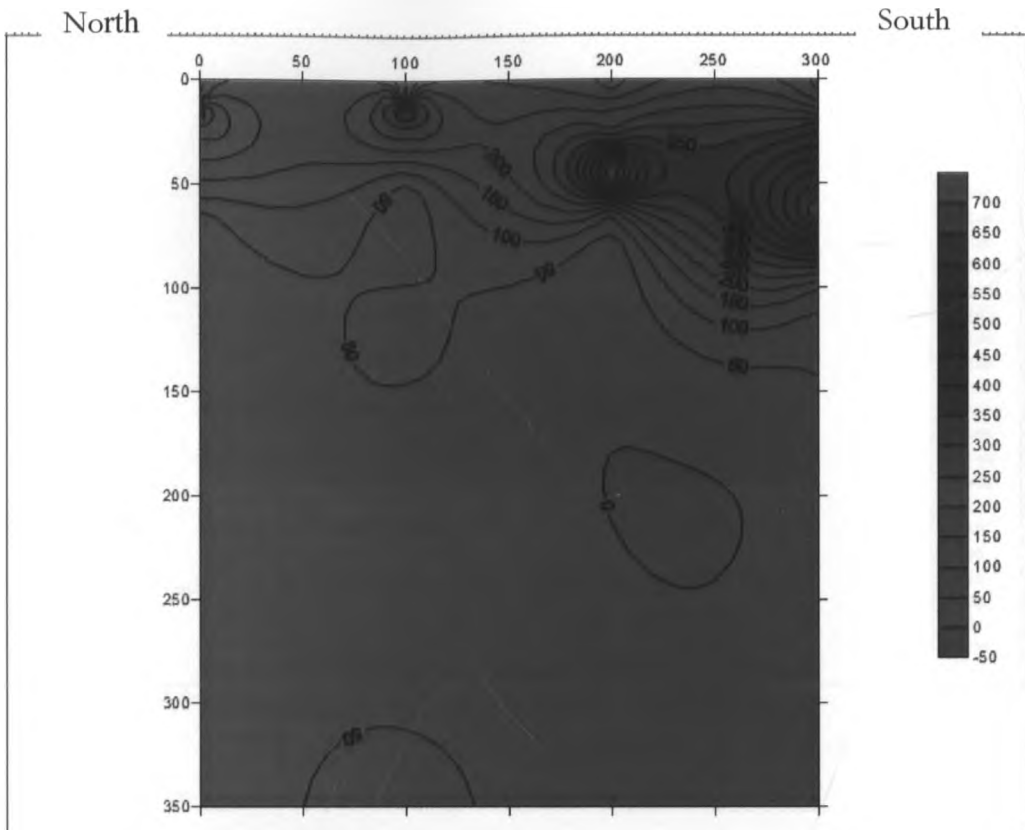


Figure 6.9a. Profile1 Vertical section of true resistivity in the N-S direction (contours in ohm.m).

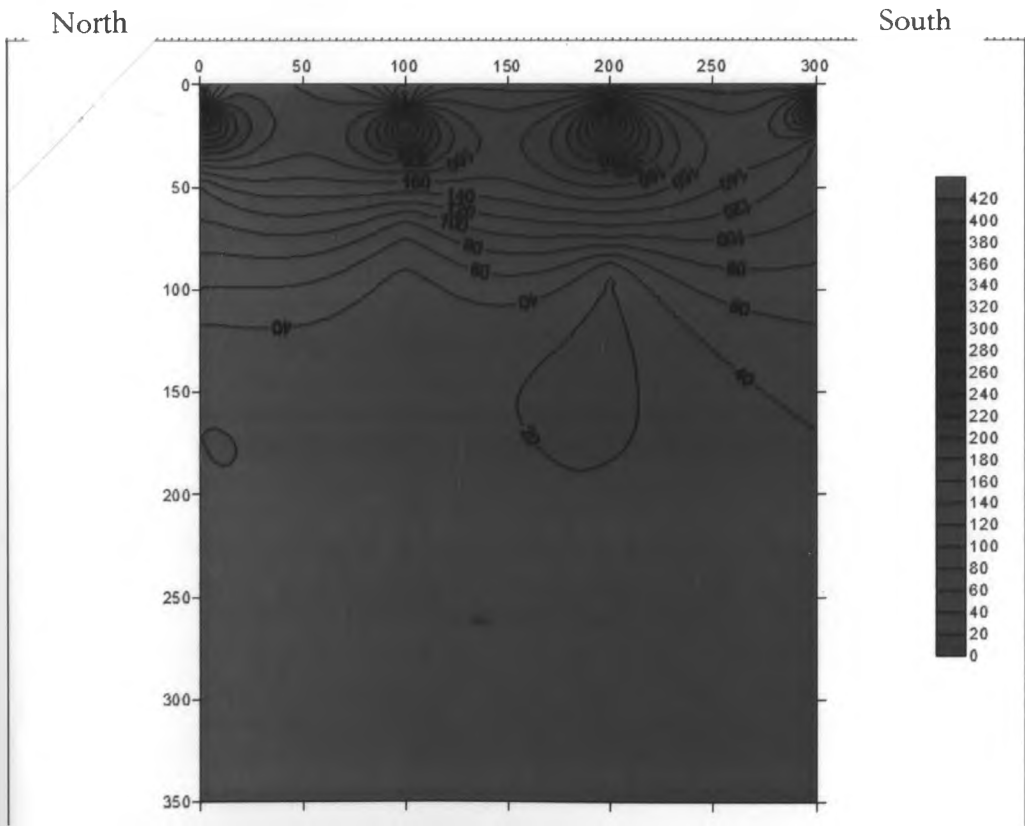


Figure 6.9b. Profile2 Vertical section of true resistivity in the N-S direction (contours in ohm.m).

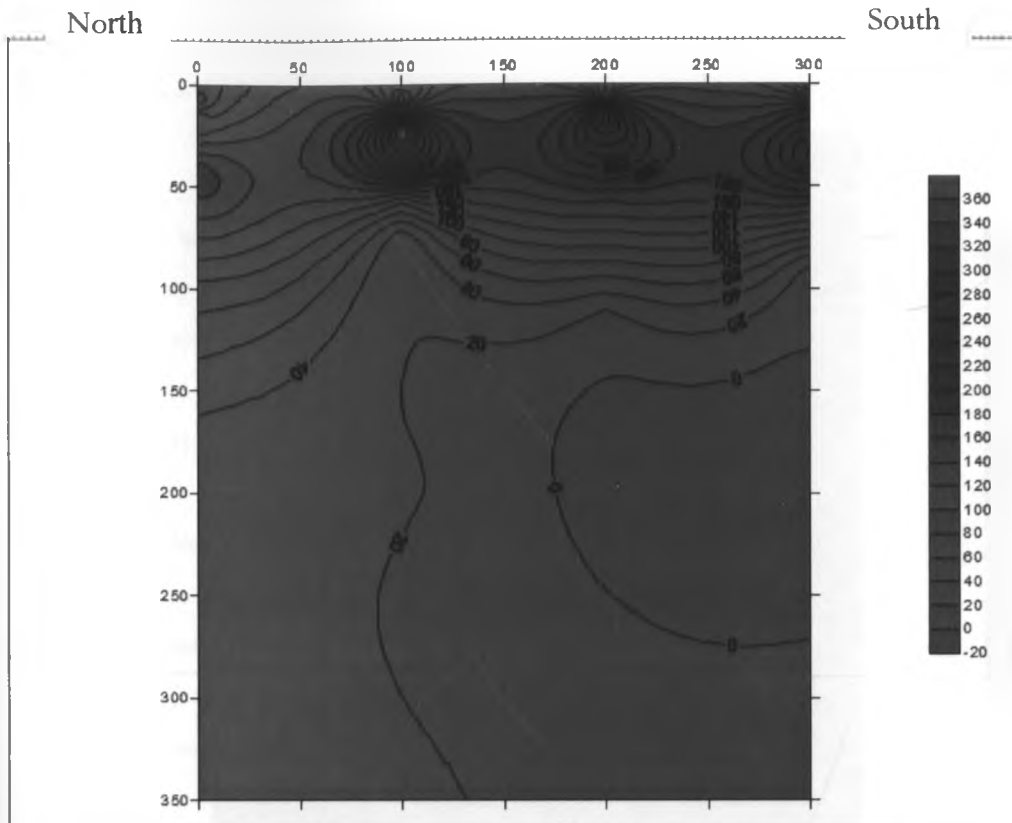


Figure 6.9c. Profile3 Vertical section of true resistivity in the N-S direction (contours in ohm.m).

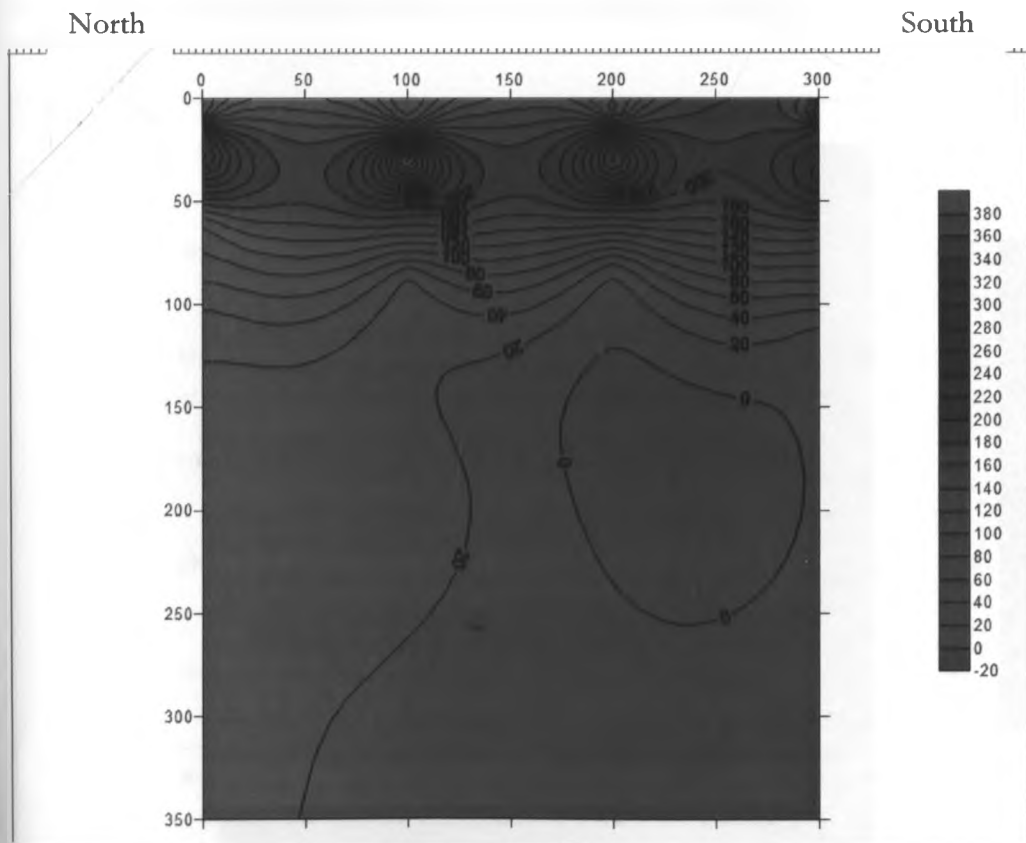


Figure 6.9d. Profile4 Vertical section of true resistivity in the N-S direction (contours in ohm.m).



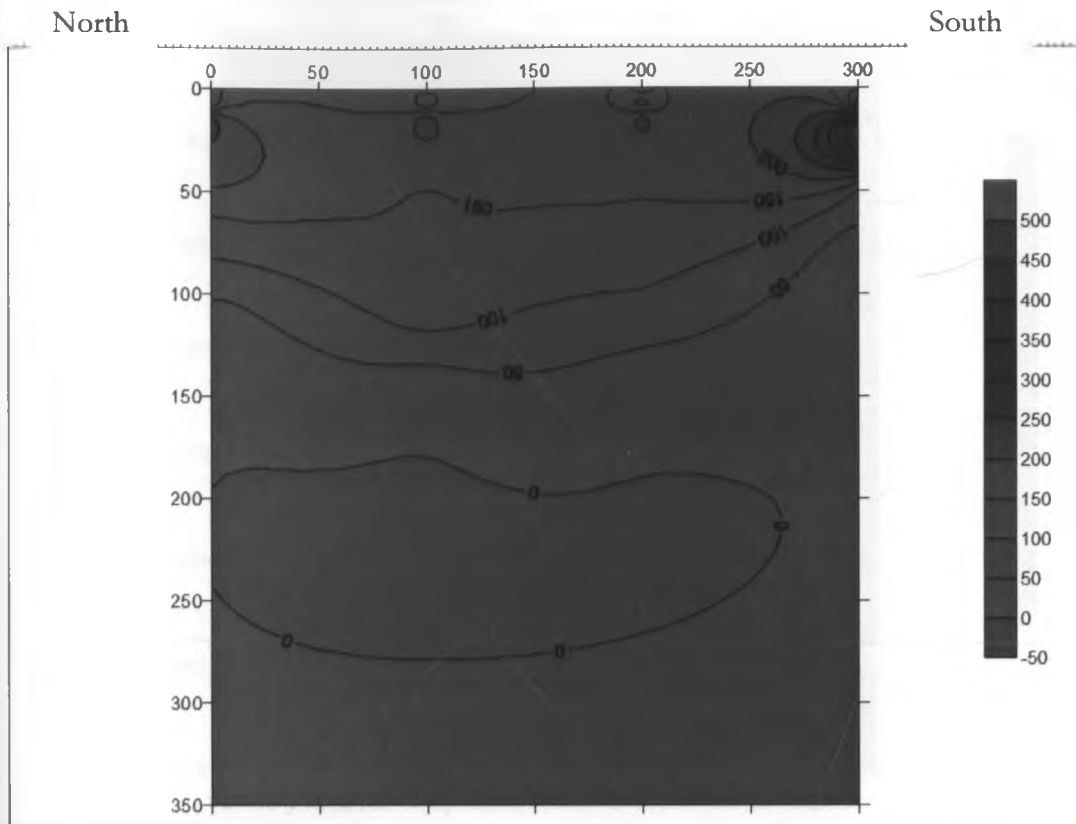


Figure 6.9e. Profile 5 Vertical section of true resistivity in the N-S direction (contours in ohm.m).

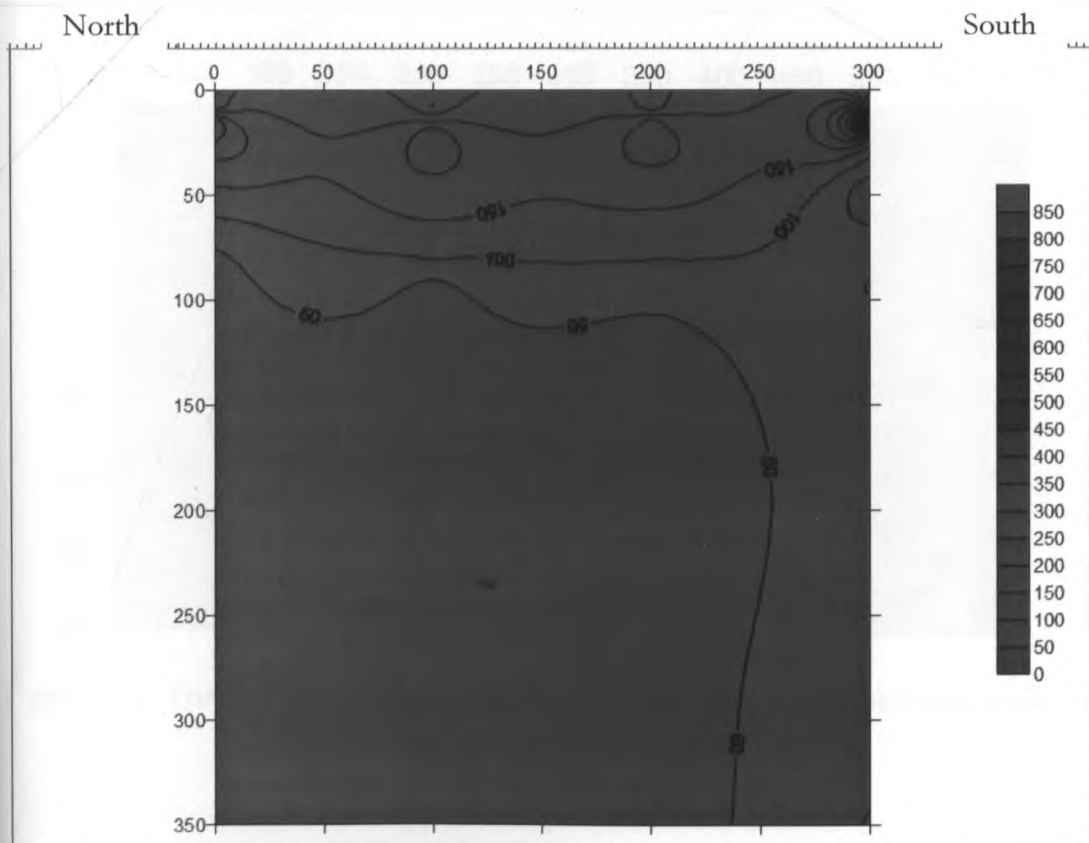


Figure 6.9f. Profile 6 Vertical section of true resistivity in the N-S direction (contours in ohm.m).

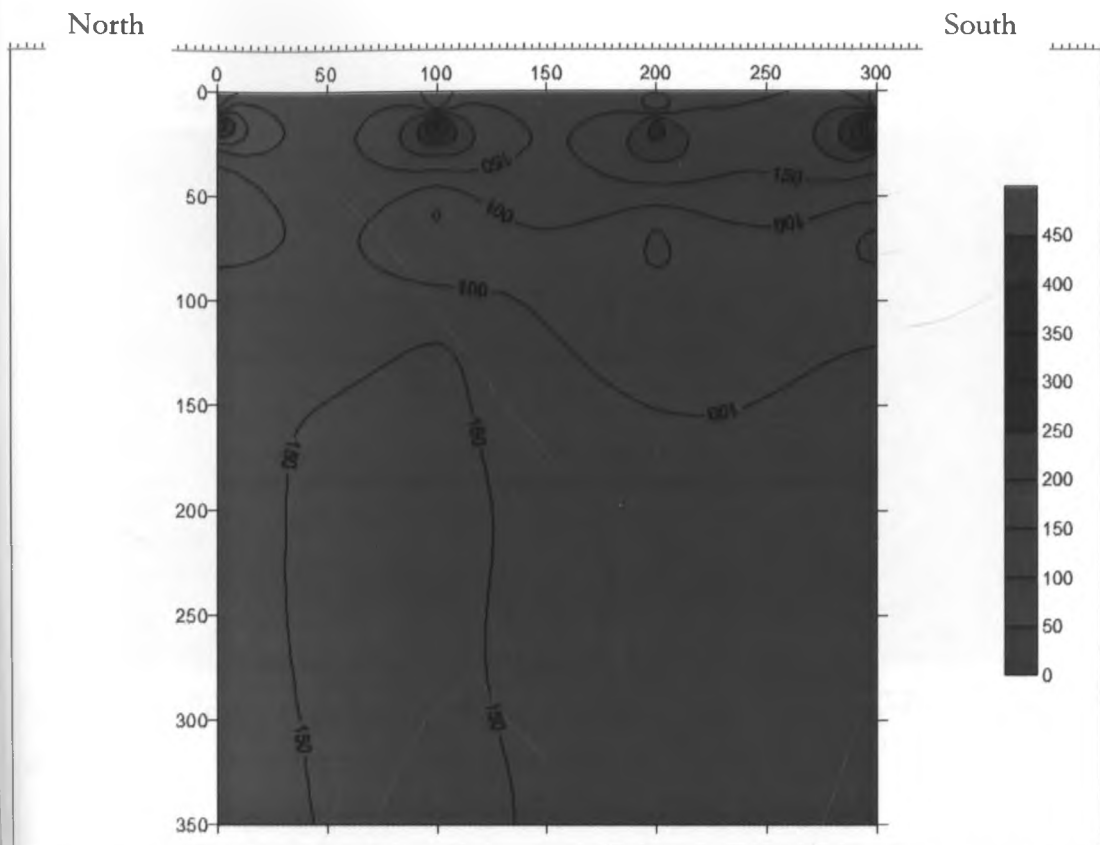


Figure 6.9g. Profile7 Vertical section of true resistivity in the N-S direction (contours in ohm.m).

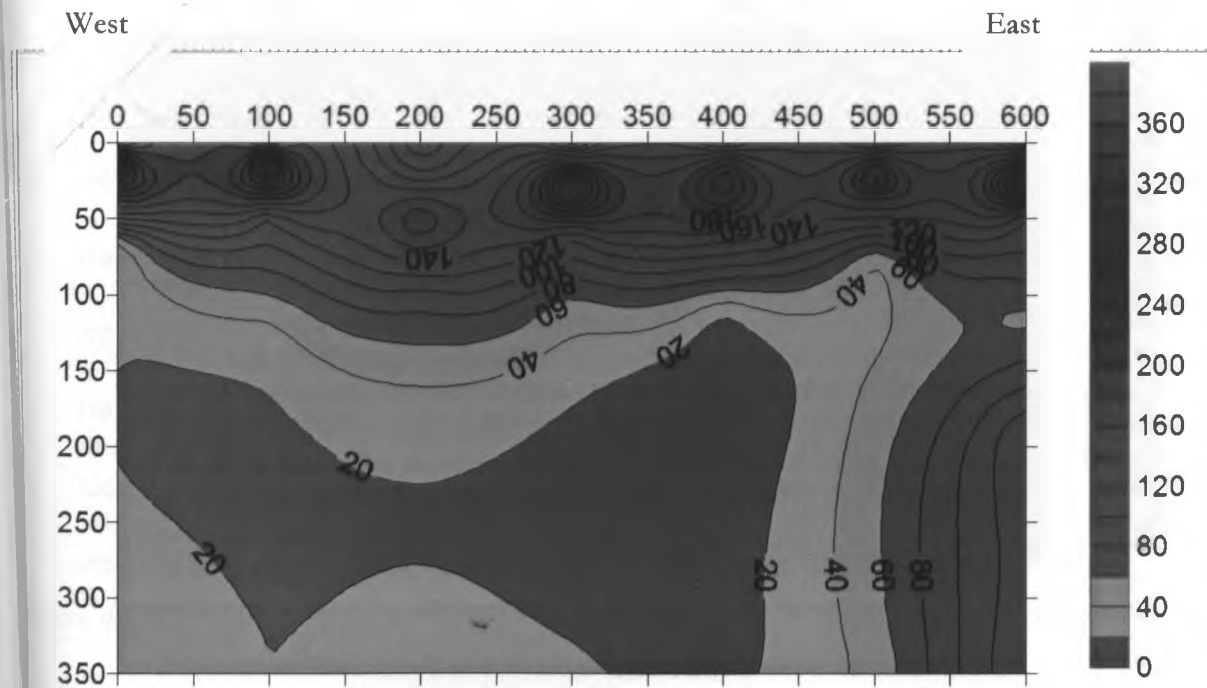


Figure 6.10a. Profile1 Vertical section of true resistivity in the W-E direction (contours in ohm.m).

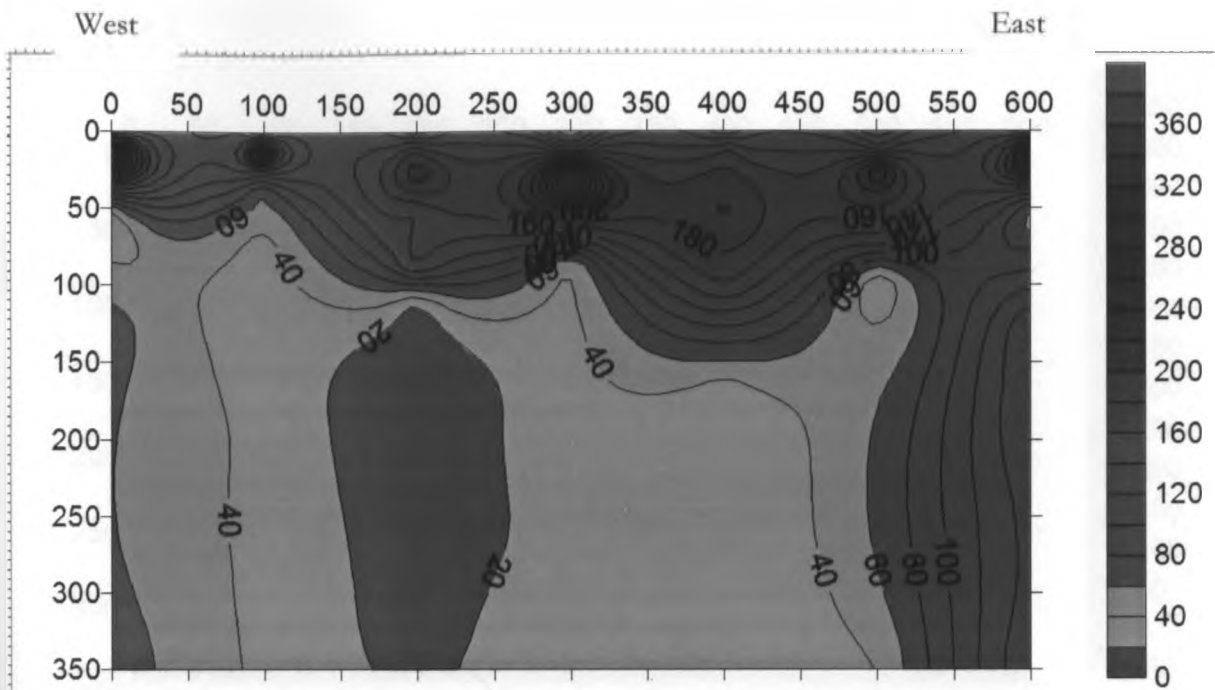


Figure 6.10b. Profile 2 Vertical section of true resistivity in the W-E direction (contours in ohm.m).

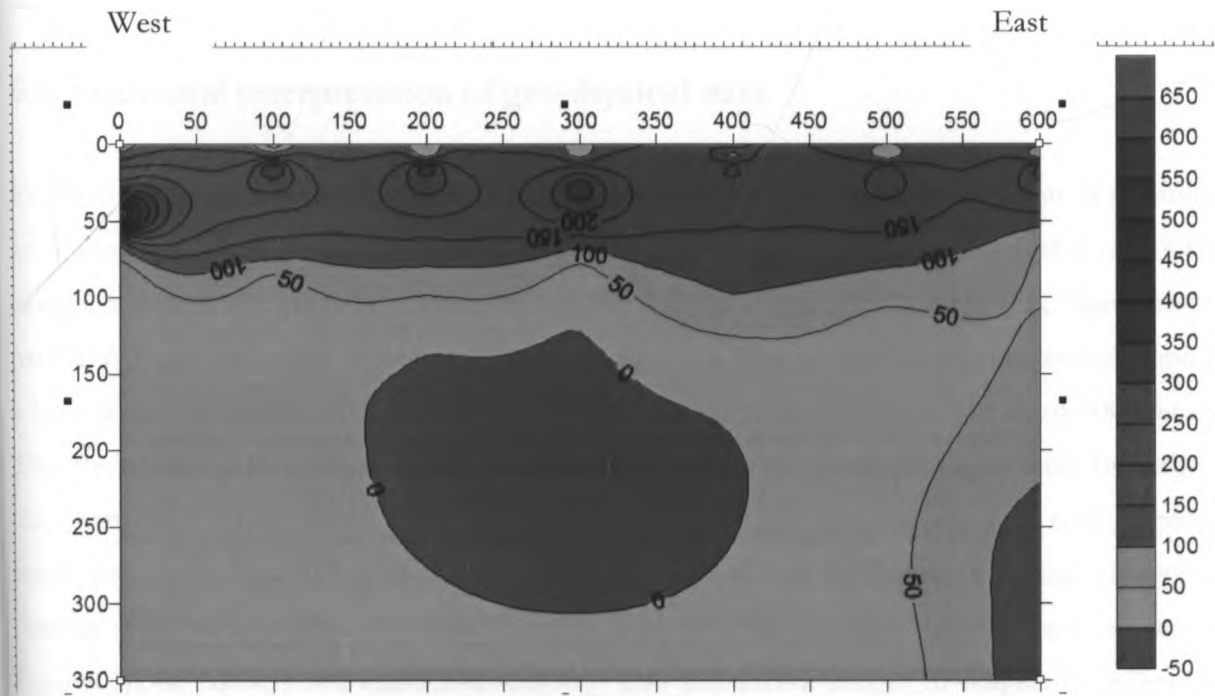


Figure 6.10c. Profile 3 Vertical section of true resistivity in the W-E direction (contours in ohm.m).

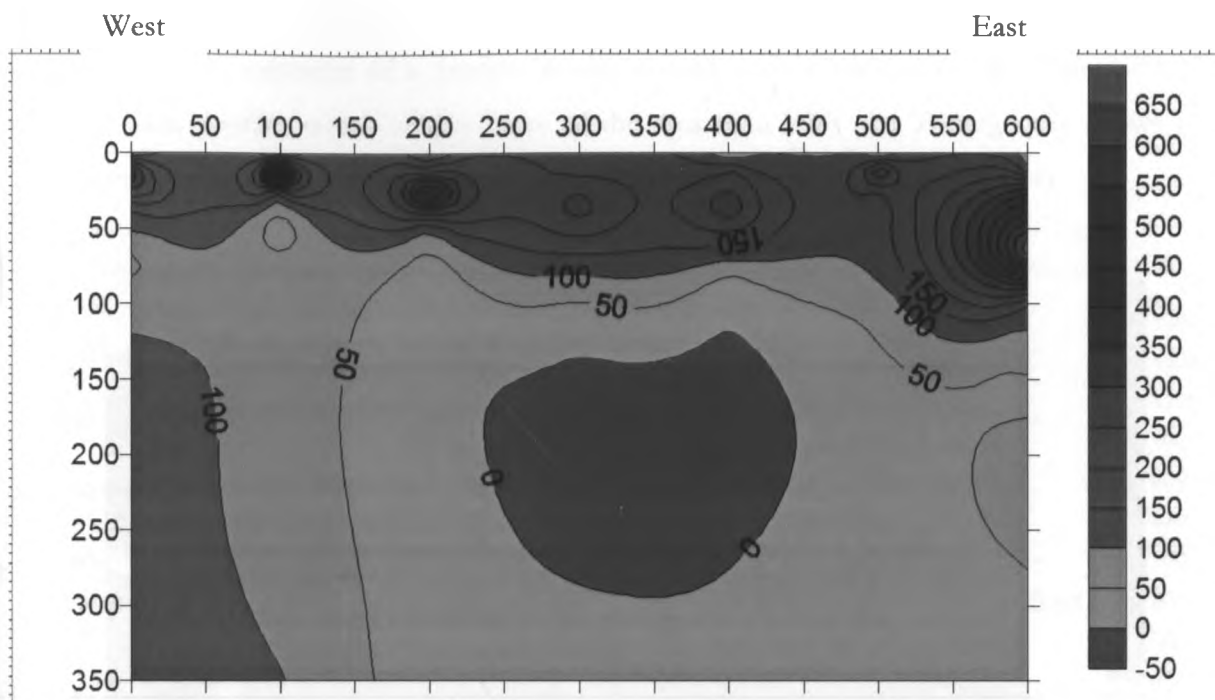


Figure 6.11. Profile4 Vertical section of true resistivity in the W-E direction (contours in ohm.m).

#### 6.4 Structural interpretation of geophysical data

Prominent structural features were not much in the mainly sedimentary environment of the study area. However, vertical and sub-vertical faults occur in areas close to the rift wall that marks the eastern margin and an area of a few metres to the western margin of the study area. Significantly, profile 7 (Fig. 6.9g.) which is running North-South in the Eastern side of the project area depicts a high resistivity material from the depth of about 10 metres to beyond the depth of 300 metres. This shows that at this point the formations are dipping against the general horizontal layering of the formations in the other profiles. This is also confirmed by Apparent resistivity contour maps made for depths of 50, 100, 150, 250, 300 and 350m shown in Figures 6.12 a-g. Magnetic profiles were done in the area in the West to East direction covering dimensions as shown in Figures 5.24a, 5.25a, 5.26a and 5.27a and they give subsurface images of magnetic susceptible materials to a depth of about 10 metres to about 60 metres. Similarly longer magnetic profiles were run in the area in the West to East direction covering 2500 metres, thus the project area being inside the grid. The interpreted magnetic profile ( Fig. 6.13) running 30 metres within the project area from the northern border indicates that at about 2000 metres to about 2300 metres the magnetic susceptible material tends to go deeper than other areas in the project area where it is shallower and horizontal. The dipping effect of the magnetic material along the eastern end of in Figure 13 and other profiles ( Appendix A, 1-4) shows a resemblance to VES and tomography

revelations of an existence of a faultline in the eastern end of the project area. Similarly, the magnetic data profiles which covers more of the area than VES and Tomography shows that there also exists a faultline to the western side of the project area ( Appendix A, 1-4).

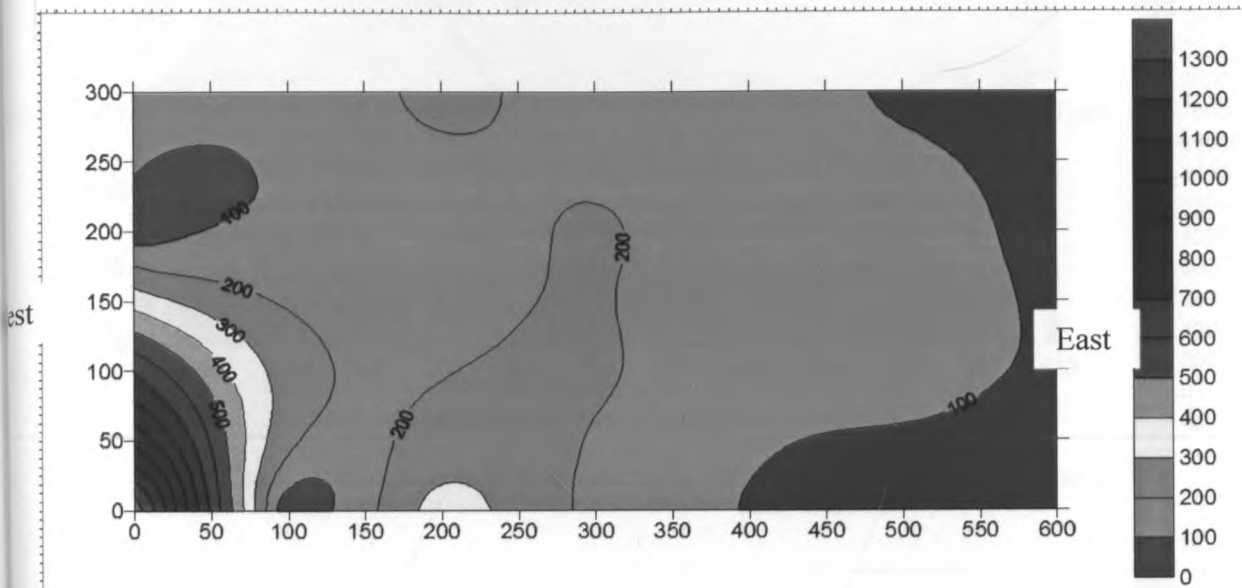


Figure 6.12a. Horizontal section of true resistivity at 50 m depth (contours in ohm.m).

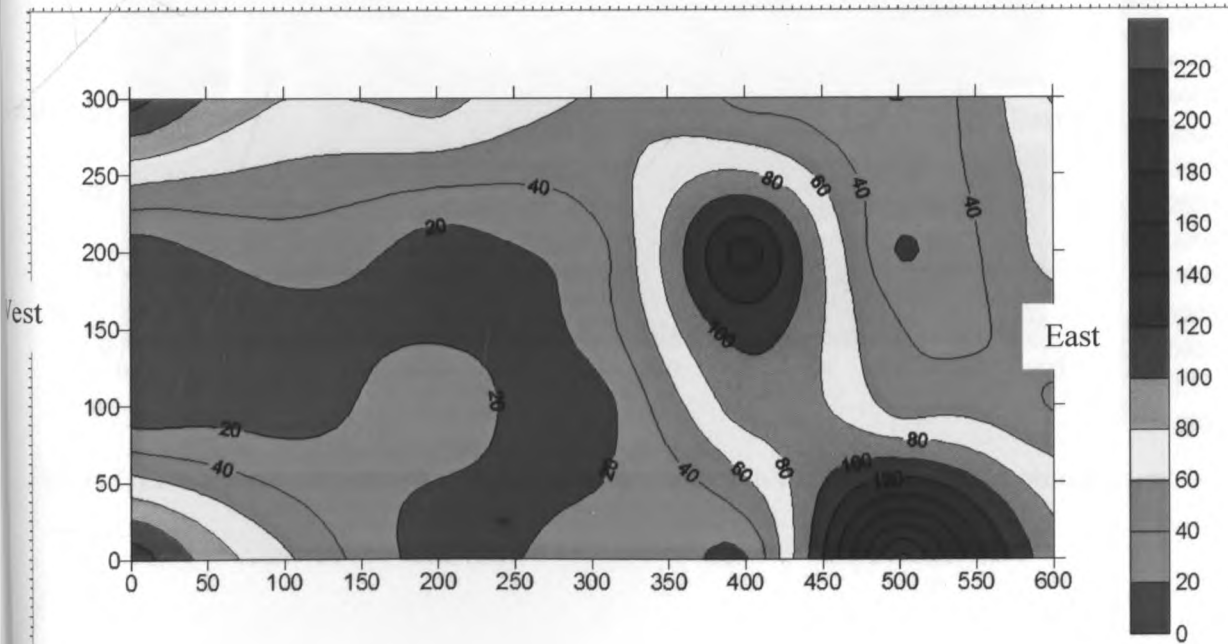


Figure 6.12b. Horizontal section of true resistivity at 100 m depth (contours in ohm.m).

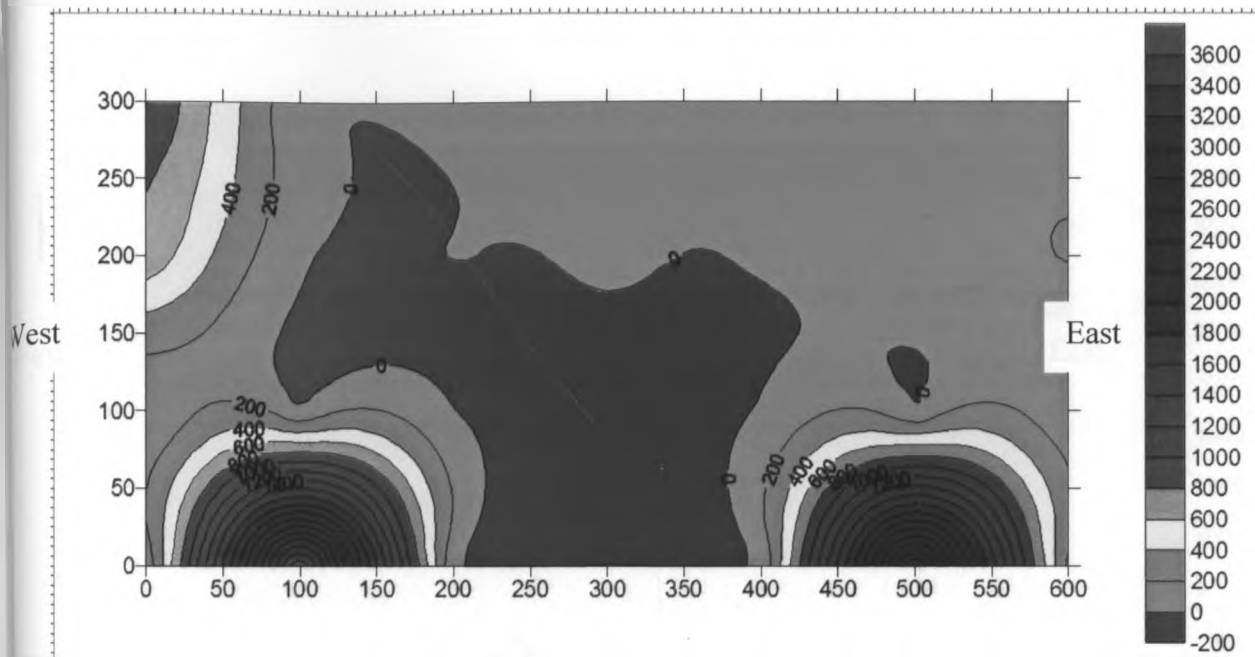


Figure 6.12c. Horizontal section of true resistivity at 150 m depth (contours in ohm.m).

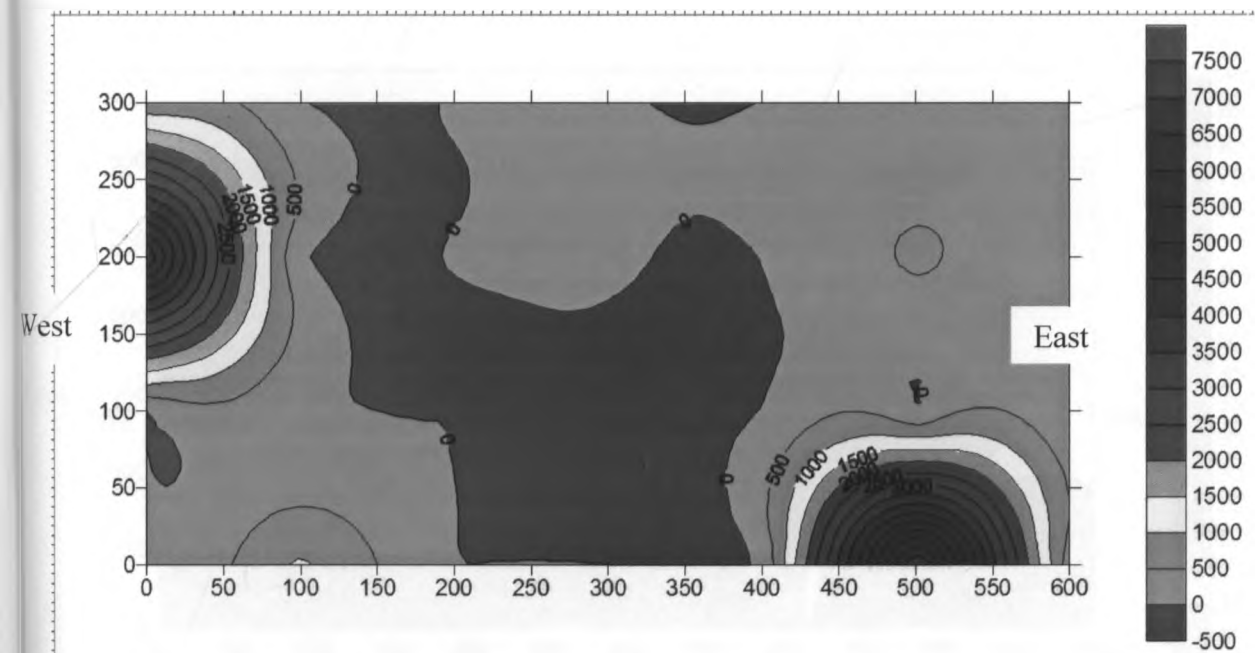


Figure 6.12d. Horizontal section of true resistivity at 200 m depth (contours in ohm.m).

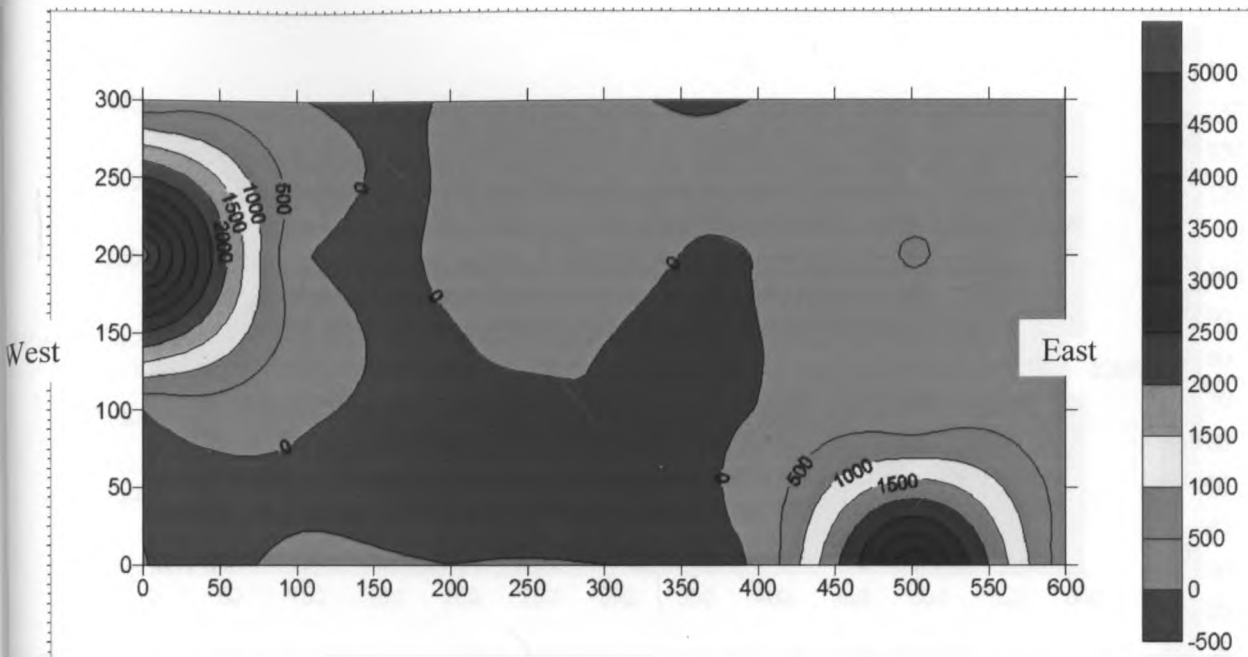


Figure 6.12e. Horizontal section of true resistivity at 250 m depth (contours in ohm.m).

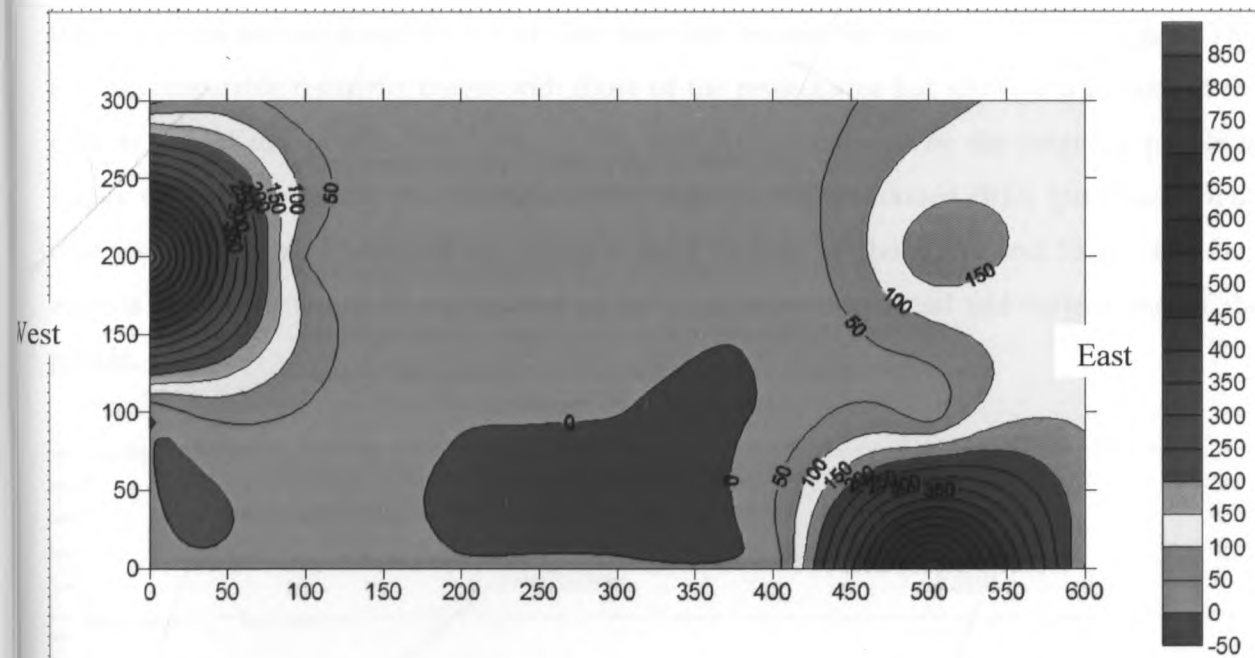


Figure 6.12f. Horizontal section of true resistivity at 300 m depth (contours in ohm.m).

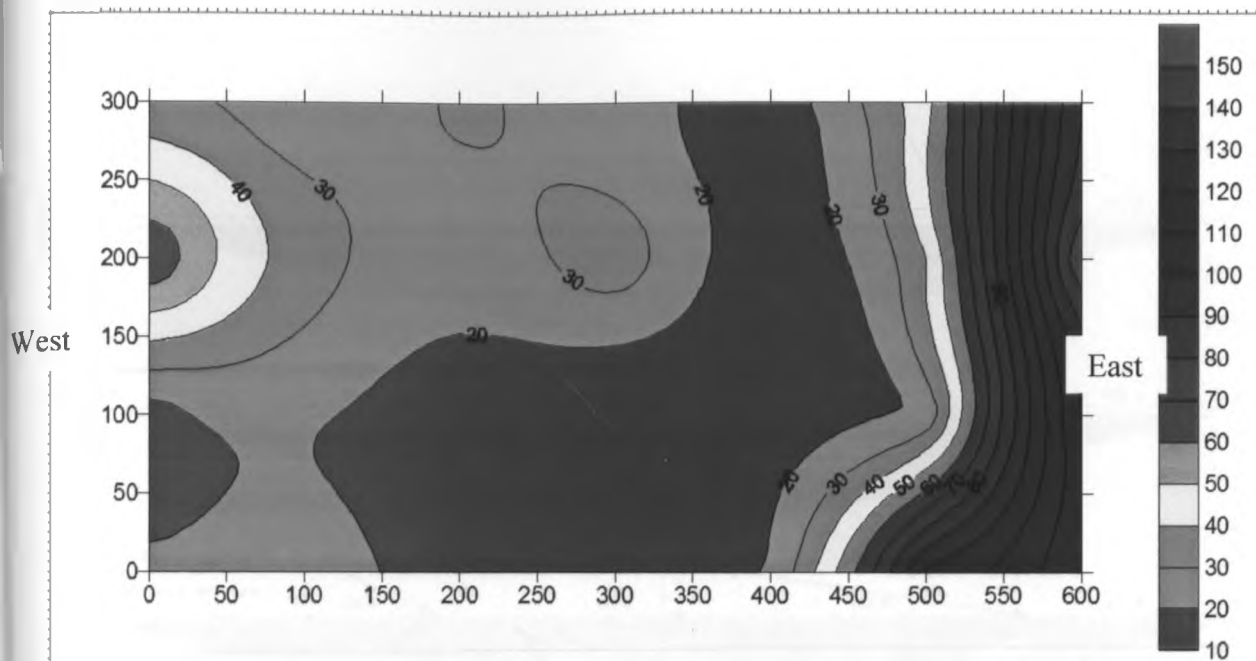


Figure 6.12g. Horizontal section of true resistivity at 350 m depth (contours in ohm.m).

Similarly, tomography profiles were done near the abandoned BHX which lies to the western of the study area and separated by a fault line and thus reveals the same subsurface picture. This shows comparable resistivity ranges with those of the project area but shows a fault zone at the eastern end of this profile (see Figure. 5.14.), and thus ascertained by the magnetic profile in Figure 6.15. The magnetic profile (Figure 6.16) through the abandoned BHX (previously BH2) demonstrates magnetic materials occupying a depth flanked by about 5 m and 55 m. The fault zone is evident at about 30 metres east of BHX, to the western end and eastern end of the profile.

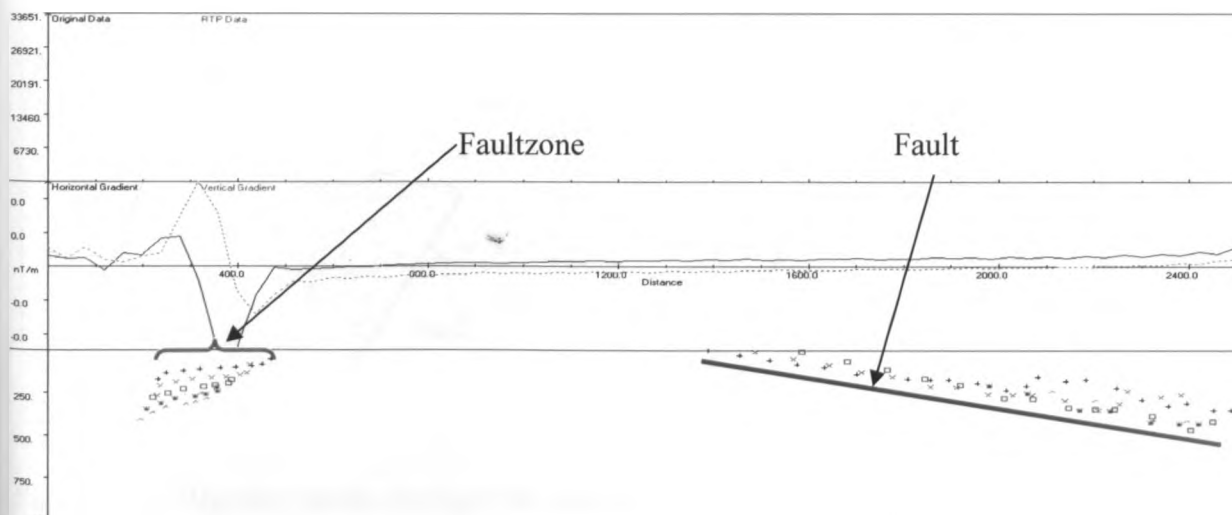


Figure 6.13. Magnetic profile processed to a depth of 1000m



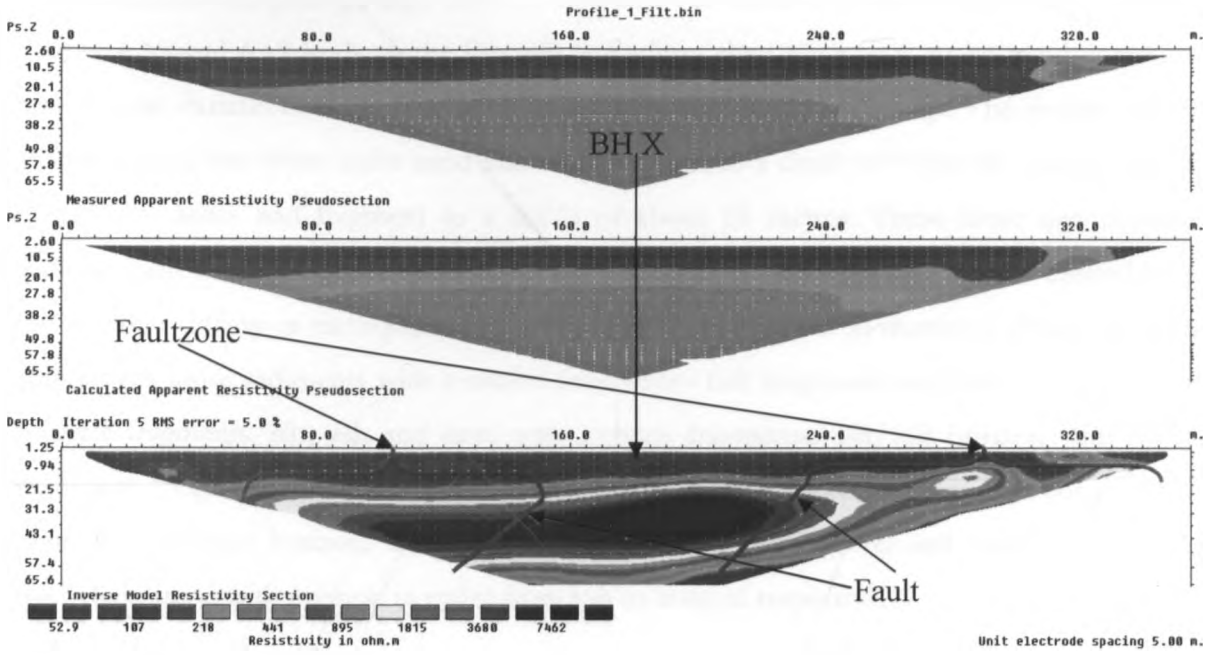


Figure 6.14. Profile 1 showing the vertical slice acquired from abandoned BHX.

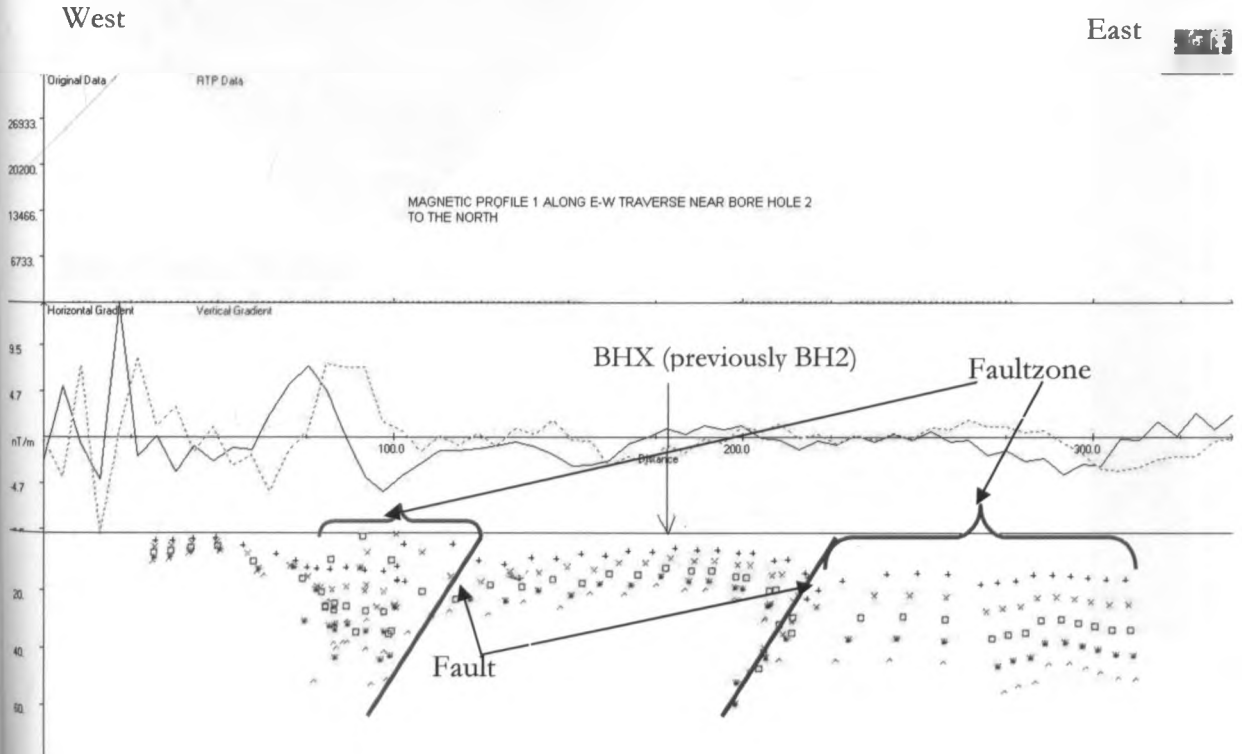


Figure 6.15. Magnetic profile through the abandoned BHX (previously BH2) showing magnetic materials occupying a depth flanked by depth of between 5 m and 55 m and fault zones.

## 6.5 Relationship between borehole lithology/structure and geophysical results and hence collapsing of boreholes

Examination of the geologic logs, ERT profiles and VES models of BHX and BH2, correlated in Figures 6.16 and 6.17 leads to the interesting findings that there seem to be good correlations between the variations in the formation resistivities and the geologic logs. The results from the analysis shows that there exists sand and silt formation to a depth of about 40 metres underlain by volcanic ashes and fragment to a depth of about 80 metres. These loose unconsolidated geologic materials are vulnerable to subsidence in circumstances where a void is created by any cause, either drilling or earthquake occurrence. The depth beyond 80 metres to about 300 metres consists of loose sediments with rounded fragments:- tuff fragments; ash horizon with tuff and trachyte fragments, silt, ash and sand with pumice fragments, ash/tuff horizon with trachyte fragments; tough trachyte rock, tough trachyte with some tuff, loose volcanic ash horizon, tough phonolitic trachyte horizon, horizon of alternated weathered gravel and mud and weathered trachyte horizon with pumice; in order from top to bottom respectively.

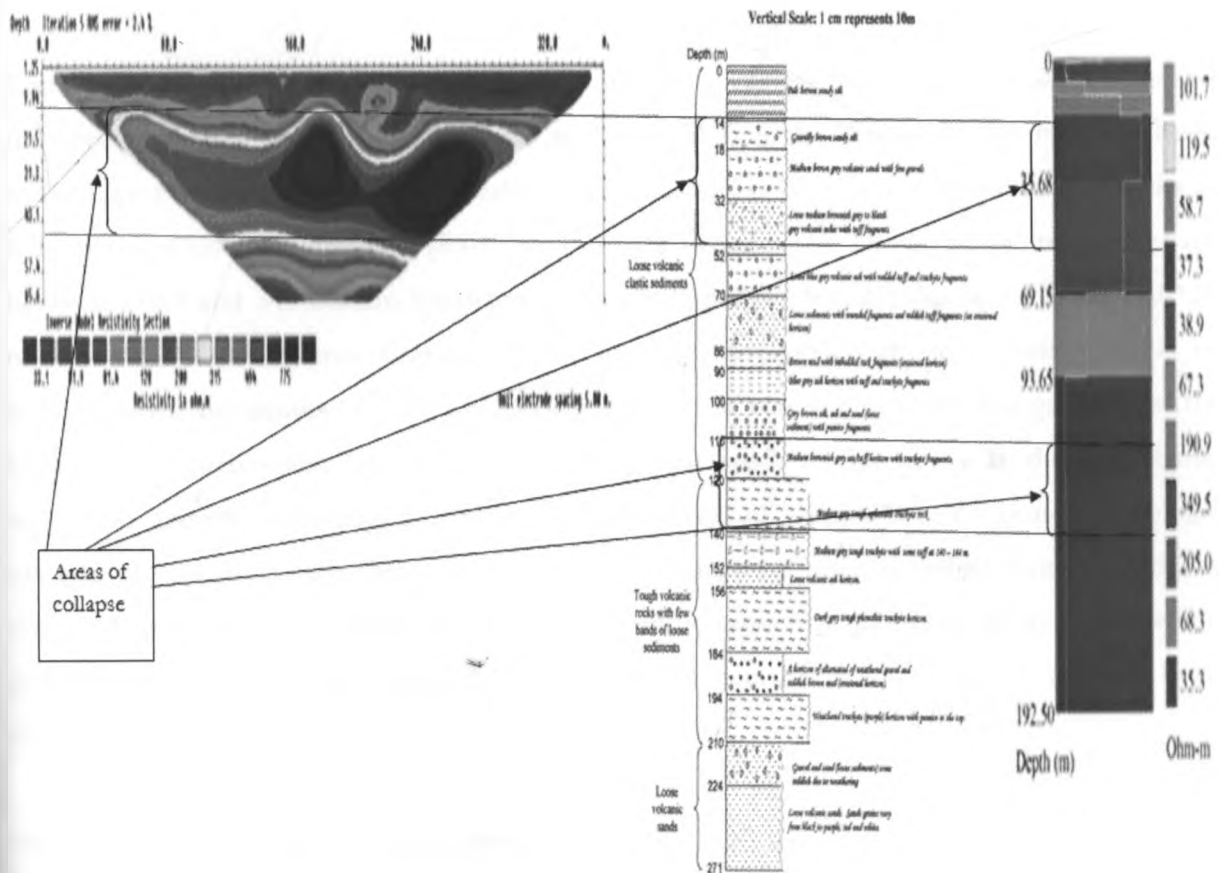


Figure 6.16. Shows correlation of ERT profile, geologic log and VES model and the specific areas where collapsing occurred during drilling of BH2.

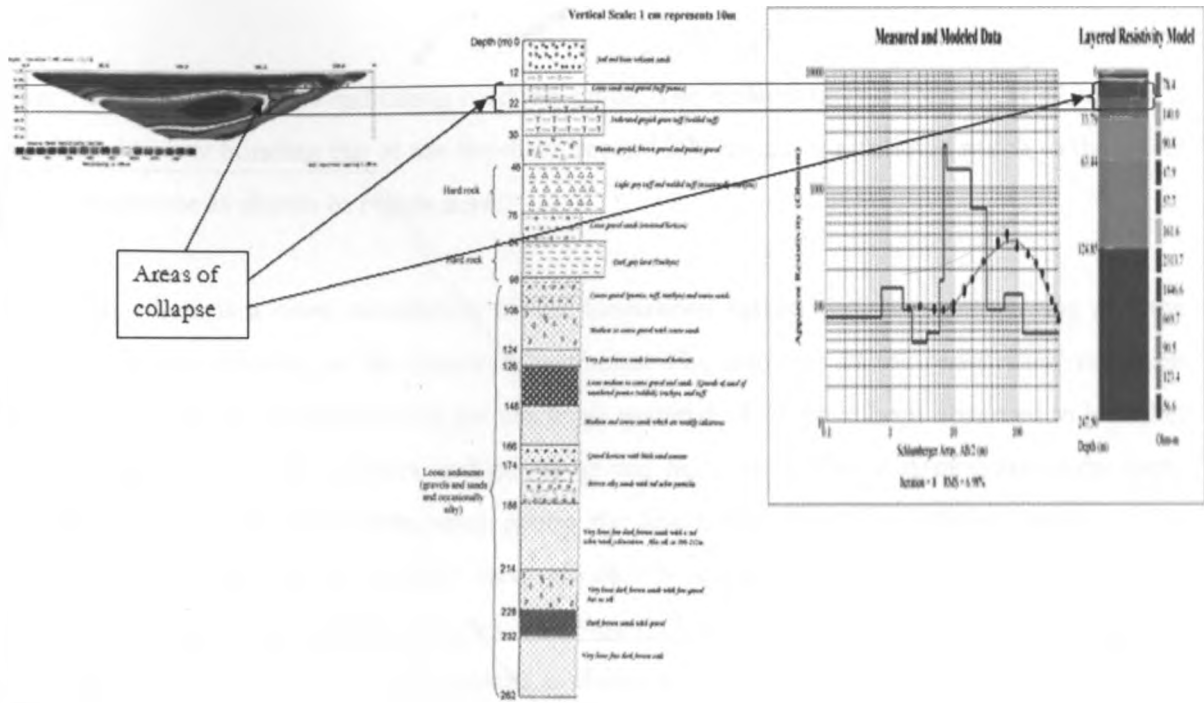


Figure 6.17. Shows correlation of ERT profile, geologic log and VES model and the specific areas where collapsing occurred during drilling of BHX.

Considerations have been made regarding the resistivity values, the borehole geologic logs and the specific depths where collapsing was recorded during the drilling of the two boreholes studied (i.e. boreholes 2 and X). In borehole 2, the areas of collapse are indicated at the depths of 8-24 metres, 110-139 metres and 189-195 metres (see Figure 6.16). The formation resistivities are between 190.9 and 349 ohm.m for depths of 8-24 metres, less 35 ohm.m for both 110-139 metres and 189-195 metres. Considering the lithologic formations at these levels, there is an indication that the depths of 8-24 metres is dominantly of very coarse sands and gravels and for both 110-139 metres and 189-195 metres are silty clay sands to fine sands. In the very coarse sands and gravels; collapsing is attributed to low levels of compaction, no bonding geologic material present, thus high chances of free fall of the material once disturbed. Consequently, in the silty clay sands to fine sands; clay is dominant and considering that these are the levels where groundwater is found, high chances of liquefaction hence the free flow of the material once disturbed.

Having the same application to the abandoned borehole X; the areas of collapse are indicated at the depths of 15-32 metres (see Figure 6.17) and beyond 200 metres where more than 50 metres formation range collapsed. The formation resistivities are between greater than 94 ohm.m for depths 42 metres which is indicative of very coarse sands and pebbles, less 56 ohm.m for both

depth beyond 200 metres indicating medium sands. The collapsing at the depth of 42 metres is attributed to low bonding but at the depth of beyond 200 metres is attributed much to the effect of the faultzone as shown in Figure 5.14.

Generally, there is a close correlation of the formations resistivities, the geologic log and the component of collapsing in the observed boreholes. The extremes of the resistivities( very high and very low) gives the extremes of the lithologic material which have been observed to be either dominantly coarse sands, pebbles and gravels giving high resistivities and/or dominantly clayey formations at depths filled with water giving the low resistivities. The extreme points of the lithologic formation are the specific areas affected by collapsing. It is important to note that formation outside the aforementioned lithologies are the areas where faulting has greatly increased the borehole collapsing problem as shown in the analysis of the abandoned borehole X. Thus the loose materials are a recipe for collapsing of the freshly drilled boreholes in this area, a problem addressed by this study.

## 6.6 Groundwater

The Olobanita well-field is renown for its high yields from boreholes tapping the aquifers in the well-field. The sounding curves (Figs.6.8i-xxviii) are very analogous which shows a KHKHK type curve with ten to twelve geoelectric layers having distinct resistivities and thicknesses. The curves and the resistivities show wet section of the formation of low resistivity at about 5 to 20 metres. The aquifer levels are noted from the depth of about 60 metres, the second aquifer at about 80 metres, the third aquifer at 120 metres and the fourth aquifer about 160 metres and a high potential aquifer at 260 metres below the ground as shown by the presented VES interpreted results. But considering the drilling results of BH2 (previously BH1) shows that in this particular point minor aquifers were noted at depths of 140-142, 182-184, 208-217 and 238-252 metres below the ground.

## CHAPTER SEVEN

### 7.0 CONCLUSION AND RECOMMENDATIONS

Nakuru town and its peri-urban areas use mainly groundwater from the the main aquifers; Olobanita, Kabatini and Baharini for domestic and industrial activites. The existence of buried river channels ( in Kabatini and Baharini) and faultlines and thick sedimentally formations ( in Olobanita) are believed to be the cause of the high yielding boreholes. However, despite the high yields in Olobanita some have been abandoned as a result un economical yields. Others were abandoned at the time of drilling mainly due to either the presence of excessive silt and clay resulting in the caving in of walls or the encounter of hard rock boulders(volcanic fragments).

The VES (VES) and the 2D Resistivity imaging allowed a distinction to be made between very high resistive volcanic sands, the moderately high resistivity freshwater saturated zone and the very low resistive clays in localised areas. The geological interpretation of the surveys correlated very well with the borehole data. Vertical faults have resulted in minor down-throwing of blocks in areas close to the rift wall on the east and some few metres to the west margins of the research area. The loose silts and volcanic sands of thick depths, the volcanic rock fragments were established to be the common causes of collapsing and blockage of freshly drilled boreholes.

2D, VES and magnetic models of the of the subsurface information of the research area have been presented. Also Apparent resistivity contour images made for depths of 50, 100, 150, 250, 300 and 350m were made. The findings of the study agree fairly well with all the available ground information and also provide answers to the groundwater problems currently existing in the study area.

Based on this work the following recommendations have been made;

- Drilling by use of mud instead of compressed air is ideal in these area which is affected by collapsing of fresh borehloes. Mud helps in consolidating the loose materials immediate to drilling rig, thus couters the caving in effect.
- It is recommended that the wells should be drilled with modern equipment preferably geophysically logged with Long Normal (LN) and Short Normal (SN) resistivity, SP, natural gradient, caliper and gamma - gamma radiation (neutron).

- Grouting should be applied during the drilling process. Grouting is the act of injecting certain substances into the void of earth materials to reduce or eliminate their permeability, consolidate them, or increase their strength. Grouting or cementing well casing involves filling the annular space between the casing and the drilled hole with suitable slurry of cement or clay.
- Some wells must be drilled and preserved solely for observation purposes (i.e. they should not be used for production purposes) to help in regulation of the extraction of ground water from this well field.

## REFERENCES

Anderson, N. L., 2006. Selection of Appropriate Geophysical Techniques: A Generalized Protocol Based on Engineering Objectives and Site Characteristics. Proc., 2006 Highway Geophysics- NDE Conference, 2006, pp. 29–47. Available at <http://2006geophysics.mst.edu/>. Available at [http://onlinepubs.trb.org/onlinepubs/nchrp/nchrp\\_syn\\_357.pdf](http://onlinepubs.trb.org/onlinepubs/nchrp/nchrp_syn_357.pdf).

Ayeneu, T. & Becht, R., 2008. Lakes comparative Assessment of the Water Balance and Hydrology of selected Ethiopian and Kenyan Rift Lakes, Lakes & Reservoirs: Research and Management 2008 13: 181–196. Journal compilation © 2008 Blackwell Publishing Asia Pty Ltd.

Barongo, J. O., 2008. Groundwater exploration in Nakuru basin. [report] (Personal communication, 2 June 2010).

Clarke, M. C. G., Woodhall, D. G., Allen D. & Darling, G., 1990. Geological, volcanic and hydrological controls on the occurrence of geothermal activity in the area surrounding Lake Naivasha, Kenya. Kenyan Ministry of Energy, Nairobi, Kenya.

GOK, 1999. Sessional Paper No. 1 of 1999 on National Policy on Water Resources Management and Development.

Institute of Economic Affairs, 2007. A Rapid Assessment of Kenya's Water, Sanitation and Sewerage Framework. Published by the IEA 5th Flr. ACK Garden House, 1st Ngong Avenue, Nairobi, Kenya.

Keller, G.V., & Frischknecht, F.C., 1966. Electrical Methods in Geophysical prospecting. Pergamon Press, 517 pp.

Kuria, Z. N., 2006. Hydrogeology notes. Published by the University of Nairobi, Nairobi Kenya.

Kuria, Z.N., 1999. Hydrogeology of Lake Nakuru Drainage Basin using GIS data and electrical resistivity survey, Unpublished M.Sc. Thesis, University of Nairobi, Nairobi, Kenya.

Loke, M.H. & Barker M.,1996. Rapid least-squares inversion of apparent resistivity pseudosections by a quasi-Newton method, *Geoph. Prosp.*, 44, 131-152.

Mathu, E.M., 2008. Groundwater exploration in Nakuru basin. [report] (Personal communication,10 June 2010).

McCall, G. J. H., 1957. Geology and Groundwater conditions in the Nakuru area. Technical Report No. 3, Ministry of Works (Hydraulic Branch), Kenya.

McCall, G. J. H., Baker, B. H. & Walsh, J., 1965. Late Tertiary and Quaternary sediments of the Kenya Rift-Valley. Paper read at Symposium No. 29, Wenner-Gren Foundation for Anthropological, Vienna.

Mooney, H. M. & Wetzel, W. W., 1956. The potentials about point electrodes and apparent resistivity curves for a two, three and four layer earth. University of Minnesota press.

MoWI, 2006. The National Water Resources Management Strategy (NWRMS) (2006-2008): First Edition - January 2006, Nairobi.

Nyambok, I.O. Bhogal, P.S. & Bwire-Odhiambo, S., 1993. Hydrogeology and hydro geochemistry of the groundwater resources of the Rift Valley, Nakuru North, GSK, Report, Proceedings of the Fifth conference on the Geology of Kenya, Nairobi, Kenya 92p.

Reynolds, J.M., 1998. An introduction to applied and environmental geophysics: Wiley and Sons.

Robert B. & David H., 2002. Towards an understanding of human impact upon the hydrology of Lake Naivasha. *Hydrobiologia* 488, 1-11.

Serson, P.H., 1962. A Simple Proton Precession Magnetometer, Dominion Observatory, Ottawa, Canada, 1962 Serson, P.H., U.S. Patent No. 3,070,745, 1962.



Sirles, P. C., 2006. NCHRP Synthesis 357: Use of Geophysics for Transportation Projects, Transportation Research Board of the National Academies, Washington, D.C., 2006.

Sporry, R., 2001. Lecture material on Resistivity. Earth System Analysis Department, ITC.

Tuinhof, A., 2001. "Groundwater Resources Component." In World Bank Mission Aide-mémoire, Kenya Water Resources Management Strategy, September 2001.

World Bank, 2000. World Development Report 2000/2001: Attacking Poverty. World Bank, Washington, D.C.

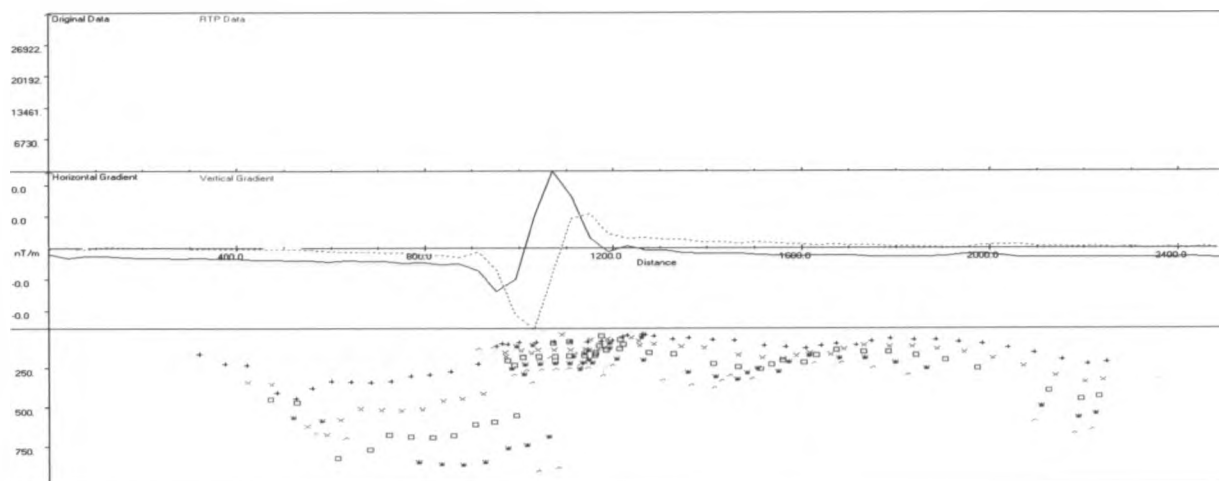
Yujie Shi., 2008. Rift Valley Water Supply and Sanitation Project Nakuru works. ZHONGHAO Overseas Construction Engineering Company limited. [report] (Personal communication, 20 December 2009).

# APPENDICES

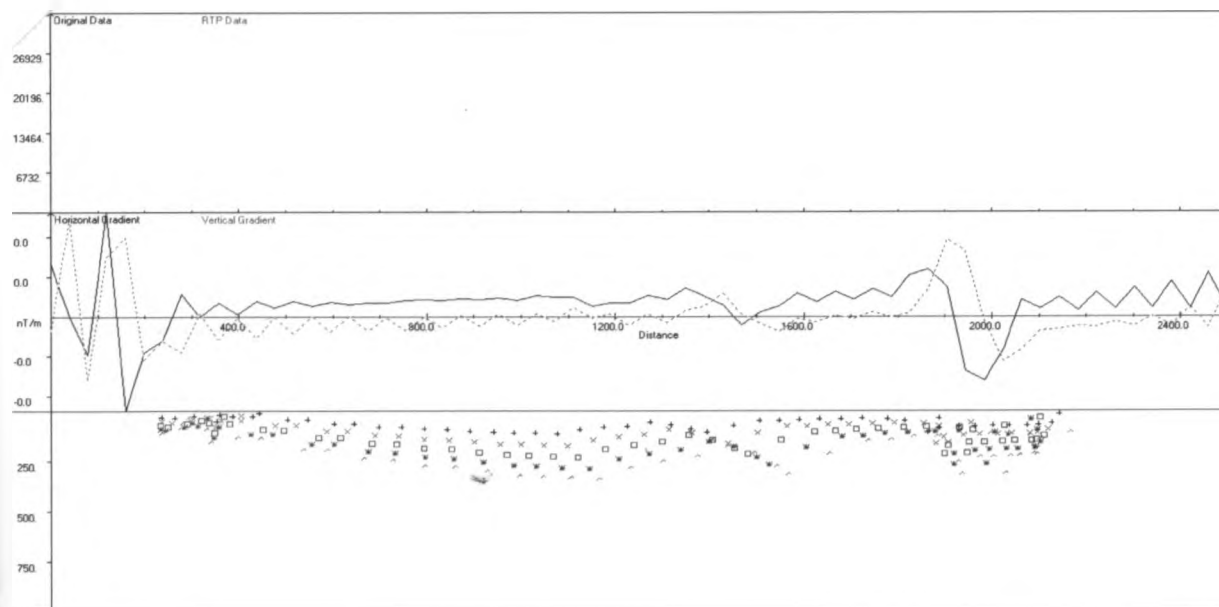
## APPENDIX A

1. Magnetic profiles (1-4) run in the area in the West to East direction covering 2500 metres at intervals of 100 metres showing subsurface magnetic materials and faultzones.

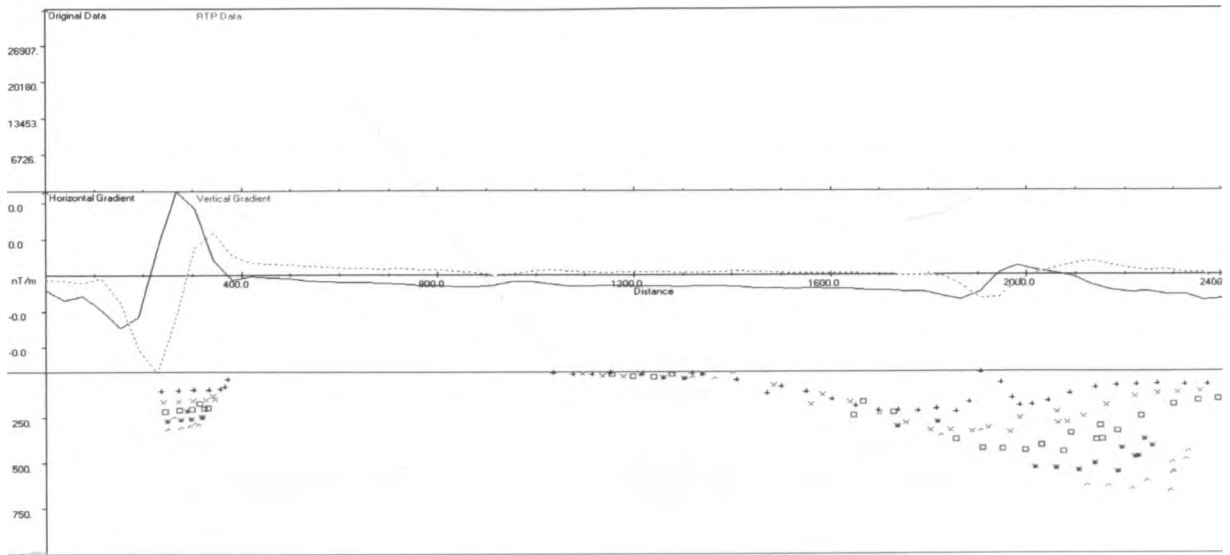
### 1. Magnetic profile 2 to a depth of 1000m



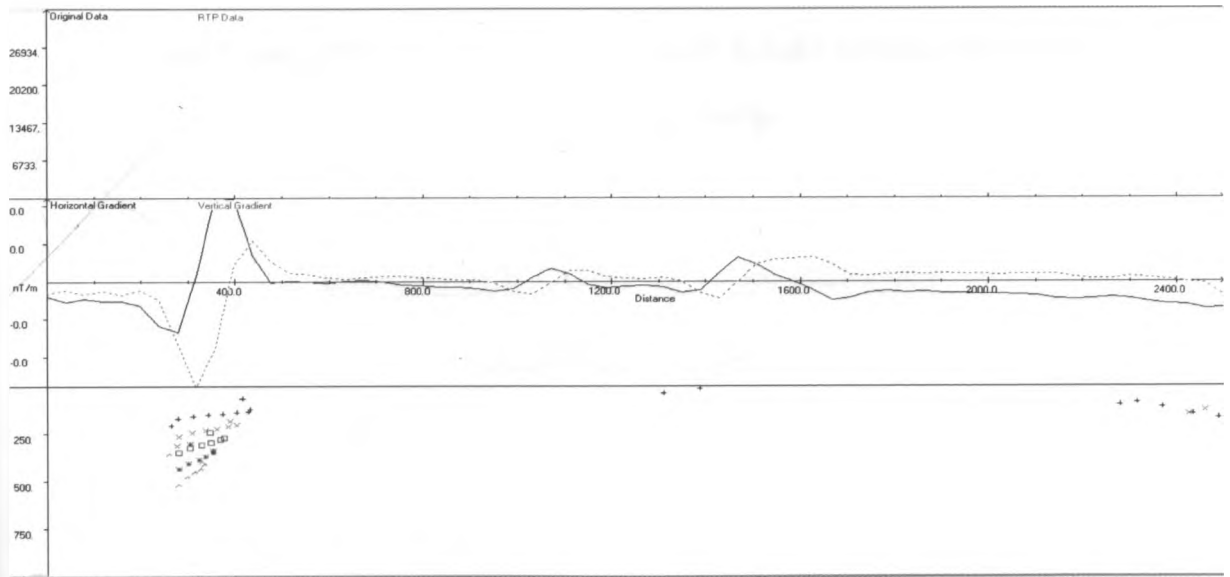
### 2. Magnetic profile 3 to a depth of 1000m



### 3. Magnetic profile 4 to a depth of 1000m



### 4. Magnetic profile 5 to a depth of 1000m



## APPENDIX B

1. Concrete field data on borehole completion report-Olobanita Borehole No. 1 showing areas affected by collapsing during drilling operations.



GAUFF INGENIEURE GmbH & Co KG - JBG  
Bernstrasse 45  
D-60437 Frankfurt am Main  
Germany

Tel: +49-69-5 00 08-0  
Fax: +49-69-5 00 08-111  
E-mail: jbgafnca@gauff.com



**RIFT VALLEY WATER  
SERVICES BOARD**

Giddo Plaza - Office 25  
George Morara Road  
P.O BOX 2451  
NAKURU, KENYA

Tel: +254 - 51 - 2213557  
E-mail: rvwsb@afncaonline.co.ke

### **RIFT VALLEY WATER SUPPLY AND SANITATION PROJECT NAKURU WORKS**

### **BOREHOLE COMPLETION REPORT**

**OLOBANITA BH NO.1**

PREPARED BY : PETER NJOROGE GITAU  
COMPILED BY : JOSHUA ICHANG'I WERU

JULY 2008

**BOREHOLE DRILLING PROGRESS ASSESSMENT CHECKLIST**

The drilling supervisor/driller and/or any responsible drilling representative should explain the following parameters and if possible provide any other information relevant to the project's drilling phase which not covered below.

1. Date of assessment 10/04/2008

2. Project Name OLOBANITA BOREHOLE - 1

Total Drilled Depth (m) 271.0 Borehole Diameter 350mm

3. What is the current Water Rest Level in meters? 130m below ground level

4. Indicate all Water Struck Levels and their estimated airlifted yields

i. 140

ii. 182

iii. 208

iv. 238

25  
#2 X  
0.30

5. Outline thicknesses of various aquifer zones encountered in meters and their estimated airlifted yields  
Classify the aquifers as **Minor or Major**

i. 140 - 142

ii. 182 - 184

iii. 208 - 217

iv. 238 - 252

v. \_\_\_\_\_

6. For quick and accurate correlation of aquifer zones with geological logs, did the drilling contractor indicate specific water struck levels and their estimated yields on the sample bags of the corresponding geological logs? If no, please explain, Estimated yield could not be measured since we are using mud drilling and occasionally we lost circulation. The contractor feared that if airlifting was done without the casings in the borehole, the borehole would collapse.

7. Samples of clearly labelled geological logs should be brought to Groundwater Survey's office in Nairobi for analyses and reporting purposes, after which the logs can be collected.

8. What are the drilling Supervisor's/ Driller's/ drilling crew's remarks on

i. Difficulties encountered during drilling e.g.

a) Any caving in (collapsing of walls) problem? Yes If any at what depth(s)

22 - 24 m

b) Any blockage of the hole by boulders? Yes, If any at what depth(s)

At 110 m there were boulders falling from the upper level

c) Explain any other problem(s) encountered during drilling

Since we were using mud drilling from 217m - 277m, a lot of water was required

ii. Any difficulties encountered during collection of geological logs in relation to nature of the airlifted cuttings e.g. airlifting of volcanic ashes mixed with plenty of water might appear as very turbid water or slurry without any noticeable fragments. Please explain

N/A

iii. Rate of Penetration. (was it recorded or not?) If yes, please attach its copy. If no, please explain why

iv. General progress of drilling works Since the borehole diameter is big, the rig could not airlift the cuttings to the surface

v. Any other remarks? Considering the method of drilling, time taken to finish this borehole was good